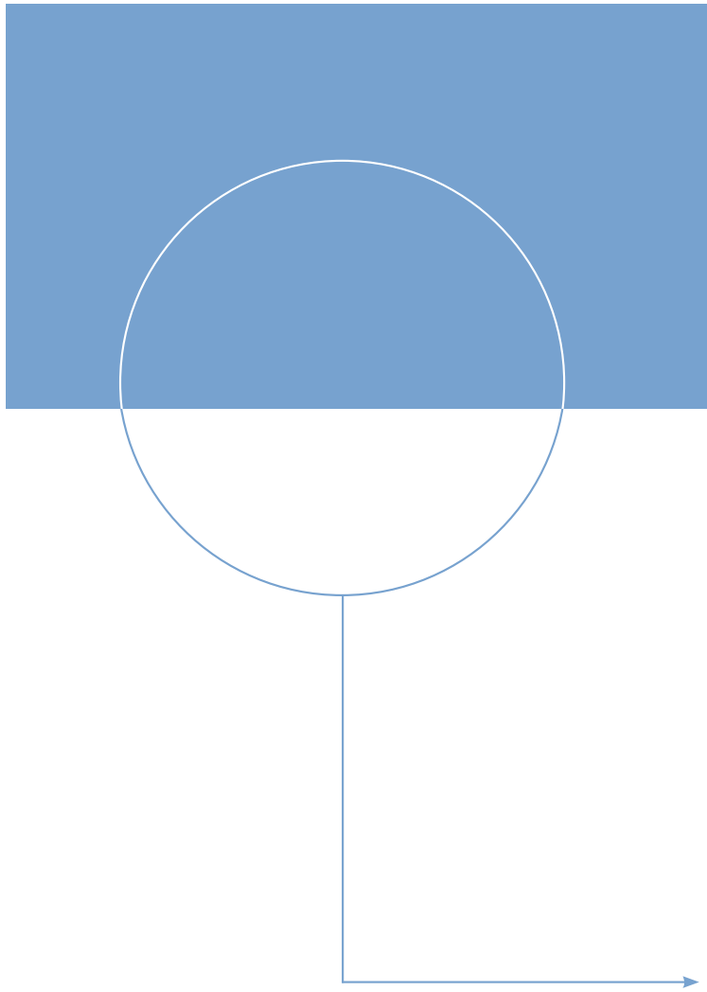

Master's thesis

2021

Yeray González, Arkaitz Rabanal

NTNU
Norwegian University of
Science and Technology
Faculty of Information Technology and Electrical
Engineering
Department of Electric Power Engineering

Yeray González
Arkaitz Rabanal

Adaptive Control of HVDC Transmission Systems

Designing a stability-preserving energy-balancing outer loop

June 2021

NTNU
Norwegian University of
Science and Technology

NTNU
Norwegian University of
Science and Technology

NTNU

Norwegian University of
Science and Technology

Adaptive Control of HVDC Transmission Systems

Designing a stability-preserving energy-balancing outer loop

Yeray González

Arkaitz Rabanal

Master in Renewable Energy in the Marine Environment

Submission date: June 2021

Supervisor: Gilbert Bergna-Díaz

Co-supervisor: Raymundo E. Torres-Olguin

Norwegian University of Science and Technology

Department of Electric Power Engineering

To our supervisor, Professor Gilbert Bergna-Díaz, for his support, dedication and endless willingness to help from the early beginning of the Master's Thesis. Without your guidance and perseverance this work would have never been possible.

Contents

List of Figures iv

List of Tables vi

1 INTRODUCTION 3

1.1 General Introduction . . . 3

1.2 Objectives . . . 7

1.3 Limitation of Scope . . . 7

1.4 Thesis Structure . . . 8

2 NON-LINEAR CONTROL THEORY PRELIMINARIES 9

2.1 Non-linear System Equilibrium . . . 9

2.2 Port-Hamiltonian Representation . . . 9

2.2.1 Nonlinear Incremental Model . . . 11

2.3 Lyapunov Function Theory . . . 12

2.4 Passivity Based Control . . . 13

2.5 Immersion & Invariance . . . 15

3 ENERGY MODELLING AND PI-PBC CONTROL FOR A 2L-VSC HVDC SYSTEM 19

3.1 Systems Modelling . . . 19

3.1.1 Model description of the 2L-VCS . . . 19

3.1.2 Model description of the HVDC transmission line . . . 21

3.2 Port-Hamiltonian Representation . . . 22

3.2.1 Port-Hamiltonian representation of 2L-VSC . . . 22

3.2.2 Port-Hamiltonian representation of HVDC transmission line . . . 24

3.3 2L-VSC Open-Loop Stability . . . 25

3.4 2L-VSC Stability Certificate . . . 29

3.4.1 Lyapunov function for the physical model . . . 29

3.4.2 Application of the incremental model . . . 30

3.4.3 Lyapunov function for the incremental physical model . . . 31

3.4.4 PI-Passivity based controller . . . 32

3.4.5 Lyapunov function for the physical and the virtual model . . . 35

4 DESIGN OF THE PARAMETERS ESTIMATORS 37

4.1 Single Estimation of I_T . . . 37

4.1.1 Definition of $\beta(q_c)$ from Lyapunov function . . . 38
4.1.2 Definition of $\beta(q_c)$ from the desired behaviour . . . 39
4.2 Single Estimation of G . . . 39
4.2.1 Linearized G estimator from $\dot{q}_c$ . . . 40
4.2.2 Non-linearized G estimator from $\dot{q}_c$ . . . 41
4.3 Combined Estimation of I_T and G . . . 41
4.4 Single Estimation of R . . . 43
4.4.1 R estimator from inductance direct flux ($\dot{\psi}_d$) . . . 43
4.4.2 R estimator from inductance quadrature flux ($\dot{\psi}_q$) . . . 45
4.4.3 R estimator from the inductance direct and quadrature fluxes together . . . 46
4.5 Combined Estimation of R and G . . . 48
4.6 Estimator's Energetic Interpretation . . . 51
4.7 Energy Balance Based Adaptive Controller . . . 53

5 SIMULATIONS **55**
5.1 Description of Matlab/Simulink Models . . . 55
5.2 Open-Loop Control . . . 56
5.3 PI-Passivity Based Control . . . 58
5.3.1 PI-PBC with nominal parameters . . . 58
5.3.2 PI-PBC with erroneous parameters . . . 59
5.4 Adaptive Passivity Based Control . . . 61
5.4.1 Estimation of I_T . . . 62
5.4.2 Estimation of G . . . 63
5.4.3 Estimation of I_T and G . . . 64
5.4.4 Estimation of R . . . 65
5.4.5 EBBA outer-loop: Estimation of R and G . . . 68
5.4.6 Two terminal HVDC system . . . 73
5.5 Discussion of Results . . . 78

6 CONCLUSIONS AND FUTURE WORKS **79**
6.1 Conclusions . . . 79
6.2 Future Works . . . 79

Bibliography **81**

Appendix **85**

A Mathematical Developments **85**

A VSC Matrix Representation 85

B Park Transformation 86

C VSC Incremental Passive Output 89

D Final Steps for the Obtention of Expressions of the Modulation Indices 90

D.1 Development of direct modulation index 91

D.2 Development of quadrature modulation index 91

B Sets of Equations for VSC converters **92**

A Set of equations from the point of view of a rectifier operation and as a function of inductor fluxes and capacitor charge 92

B Set of equations from the point of view of a rectifier as a function of inductor's currents and capacitor's voltage 92

C Set of equations from the point of view of an inverter as a function of inductor's fluxes and capacitor's charge 92

D Set of equations from the point of view of an inverter as a function of inductor's currents and capacitor's voltage 92

C Proofs **93**

A Proof 1: Property of a Skew-Matrix 93

B Proof 2: Incremental Hamiltonian Gradient 93

C Proof 3: Relation Between Input Matrix and Vector 93

D Proof 4: Relation Between Passive Output Terms 94

E Proof 5: Terms Cancellation in the Physical-Virtual System Lyapunov Function . . 94

List of Figures

1 Share of renewable energy in power generation in the Sustainable Development Scenario, 2000-2030. 3

2 European supergrid. 4

3 Breakeven distance between a HVAC and HVDC line. 5

4 (a) Π and (b) T models for a transmission grid. 5

5 Block diagram of a PID-PBC. 14

6 Block diagram of a PI-PBC. 15

7 VSC model for grid forming control strategy. 19

8 VSC model for grid feeding control strategy. 21

9 Schematic representation of the FD-Π model. 22

10 Block-diagram of the proposed PI-PBC. 32

11 Interconnection between VSC and PI-PBC. 34

12 Schematic representation of EBBA outer-loop. 53

13 HVDC Simulink Model diagram. 55

14 VSC AC currents and DC voltage in an open-loop control. 57

15 Injected active and reactive powers into the grid in an open-loop control. 58

16 VSC AC currents and DC voltage with PBC strategy 59

17 Systems Lyapunov function and its time-derivative 60

18 VSC AC currents and DC voltage with PBC strategy and erroneus parameters . . 60

19 Active and reactive powers with PBC strategy and erroneus parameters 61

20 VSC AC currents and DC voltage with I&I philosophy for I_T estimation. 62

21 I_T estimation. 63

22 VSC AC currents and DC voltage with I&I philosophy for G estimation. 64

23 Conductance estimation for a 10% of initial error. 65

24 VSC AC currents and DC voltage with I&I philosophy for I_T and G estimation. . 66

25 Transmission current and conductance estimation for a 10% of initial error. 66

26 VSC AC currents and DC voltage with I&I philosophy for R estimation from one equation. 67

27 Inductor resistance estimation for a 10% of initial error. 68

28 VSC AC currents and DC voltage with I&I philosophy for R estimation from two equations. 69

29 Inductor resistance estimation for a 10% of initial error. 69

30 VSC AC currents and DC voltage with I&I philosophy for R and G estimation. . . 70

31 R and G estimations. 71

32 R and G estimations for different inductance and capacitance error. 71

33 Zoom of R and G estimations for different inductance and capacitance error. . . . 72

34 VSC AC currents and DC voltage with I&I philosophy for R and G estimation and for different inductance and capacitance error. 72

35 Zoom of VSC AC currents and DC voltage with I&I philosophy for R and G estimation and for different inductance and capacitance error. 73

36 VSC AC currents and DC voltage with I&I philosophy for R and G estimation and for different inductance and capacitance error (Grid feeder control with DC transmission grid). 74

37 Zoom of R and G estimations for different inductance and capacitance error (Grid feeder control with DC transmission grid). 74

38 Both terminals AC currents and DC voltages. 76

39 DC transmission line current (Reference from terminal 2 to 1). 76

40 Zoom of both terminals DC voltages and DC transmission line current. 77

41 Both terminals R and G estimations. 77

List of Tables

1 Electrical Nominal Values of the System 56

2 Converter Passive Elements (per phase) 56

3 PI-PBC proportional and integral parameters 58

4 I_T estimator parameters 62

5 G estimator parameters 64

6 Estimator parameters of DC current and conductance 65

7 R estimator parameters. 68

8 AC resistance and DC conductance estimator parameters 70

9 Terminals PI-PBC and EBBA controler parameters 75

10 Terminal references though the simulation 75

ABSTRACT

The large-scale introduction of offshore renewable generation will indeed require a multi-terminal HVDC transmission system—based on voltage source (power) converters—in order to efficiently transfer the offshore power to shore over long distances. The conventional power converter control solutions associated to this technology (typically based on standard current control methods) have been designed to satisfactory operate near a single nominal operating point. This makes them inherently unsuitable for guaranteeing uninterrupted operation (stability) of the system in the event of an unexpected large signal-disturbance. Moreover, the offshore HVDC grid architecture complexity is expected to increase as more lines and renewable energy sources are connected to the grid. It then seems desirable to find control alternatives able to operate the system with large-signal stability guarantees, preserved regardless of any topological change or system disturbance size—and therefore avoiding any costly operational interruption of the system.

This manuscript presents the *Energy Balance Based Adaptive (EBBA)* outer-loop rooted in the *Immersion & Invariance* methodology, which replaces the traditional outer-loops while preserving the large-signal stability certificate on 2 Level VSCs. This novel controller places particular emphasis on the estimation of the system parameters, crucial for the converter load-flow computation. Additionally, for the development of this Master's Thesis *port-Hamiltonian* representation, *Lyapunov* theory and *Passivity Based Control* strategy are used.

1 INTRODUCTION

1.1 General Introduction

The current development and growing trends are expected to have huge impact on the global primary energy consumption over the next few decades. According to the International Energy Outlook 2019 [41], the U.S. Energy Information Administration (EIA) expects a growth of nearly 50% between 2018 and 2050; influenced by the strong economic development in Asia. Closely related to it, as consequence of the growth in end-use consumption, the electricity generation is expected to increase a 79% from the same time period. This can be interpreted as a direct consequence of the rising population and living standards in non-OECD countries and the electrification of the transportation sector, especially due to the plug-in vehicles and rail.

However, the way in which this increase will occur is not independent of the actual climate scenario. For that reason, several global institutions have set forth ambitious energy plans; betting strongly on a massive inclusion of renewable energy sources (RES) in the energy system. This is the case of the objectives for 2030 and 2050 proposed by the European Union (EU), when the RE are expected to provide the 32% and 100% of the electricity, respectively [14, 33]. The impact of these kind of legislation may imply a worldwide renewable energy consumption increase of 3.1% per year. As a consequence of this transition trend, the EIA predicts renewable energy will be the most used energy source by mid 2040s decade. Figure 1 depicts the predicted share of renewable energy in the power generation according to the sustainable development scenario publish by the International Energy Agency (IEA) in 2020 [18].

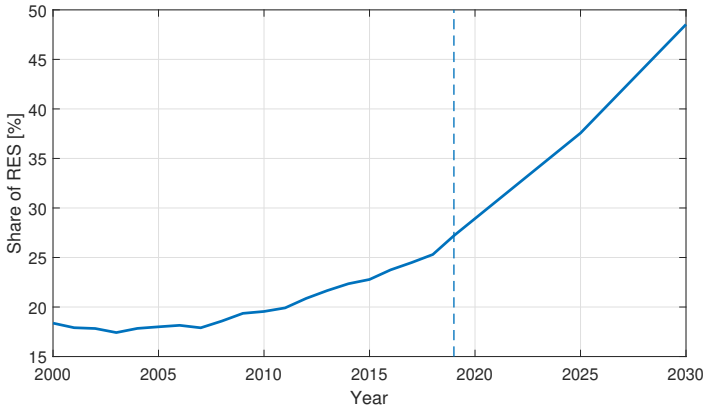

Figure 1: Share of renewable energy in power generation in the Sustainable Development Scenario, 2000-2030.

But, at the same time, this energy transition poses different challenges, which agents involved have to be able to solve. One of those challenges is the creation of efficient energy interconnections among large areas, including neighbouring countries and regions. This crucial step will contribute to reduce the dependence on the local predominant RE resource; i.e., a large enough grid including European and northern-African countries would count on the wind resource of the North Sea and the photovoltaic one of the countries of the south, among which the commissioned solar thermal projects in the north of Africa stand out. This kind of systems are known as supergrids (example shown in figure 1), which shares trans-national resources and, consequently, enormous RE potential.

Indeed, the implementation of supergrids, such as the one interconnecting Europe and North Africa shown in figure 2, and a further progress in the energy transition goes hand in hand with the development of technology that supports it [34]. This is the case of *High Voltage Direct Current (HVDC)* technology, which is probably the key technology for integrating large-scale RES. This kind of transmission system enables bulk energy transmission along great distances and the interconnection of different frequency HVAC grids. This is crucial as lots of RES are in remote locations, such as large water reservoirs or off-shore wind farms far away from the centres of consumption.

Figure 2: European supergrid.

The use of HVDC technology took off in the mid 1950s, thanks to research on high power electronics and advanced electronic control in the two previous decades. Major advances in the field enabled the commissioning of the first commercial transmission link in 1954 in the middle of the Baltic Sea, feeding the Swedish island of Gotland. Furthermore, it is of interest to mention that this link is still operational, focused on transmission of wind power to mainland [2].

Although historically HVAC technology was predominant, the development of the mercury arc valves made the use of HVDC systems increase rapidly during the following years [35]. At the same time, in use voltage levels rapidly augmented from values of 110 kV to five or seven times the initial one. Such had been the interest in high voltage developing, that a transmission project of 1150 kV was built with testing purposes in the former Soviet Union.

The continuous development of AC transformers was the main reason of HVAC being historically the predominant transmission technology, reason why the terminal costs of this kind of installations are considerably lower at present. Nevertheless, its major drawback is the excessive reactive current drawn by the cable's reactive element. This is directly related to the increase of cable's losses as the line length is incremented. For that reason, reactive compensation technology is required, generally known as *flexible AC transmission systems* (FACTS). However, these elements augment the AC line cost per unit length.

On the other hand, recently introduced HVDC technology makes the energy transmission more cost-effective for longer distances, as the reactive losses are neglected in this state. Moreover, this scheme adds some other benefits such as the use of submarine and underground cables over long distances, relatively easy full control of the power flow, embedded stability, smaller footprint or reduced magnetic fields when compared to AC lines. Nonetheless, as the technology development is more recent, the constructing costs are considerably higher.

As a result, when discussing the usage of HVDC transmission systems, the most determining factor to consider is the so-called *breakeven distance*, which directly implies the economic feasibility of HVDC projects compared with HVAC [22]. For that reason, particular studies have to be done for every single case, as different technical and economic specifications and combinations could affect the result, obtaining the particular distance for each of the cases. An illustrative example is shown in figure 3.

Going in-depth on HVDC transmission lines, their modelling should be undertaken considering the balance between accuracy and complexity. Π and T models have been traditionally used considering their relatively good performance in spite of their simplicity.

In figure 4, both possible modellings are shown, being the disposition of the different components the main existing difference. In T models of transmission line, the shunt capacitance is positioned entirely in the middle of the line, while half of line resistance and reactance are assumed to be at

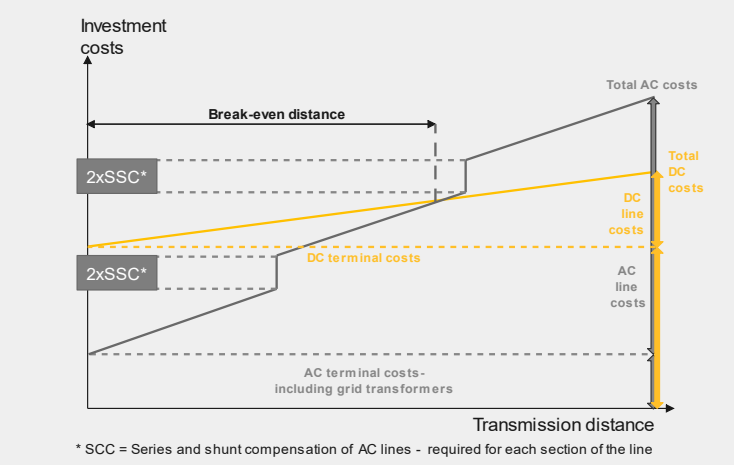

Figure 3: Breakeven distance between a HVAC and HVDC line.

each side of the shunt capacitance. On the other hand, Π model presents half of shunt capacitance on each of the terminals, also called sending and receiving ends; while the whole resistance and reactance is in the middle of both of them. One of the main differences is where the flowing of the capacitive charging current is located. In the case of T model, this flows through half of the transmission line, while in Π this is shared by the transmission and the receiving end [11, 43].

It is interesting to highlight the predominance of the use of cascaded-Π models for those lines with great length, whose capacitance has to be properly distributed. However, such models fail to capture the frequency-dependent characteristics of the cable, which are essential to account for the damping effects of the system [6, 12].

In relation to this, a continuous development of transmission models has been crucial in order to capt an accurate representation of the HVDC transmission technology performance, specially when talking about cable-based connections over long distances. This is due to the presence of significant inductance and stray capacitance in the system, which cause multiple LC resonance frequencies; being damped oscillations, over-voltages and instability due to interaction with power electronic converters and their control systems the major problems to be faced [13].

On the other side, HVDC converters are responsible of adapting the power from AC to DC side and vice verse, and therefore, the control strategies are implemented directly over these terminal. They can be classified into two main groups depending on the switching technology: *Line Commutated Converters* (LCCs) and *Voltage Source Converters* (VSCs).

Line Conmutated Converters, which were used in early designs, are generally thyristor based technology; reason why they can be referred as *"classic HVDC systems"*. This is because self-conmutated power devices were unavailable in the early stages of the technology development.

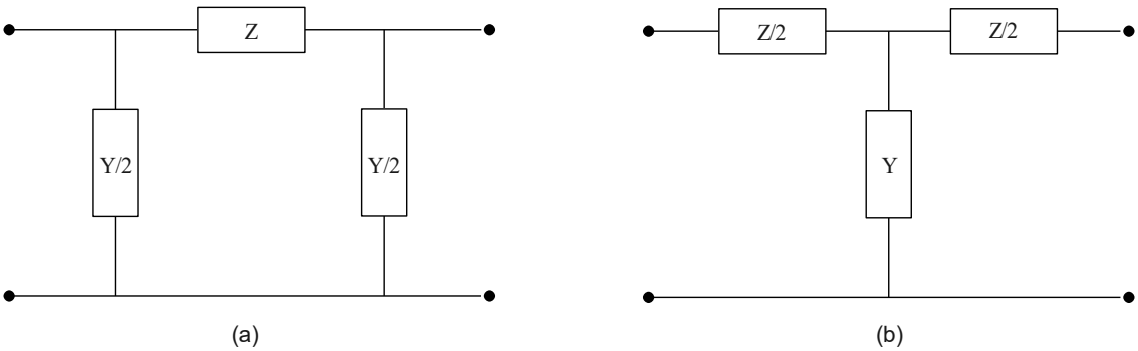

Figure 4: (a) Π and (b) T models for a transmission grid.

Due to the switching device's nature, the current's direction needs to remain invariant, so DC polarity needs to be changed if the power direction is wanted to be reversed. The major LCCs' advantage are the lower station losses and costs, which enable higher converter ratings.

However, there is a major drawback for this technology, which is the high reactive power consumption at terminals. This can vary up to 50-60% of the rated reactive power. LCCs are generally applied when there is a high *Short Circuit Ratio* (SCR), i.e. when the grid is strong enough.

On the other hand, *Voltage Source Converters* appear as a relatively recent HVDC system, fundamentally based on the development of self-commutated devices. These are mainly the *insulated gate bipolar transistor* (IGBT), which combines the controllability of MOSFET and the reliability of BJT.

If this technology is compared to LCC, the size is drastically reduced, as no reactive power compensators or AC filters are required in this case. However, the losses increase when compared to the traditional technology. For a two level converter, losses can reach a 1.4%, while in LCCs it is of 0.8%; thus, the power ratings are lower. Even so, VSCs are the major trend when talking about HVDC systems, as they can provide more accurate control and resulting waves.

The commutation control of this technology is generally based on *Pulse Width Modulation* (PWM) control; aiming to produce the most accurate sinusoidal AC voltage wave from DC and vice versa. This is perfectly feasible with the primary converters, called 2-level VSC. Still, this typologies limit the resulting voltages and add harmonic content whenever the required RMS voltage differ substantially from the DC voltage. For that reason, *Modular Multilevel Converters* (MMCs), which is a natural evolution of 2-level converter, appear to be a fitting solution for obtaining better-quality AC signals. This is because of the addition of a higher number of switches, helping to move towards a large number of voltage levels. Consequently, the switching frequency of each module is reduced, and so does the number of filters and switching losses.

The traditionally used control for these VSC converters consists on two main loops: an inner-loop responsible for carrying system's currents to their respective references, and an outer-loop which computes the needed current references based on the given active and reactive powers and voltages references.

Controlled currents are usually represented in a non-stationary *dq0-framework*, becoming these currents constant during steady-state operation. Thanks to this feature, traditional *Proportional-Integral-Derivative (PID)* controllers are able to bring the error between the measurements and references to zero.

In case of the inner loop, both direct- and quadrature-currents' PID controllers must be tuned in order to cancel the dominant poles of the converter's dynamic, allowing an appropriate control of the VSC behaviour. The dominant pole will be defined by the RL filter between the converter and the grid; thus, the time constant $\tau = \frac{L}{R}$ should be canceled.

Conversely, the outer-loop generates a d-current reference from a previously requested active power or DC-side voltages. Taking into account that the DC voltage dynamic is dependant on the injected or absorbed AC active power, a single converter cannot control both at the same time. The quadrature current reference is also computed by an outer-loop. In this case the q-current is controlled to get the asked reactive power or PCC's voltage level, since both of them are strongly coupled in medium and high voltage AC systems.

Note that, to be able to neglect the inner-loop in the tuning of the outer-loop's parameters, the former must be sufficiently faster than the latter.

Nevertheless, the global stability of these control strategy have not yet been proven analytically. Thus, multiple numerical simulation must be carried out in order to be sure of the robustness and stability of the system. This fact takes even more relevance in multi-terminal HVDC systems, where the integration of new components must be carefully analysed aiming not to compromise the whole system.

Consequently, the main motivation behind our work is to contribute towards the design of *robust controllers with large-signal stability guarantees* able to suitably operate HVDC systems even when subjected to unwanted large disturbances. At the same time, particular consideration is given to control alternatives with *Plug & Play* philosophy, which would enable electrical grids to grow without requiring a significant update of the controllers, while preserving the overall stability certificate.

For that purpose, the passivity feature of the system will be exploited by means of a *Proportional-Integral Passivity Based Control (PI-PBC)*. This control philosophy enables an energetic interpretation of the control, which allows the mathematical interconnection of the physical and virtual systems, i.e. the converter and the control. Nevertheless, this strategy requires the knowledge of the desired equilibrium point of the system, which, in turn, requires the knowledge of the exact value of the system parameters.

Towards this end, the implementation of the *Immersion & Invariance (I&I)* methodology appears to be a promising solution, enabling to obtain the exact parameters that can guarantee the desired equilibrium point and which does not destroy the stability certification that has been previously obtained thanks to Lyapunov theory and the *PBC* strategy.

1.2 Objectives

This work aims to develop an analytical adaptive controller for non-linear systems, specifically focused on HVDC converters and systems, trying to improve the possible lack or wrong knowledge of system parameters. This will be particularly based on *Passivity-Based Control* and the *Immersion & Invariance* methodology, which are explained in due course.

Accordingly, this present work has different objectives, which are identified as follows.

- First, we aim to obtain a suitable analytical nonlinear (incremental) model for a single 2-Level Voltage Source Converter (VSC), in both grid-feeding and grid-forming configurations, under the Port-Hamiltonian formalism, which eases the PBC design.
- Second, we aim to overcome the lack of knowledge over the physical system by means of the design of a parameters estimator, based on the immersion & invariance methodology.
- Finally, to validate the proposed adaptive controller through numerical simulation, testing both grid forming and grid feeding configurations, and increasing the complexity of the model.

In order to achieve all the objectives, and although this work is fed by the contributions from several references in the literature, the article *Adaptive PI Stabilization of Switched Power Converters* [17] of Dr. Hernandez-Gomez deserves special mention, since it provided the main idea for the project. Likewise, the recent paper *PID passivity-based Control of Power Converters: Large-signal Stability, Robustness and Performance* by Daniele Zonetti brought the basis for the understanding of PI-PBC strategy on VSC converters.

Despite the infinite research possibilities in this field, it is always important to take into consideration the limited time available for this Master Thesis development. For this reason, this work is focused on very specific objectives. Notwithstanding all of this, all possible complementary improvements are not discarded at all and they are included in the following section 1.3.

1.3 Limitation of Scope

As mentioned above, the current work has been developed in less than half a year. For that reason, different simplifications have been assumed so that the main objectives of the Master's Thesis can be achieved. These assumptions are covered deeper in the following lines.

Firstly, it is well known that the modular multilevel converter (MMC) technology has established itself as the most suitable technology fot multi-terminal HVDC systems. However, for simplicity

reason and time limitations, we focus our attention to its predecessor, the two-level voltage source converter (2L-VSC). This decision is justified given that i) the main focus of the work is on investigating the potential of the I&I adaptive control method for the HVDC scenario, and ii) it is likely that the results can be easily extended to the MMC.

Secondly, aiming to simplify as much as possible the model operation, the following assumptions are considered. On one hand, the *current inertia* provided by the filter inductors is assumed to be large enough compared to the time constant of the switching action of the system so that the model is continuous. This assumes that both the modulation indices in the *abc* framework as well as the AC currents are considered purely sinusoidal. This decreases the relevance of current conditioning in relation to harmonics and quality.

On the other hand, the synchronisation of the converters to the network via PLLs is not taken into account. Again, this decision is justified given that i) the main objective is to highlight what the main contribution of the work is, rather than complementary features, and ii) the faster dynamic of the synchronisation process compared to the estimator ones makes this aspect possible to neglect to a certain extent.

Furthermore, we also assume that the transmission line parameters are known and available for load flow calculations. This strong assumption allows us to direct our focus to the estimations of the inner resistances and conductance of the power converters. Indeed, a more complete adaptive control design would also take the uncertainty of the line resistances into account, yet we leave this extension for future works.

Finally, decentralized and distributed control appear as the alternatives to facilitate the implementation of electrical systems in which the power flow is multi-directional. However, in a same way as in the previous point, a traditional centralized control scheme is assumed to simplify the system operation and estimator implementation. Again, alternative control modes are left for future improvements.

1.4 Thesis Structure

The remainder of this Thesis manuscript is structured as follows. Sections 2 and 3 follow parallel complementary paths: while the former gives the underlying theoretical framework necessary to understand the required concepts, the latter presents the application of such a framework to the specific case of the 2L-VSC. More precisely, section 2 presents a more formal approach, including the required theorems and lemmas; while in section 3 an informal interpretation is given, aiming to create a didactic summary that can serve as a basis for future master students not so familiar with nonlinear control to get acquainted with the necessary knowledge of this line of research.

Furthermore, section 4 is dedicated specifically to the I&I philosophy. More precisely, this section describes, in chronological order, our five different I&I implementation attempts, varying both the parameters to be estimated as well as the strategy undertaken. Ultimately, these attempts lead to our main result: a large-signal stability preserving outer-loop control based on the internal power-balance of the 2L-VSC. In section 5, different simulations results are presented, together with an analysis and discussion of the different estimators performance. Section 6 concludes the Thesis along with some hints for future works.

Finally, an appendix is attached in the last pages of the document, in which proofs, mathematical developments and theoretic background are included. This is since to some of them are well-known by people in the field or whose inclusion in the main document makes no sense for reasons of simplicity or excessive length.

2 NON-LINEAR CONTROL THEORY PRELIMINARIES

This chapter will provide some basic yet formal theoretical concepts in order to ease the understanding for potential readers not so familiarized with nonlinear control. Starting with the definition of the equilibrium point and with the open loop control solution of a non-linear system, this section will introduce the concepts of *Port-Hamiltonian Representation*, *Nonlinear Incremental Model*, *Lyapunov Function*, *Passivity Based Control* and the *Immersion & Invariance Method*.

It is worth mentioning that these concepts will be approached from a more theoretical point of view; leaving the application to the VSC to section 3.

2.1 Non-linear System Equilibrium

A physical system is said to be at equilibrium when the state-variables which represent the system are constant with respect to time. For instance, if the dynamics of a general system are expressed as in equation (1), where $x \in \mathbb{R}^n$ are the state-variables and $\dot{x} = \frac{dx}{dt}$, there is an equilibrium point at $\bar{x} \in \mathbb{R}^n$ that can be written as the set of assignable equilibrium (2).

$$\dot{x} = f(x) \tag{1}$$

$$\mathcal{E} := \{x \in \mathbb{R}^n : f(x) = f(\bar{x}) = 0\} \tag{2}$$

With some loss of generality, we will be focusing on non-linear systems whose dynamic equations can be expressed as in (3), where $u \in \mathbb{R}^m$ is the control input vector of the system, the vector field $f(x) : \mathbb{R}^n \to \mathbb{R}^n$ and the input matrix $g(x) : \mathbb{R}^m \to \mathbb{R}^n$ [50].

$$\dot{x} = f(x) + g(x)u \tag{3}$$

The set of equilibrium of this kind of systems can *sometimes* be expressed as function of state variables only, avoiding the control or input vector in the expression. Then, the assignable equilibrium point of (3), characterized by

$$0 = f(\bar{x}) + g(\bar{x})\bar{u},$$

can be alternatively written as (4).

$$\mathcal{E} := \{x \in \mathbb{R}^n : g^{\perp}(x)f(x) = 0\}, \tag{4}$$

where $g^{\perp}(x)$ is a full-rank left annihilator of $g(x)$. On the other hand, the input vector's solution at the equilibrium can be computed as a function of the states as shown below.

$$u(\bar{x}) = -g^{+}(\bar{x})f(\bar{x}), \tag{5}$$

where $g^{+}(x)$ is the Moore-Penrose left pseudoinverse of the matrix $g(x)$ shown in equation (6).

$$g^{+}(x) = \left(g^{\top}(x)g(x)\right)^{-1} g^{\top}(x) \tag{6}$$

2.2 Port-Hamiltonian Representation

Depending on the representation, the dynamics of the same *physical* system of interest can be written in a variety of forms. The election of the representation depends not only on the system

itself, but it is also chosen in order to facilitate the development of the model to achieve the desired result.

For instance, a well-known mathematical model is the state-space representation, which is able to represent multiple-input multiple-output (MIMO) systems that are described by first order differential equations. For *linear* systems, this representation is written by the set of equations (7).

$$\begin{cases} \dot{x} = Ax + Bu, \\ y = Cx + Du. \end{cases} \tag{7}$$

where $x \in \mathbb{R}^n$ are the state variables of the system, $\dot{x}$ are the first order time-derivatives of state variables, $u \in \mathbb{R}^m$ is called input or control vector, $y \in \mathbb{R}^q$ is called output vector, $A \in \mathbb{R}^{n \times n}$ is the state matrix, $B \in \mathbb{R}^{n \times m}$ is called input matrix, $C \in \mathbb{R}^{q \times n}$ is the output matrix and $D \in \mathbb{R}^{q \times m}$ is called feed-forward matrix [20].

Similarly, a set of dynamic equations describing a nonlinear systems can be also arranged in multiple forms. Looking at literature [17, 29], a commonly used representation is:

$$\begin{cases} \dot{x} = f(x) + g(x)u, \\ y = h(x) + j(x)u. \end{cases} \tag{8}$$

However, even though the above mathematical model could be used for the representation of a VSC converter, since HVDC lines are composed by multiple components such as transmission lines and two or more converters, a model which allows an easy interconnection of different systems is preferred. Thus, any port-based model would be advisable.

Port-Hamiltonian representation fulfills the needed characteristics, since it combines the views of the Hamiltonian mechanics and the theory of port-based modelling [40], which allows the representation of complex systems by the interconnection of simpler blocks. This provides a unified framework for the modeling of systems belonging to different physical domains [42].

The Hamiltonian formulation of classical mechanics is formalized in a geometric way. The underlying geometric structure of port-Hamiltonian systems is determined by the interconnection structure of the system. This motivated to consider Dirac structures instead of Poisson structures as in traditional Hamiltonian formulation. This enabled to define Hamiltonian systems with algebraic constraints [38].

The main advantages that this mathematical representation brings to the project are listed below:

- A composition of Dirac structures are again a Dirac structure. Thus, a power-conserving interconnection of port-Hamiltonian systems is again a port-Hamiltonian system [42], what is of great relevance for the conservation of the stability certification.
- It enables an easy interpretation of physical properties such as conservation laws and energy considerations, including the shaping of energy-storage and energy-dissipation.
- It allows the integration of control, since it admits the extension of physical models with virtual system components [42]. This feature is applied later in section 3.4.4.

For the sake of brevity, we limit our attention to the modelling of switched power converters and transmission lines via the port-Hamiltonian formalism. Thus, for our application of interest, the representation takes the form given in equation (9) [17, 50].

$$\dot{x} = \left(\mathcal{J}_0 + \sum_{i=1}^{m} \mathcal{J}_i u_i + \mathcal{R} \right) \nabla \mathcal{H}(x) + \left(G_0 + \sum_{i=1}^{m} G_i u_i \right) E \tag{9}$$

where $\mathcal{J}_i$ are the interconnection matrices with $i \in \{0, 1, ..., m\}$, u_i is the i^{th} element of the control vector, $\mathcal{R} = \mathcal{R}^\top \geq 0$ is the dissipation matrix, the vector $E \in \mathbb{R}^n$ contains the external sources and $G_i \in \mathbb{R}^{n \times n}$ represents the interconnections with external sources.

The interconnection matrices $\mathcal{J}_i$ capture the power preserving topological changes of the system introduced by the switches. Consequently, these matrices are skew-symmetric, i.e. they follow the structure given in (10). An interesting property of this kind of matrix for latter developments is that if $\mathcal{J}$ is a skew-matrix and $c \in \mathbb{R}^n$ is a column vector, then $c^\top \mathcal{J} c = 0$. A proof of this properties can be found in appendix C.

$$\mathcal{J} = -\mathcal{J}^\top \tag{10}$$

The Hamiltonian $\mathcal{H}(x)$ is a scalar function describing the energy-storage of the system, e.g. the energy in the inductances and capacitors in case of a power converter (see equation (11)). The effort of the energy-storing elements (currents and voltages) is then expressed by the Hamiltonian gradient $\nabla\mathcal{H} = \frac{\partial \mathcal{H}}{\partial x} \in \mathbb{R}^n$ [40].

$$\mathcal{H}(x) = \frac{1}{2} x^\top Q x, \qquad Q = Q^\top > 0 \tag{11}$$

In the specific case of a 2L-VSC, which has just fixed sources without any switching, G_i matrix can be omitted from (9). Then, the result from $G_0 E$ is simplified to E, obtaining the reduced expression (12) [17]. The development of the converters model up to the equation below is later presented in section 3.

$$\dot{x} = \left(\mathcal{J}_0 + \sum_{i=1}^{m} \mathcal{J}_i u_i + \mathcal{R} \right) \nabla\mathcal{H}(x) + E \tag{12}$$

It is worth mentioning that physical systems that are able to be represented under the port-Hamiltonian formalism, fall into the broader class of *passive* systems, making the former a natural starting point for the passivity-based control design [40], a characteristic that was widely used in [50]. Additional details on the PBC control of interest will be explained in section 2.4 and is applied to a 2L-VSC converter in section 3.4.4. However, before being able to apply this kind of controller, the nonlinear incremental model must be understood.

2.2.1 Nonlinear Incremental Model

From a general perspective, the concept of *passivity* characterizes dynamical systems that cannot store more energy than the energy supplied to them, i.e. that cannot generate power [32]. From this definition, it can be assumed that a VSC converter is passive. These energy conservation principles can later be restated to design stable control laws, especially in the case of large and complex control systems—via Lyapunov's direct method (section 2.3).

The idea behind PBC, which is itself rooted in Lyapunov theory, is based on bringing the stored energy of the system to its minimum. Unfortunately, the implementation of this strategy directly to the Hamiltonian energy function would bring the state variables to zero, practically switching-off the converter.

One possible way of applying this control strategy with a non-zero equilibrium point is to instead base the control design on the *incremental model*, whose state variables are the deviations between original variables and the desired equilibrium point called incremental variables, i.e. $\tilde{(\cdot)} := (\cdot) - \bar{(\cdot)}$ [19].

This new model is obtained after subtracting the solution of the system for the particular case of the desired point of equilibrium (13) from the port-Hamiltonian model. In such a way, the energy-based representation is developed up to an expression containing a Hamiltonian term with

the form of (14). Refer to section 3.4.2 for a step by step derivation of the incremental model of the 2L-VSC.

$$\dot{\tilde{x}} = 0 = \left(\mathcal{J}_0 + \sum_{i=1}^{m} \mathcal{J}_i \bar{u}_i + \mathcal{R} \right) \nabla \mathcal{H}(\bar{x}) + E \tag{13}$$

$$\mathcal{H}(\tilde{x}) = \frac{1}{2} \tilde{x}^\top Q \tilde{x} = \frac{1}{2} (x - \bar{x})^\top Q (x - \bar{x}) \tag{14}$$

The new Hamiltonian function is then a quadratic function which has its minimum at the point of desired equilibrium, enabling its used as Lyapunov function for non-zero equilibrium point systems.

2.3 Lyapunov Function Theory

When studying dynamical systems, different types of stability problems are generally found, where the stability of equilibrium points stands out. As referred in section 2.2.1, the *nonlinear incremental model* can be combined with Lyapunov's direct method for nonlinear autonomous systems to bring the stored energy to zero, reaching one of the mentioned equilibrium points and, consequently, forcing the system to be stable. This is further explained in the following lines.

Consider an autonomous nonlinear dynamical system:

$$\dot{x} = f(x),\ x \in \mathbb{R}^n \tag{15}$$

where the function (this is, the vector field) $f : \mathbb{R}^n \to \mathbb{R}^n$ satisfies a sufficient condition for the existence and uniqueness of a solution. The solution of (15), starting from x at t= 0 is called system trajectory. $\bar{x} \in \mathbb{R}^n$ can be defined as an *equilibrium solution* of (15) if $f(\bar{x}) = 0$. This means the equilibrium point is a solution that does not change in time and, hence, they are degenerated solution curves that do not move [36]. By translating the origin to the equilibrium point $\bar{x}$ by means of incremental model, zero can be made an equilibrium point. For the sake of simplicity, henceforth the origin is assume as an equilibrium point of (15) [37, 46].

Once the concept of equilibrium points is defined, Lyapunov's second method for stability can be used to prove the *asymptotic* stability of a system by finding an scalar function $\mathcal{V}(x)$, where x is the state variables vector and $\mathcal{V}(x)$ is called *Lyapunov Function (LF)*. This function must satisfy the following conditions:

1.
$$\mathcal{V}(x) > 0 \quad \forall \quad x \neq 0 \tag{16}$$

2.
$$\mathcal{V}(0) = 0 \tag{17}$$

3.
$$\dot{\mathcal{V}}(x) = \underbrace{\frac{\partial \mathcal{V}(x)}{\partial t} = \frac{\partial \mathcal{V}(x)}{\partial x} \frac{\partial x}{\partial t}}_{\text{Chain rule}} = \nabla \mathcal{V} \cdot f(x) < 0 \quad \forall \quad x \neq 0 \tag{18}$$

4.
$$\dot{\mathcal{V}}(0) = 0 \tag{19}$$

If $\dot{\mathcal{V}}(x)$ is negative, the function will decrease along the trajectory of (15) passing through x. A $\mathcal{V}(x)$ is positive definite if $\mathcal{V}(0) = 0$ and $\mathcal{V}(x) > 0$ for $x \neq 0$ as shown in the first condition. It is positive semi-definite if it satisfies the weaker condition $\mathcal{V}(x) \geqslant 0$ for $x \neq 0$. A function $\mathcal{V}(x)$ is negative definite or semi-definite if $-\mathcal{V}(x)$ is positive definite or semi-definite respectively [21].

However, different kind of stabilities can be distinguished depending on the *region of attraction* (ROA), this is, the domain of the states x from which the system converges to the equilibrium point or the "safe" subset of the state space in which the system tends to stability asymptotically [8, 25].

Firstly, if $\mathcal{V}(x)$ is a Lyapunov function, then the equilibrium is Lyapunov stable.

When the Lyapunov-candidate-function (LCF) $\mathcal{V}(x)$ is locally positive definite and the time derivative of the LCF $\dot{\mathcal{V}}(x)$ is locally negative definite, following (20); for the the subset $\mathcal{B}$, the equilibrium is proven to be *locally asymptotically stable*.

$$\dot{\mathcal{V}}(x) < 0 \quad \forall \quad x \in \mathcal{B} \setminus \{0\} \tag{20}$$

It is also important to remark that the system could also be proven to be asymptotically stable even when $\dot{\mathcal{V}}(x) \leq 0$ through LaSalle's invariance principle.

Finally, if the LCF is globally positive definite and the time derivative of the LCF is globally negative definite, following (21); for all the state space the equilibrium is proven to be *globally asymptotically stable*.

$$\dot{\mathcal{V}}(x) < 0 \quad \forall \quad x \in \mathbb{R} \setminus \{0\} \tag{21}$$

Where the LCF is positive definite, or radially unbounded, when

$$\|x\| \to \infty \Longrightarrow \mathcal{V}(x) \to \infty$$

Furthermore, it is important to highlight in support of what is explained in the following sections that if a system is asymptotically stable in the Lyapunov sense and the Lyapunov function is the sum of two positive definite functions, then the system can be represented as the feedback interconnection of two passive systems [24].

Considering the LF stabilities, the nonlinear incremental model can be used to make a change of variable or *offsetting*, where the wanted operating point is settled as the equilibrium point, as will be developed in section 3. Likewise, there is no a general technique for constructing a LCF, nevertheless, a good starting point of a Lyapunov function candidate for physical systems can be based on the stored energy.

2.4 Passivity Based Control

During the last decades *Passivity Based Controllers* (PBCs) emerged as a non-linear control method which successfully exploits the physical structure of the systems, increasing in popularity as a building block for controller design [32]. As mentioned in previous sections, passive power systems could be defined as non-energy generator structures, whose difference between input and output power is just dissipations or energy storage. As stated by Dr. Lozano in [24], "Passivity is a useful analysis tool in the sense that the results can easily be interpreted in terms of energy in the system".

As PBC is generally based on the passive energy balance of the system, this strategy is suitable for the use of second method of Lyapunov theory as a stability certification [42]. Note that, as said in section 2.3, a good starting point for finding a Lyapunov function candidates for physical systems is the stored energy of the system. A proof of this can be found in [39], where a control is designed for the classical problem of stabilization of an inverted pendulum on a cart based on the passivity property of the system, using both a port-Hamiltonian representation of the model and the Lyapunov theory.

In the literature it can be found a variety of control architectures based on this method. Among others, in [44] passivity based a fractional-order PID (FoPID-PBC) is implemented in a hardware-

in-loop experiment for a grid-connected PV inverter via energy reshaping. Interconnection and damping assignment PBC (IDA-PBC) is studied in [26] and [47], which allows shaping the energetic properties of one or interconnected multi-system in a power-preserving manner. In this strategy the partial differential equations (which describes the system's behaviour) that must be solved are parameterized by three matrices related with the interconnection between the subsystems. These matrices can be seen as a dynamic couplings that allow the propagation of dissipation. Moreover, PBC strategy can be also applyied to traditional PID controller. In this case, the input of the controller is not an error between a variable reference and its measurement, but the passive output of the physical system. Due to this fact, the combination of PID-PBC and port-Hamiltonian systems is widely studied first in [48], and later in [9] and [10]. A block diagram of a PID-PBC is depicted in figure 5 along with its model in equation (22).

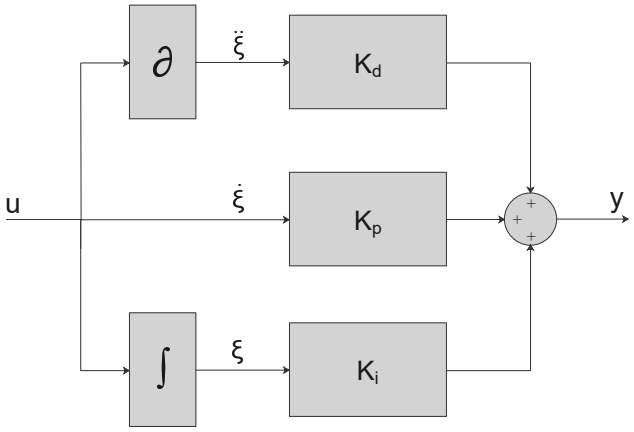

Figure 5: Block diagram of a PID-PBC.

$$\begin{cases} \dot{\xi} = u \\ y = K_p u + K_i \xi + K_d \ddot{\xi} \end{cases} \tag{22}$$

From the first stages of the methodology, different research areas have analysed the possibilities of PBC strategy in their processes. [45] studied control designs for the stability of distributed chemical processes in one spatial dimension, joining the passivity property with the second law of thermodynamics. A passivity-based perspective is also used in [3], overcoming some challenges of position, torque and impedance control of flexible joint robots. Moreover, the author emphasises the robustness of this control with respect to uncertainties of the robot.

Even though this control philosophy is not the predominant option in the electric industry, several articles can be found in the literature implementing this control successfully in multiple fields. For instance, the application of a PI-PBC is studied in [31], where a controller is designed for a permanent magnet synchronous machine based on passivity properties of the motor. Furthermore, Lyapunov theory is applied to ensure that the system is globally asymptotically stable. Another example is found in [15], where a classical PID and a PID-PBC strategy are both theoretically and experimentally compared in the control of velocity of DC motors. However, this methodology is increasingly being used in areas that are currently leading the way in progress, such as power electronics.

In this latter field, incremental passivity based control is combined with generalized PI observer for the control of a DC-DC converter in [16]. With this structure the author is able to estimate the time-varying uncertainties in the output voltage and inductor current, proving the robustness by means of experimental studies. More specifically on voltage source converters, the performance of a MMC controlled by a PI-PBC is analysed in [7].

Due to the wide research about the PI-PBC in the literature, and as the traditional PID is already rooted in the industry (what facilitates its possible future implementation) PI-PBC strategy has been chosen as control for the converters stabilization.

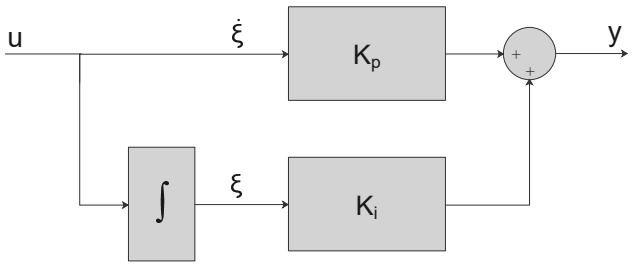

Figure 6: Block diagram of a PI-PBC.

Figure 6 depicts the block diagram representation of the used controller along with its mathematical model in (23). However, this system could be also interpreted from an energetic point of view as a I-PBC controller which is interconnected to the 2L-VSC by means of a dissipative component represented by the proportional gain. This fact is later analysed in the mathematical development performed in section 3.4.4.

$$\begin{cases} \dot{\xi} = u \\ y = K_p u + K_i \xi \end{cases} \tag{23}$$

2.5 Immersion & Invariance

Even though the given physical system could be stabilized via a PI-PBC, and this stability could be proven through Lyapunov theory, the control still would have to deal with some uncertainties in different parameters. Note that the use of incremental model forces the control to run a load flow of the system in order to compute a desired equilibrium point.

Since the model of physical systems suffer from parametric uncertainties, some small errors are inevitably introduced into the load flow, resulting in an erroneous calculated equilibrium point. The deviation of calculated point with the real equilibrium depends on the influence of each parameter in the final solution of the system.

In [50] it is proven that for current-controlled 2L-VSCs, if the PID-PBC is fed with a load flow solution near a real equilibrium point, the system will stabilize close to the desired real equilibrium and thus limiting deviations, but without exactly regulating the currents to the desired references. *Immersion & Invariance* (I&I) adaptive control could be a solution to recover the desired operating conditions prior to this deviation.

The I&I philosophy adds a new term to the classical certainty-equivalent control law, which is designed to achieve adaptive stabilisation of non-linear systems with parametric uncertainties that do not rely on the assumption of linear parameterization. As it is said in [5], the role of this new term is to shape the manifold into which the adaptive system is immersed.

A variety of articles about the implementation of this philosophy are found in the literature. In [27] I&I technique is studied for the adaptive control of linear multi-variable systems with reduced knowledge of the high-frequency gain, resulting in Lyapunov functions which contain cross-terms between the parameter errors and plant states.

[1] applies the I&I method in the stabilization of the traditional cart and pendulum system, aiming to design a functional control law and pointing the necessity of solving the partial differential equation of the immersion condition. Moreover, the design proposed in this article can be also studied from the perspective of PBC philosophy.

In another field, I&I is used by [4] to claim the possibility of design a globally convergent speed observer for general mechanical systems with k non-holonomic constraints, which main issue is recast as a problem of rendering attractive and invariant a manifold defined in the extended state-

space of the plant and the observer. The contribution is validated implementing the observer in two practical examples.

The I&I adaptive control is proposed by [23] for nonlinearly parameterized nonlinear systems, departing from the standard adaptive control and from the property of monotonicity. With this approach, the authors exploits the latter to obtain a useful strategy in the whole state-space.

Apart from the use of I&I technique for the stabilization of adaptive controllers and state observers of nonlinear systems, [30] also proves the viability of this strategy for orbital stabilization, validating their results with a simple example of a 3-phase DC-AC converter. Additionally, port-Hamiltonian representation is mentioned as a possible structure to develop a systematic procedure to apply I&I.

The method will be explained by means of a brief example with a single uncertain parameter taken from [5]. In case of a deeper insight into the topic is wanted, the reader is referred to the mentioned reference.

Consider a non-linear system represented in the form,

$$\dot{x} = f(x) + g(x)u,$$

where the functions $f(x)$ and $g(x)$ depend on an unknown parameter $\theta \in \mathbb{R}$. Then, a new variable is defined as $\theta^E \in \mathbb{R}$ (equation (24)), representing the estimation of the unknown parameter, so that $\lim_{t\to\infty} \theta^E = \theta$.

$$\theta^E \triangleq \beta(x) + \gamma \tag{24}$$

Adopting this I&I approach, the (non-robust) cancellation is avoided comparing to classical adaptive controller and it provides a means of shaping the dynamic response of the estimation error (e_θ). This is defined as,

$$e_\theta = \theta^E - \theta$$

Since the unknown parameter is constant, the dynamics of estimation errors follows the dynamic of the estimation parameter, and hence, estimation error can be developed as (25).

$$\dot{e}_\theta = \dot{\theta}^E - \dot{\theta} = \dot{\theta}^E = \dot{\beta}(x) + \dot{\gamma} \tag{25}$$

By means of chain rule, the time-derivative of $\beta(x)$ can be expressed as in (26), getting a way to introduce the dynamics of the physical system into the adaptive estimator.

$$\dot{e}_\theta = \dot{\beta}(x) + \dot{\gamma} = \frac{\partial \beta(x)}{\partial x}\dot{x} + \dot{\gamma} = \beta'(x)\dot{x} + \dot{\gamma} \tag{26}$$

Let's consider an example of a first-order nonlinear system with the form of equation (27).

$$\dot{x} = \theta x^2 + u \tag{27}$$

Then, it can be introduced to the dynamic expression of the estimation's error.

$$\dot{e}_\theta = \beta'(x)\left(\theta x^2 + u\right) + \dot{\gamma} = \beta'(x)\left((\theta^E - e_\theta)x^2 + u\right) + \dot{\gamma}$$

The first important step of I&I method is to define an update law ($\dot{\gamma}$) which linearizes or simplifies the dynamic of the estimator. In this example it should be,

$$\dot{\gamma} \triangleq -\beta'(x)\left(\theta^E x^2 + u\right)$$

Obtaining the next expression for the estimator's error dynamic.

$$\dot{e}_\theta = -\beta'(x)x^2 e_\theta$$

Finally, function $\beta(x)$ must be defined in order to get an stable system. A possibility for this example could be equation (28), for $\lambda > 0$. However, other options could be also chosen. In section 4 different methods for the definition of this function will be discussed, but in short, it could be said that the idea is to obtain a final dynamic expression that can be solved as a exponentially decaying function, such that the error between the estimated and real parameter asymptotically converges to zero.

$$\beta(x) = \lambda\frac{x^3}{3} \tag{28}$$

$$\beta'(x) = \lambda x^2$$

3 ENERGY MODELLING AND PI-PBC CONTROL FOR A 2L-VSC HVDC SYSTEM

Along this chapter, the theory explained in section 2 will be applied to the case of a 2L-VSC converter and a HVDC transmission line. Firstly, the models of both systems will be described and their port-Hamiltonian representations will be developed. Once the models are defined, open-loop stability will be checked.

In section 3.4 different mathematical tools will be used in order to obtain a global stability certificate. The explanations will be carried out in a chronological manner, obtained results and conclusions will be presented at each step. Note that one of the aims of this section is to be as didactic as possible for future readers. First, second method of Lyapunov will be developed for VSC port-Hamiltonian representation. Afterwards, in order to fulfill all the requirements needed by the second Lyapunov method, an incremental model is designed and implemented. After applying the Lyapunov method again, a proportional-integral PBC (PI-PBC) will be designed to finally fulfill all Lyapunov conditions.

3.1 Systems Modelling

Every analytical study of a physical system starts with a mathematical modelling, in which the state-variables are identified and their dynamic behaviours are described. In this first section of the chapter the modelling of both the converter and the HVDC line is performed, presenting the chosen voltage and current references for each system and modifying equations to facilitate their use in future sections.

3.1.1 Model description of the 2L-VCS

The analysed converter in this project is the well-known 2L-VSC converter, which is able to apply the desired voltage at AC-side terminals by means of an arrangement of six IGBT semiconductors. Considering the converter model shown in figure 7, the set of dynamic equations (29) governing its AC currents' behaviour can be obtained by means of *Kirchhoff's Voltage Law* (KVL). It is assumed that the converter works as inverter so the direction of the current is as indicated in the figure.

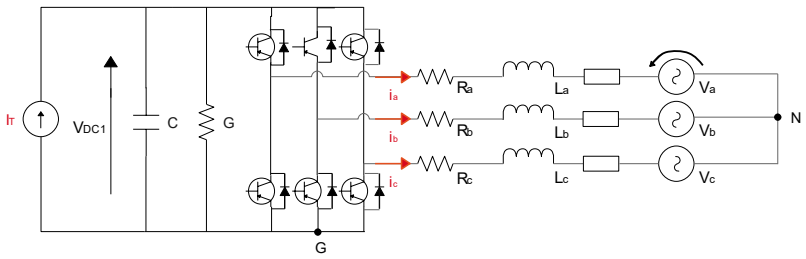

Figure 7: VSC model for grid forming control strategy.

$$\begin{cases} -v_a - \dfrac{d}{dt}(\psi_a) - Ri_a(t) + V_{QN} + u_a v_{dc1} = 0 \\ -v_b - \dfrac{d}{dt}(\psi_b) - Ri_b(t) + V_{QN} + u_b v_{dc1} = 0 \\ -v_c - \dfrac{d}{dt}(\psi_c) - Ri_c(t) + V_{QN} + u_c v_{dc1} = 0 \end{cases} \tag{29}$$

where $v_k(t)$, $k \in \{a, b, c\}$, is the AC input voltage, $\psi_k(t)$ are each inductor's flux linkage, R is a resistance in the input of the converter, $i_k(t)$ is the current through the inductors, V_{QN} is the voltage between the neutral and the negative side of the DC-capacitor, u_k is the modulation index

of each phase and $v_{dc1}(t)$ is the capacitor's DC side voltage. Note that although the modulation indices are actually Boolean objects representing the on/off state of the semiconductors, in the average model of the converter they can be handled as sinusoidal waves. Considering the different terms that appear in (29), the following definitions and properties must be taken into account.

$$L = \frac{\psi_k}{i_k} \tag{30}$$

$$C = \frac{q_c}{v_{dc1}} \tag{31}$$

$$i_C = C\frac{dv_{dc1}}{dt} \tag{32}$$

$$i_G = Gv_{dc1} \tag{33}$$

where L is the inductance of the AC-side RL linkage, C is the DC-side capacitance, q_c is the charge accumulated due to capacitances, and G is the DC-side conductance.

The dynamic of the capacitor charge charge can be expressed as in (34), using the *Kirchhoff's Current Law* (KCL), where (31), (32) and (33) are applied. Using vector/matrix notation, the final equation (35) is obtained—refer to appendix A for a detailed derivation.

$$i_a u_a + i_b u_b + i_c u_c = I_T - i_C - i_G \tag{34}$$

$$\dot{q}_c = I_T - [u_{abc}]^T [i_{abc}] - i_G \tag{35}$$

Since the dynamics above are time-variant, for simplicity, a common approach is to use time-invariant equations using Park or *direct-quadrature-zero*) transform, where the *abc* instantaneous voltages and currents are translated into a synchronously rotating framework, and where the direct-axis is linked to the a-phase voltage. This reduces the complexity of the computations and control strategy, allowing the system operator to control the active and reactive components of the current independently; or in other words, d and q axis respectively.

In any case, this transformation is widely known in the context of electrical and control engineering, for this reason why it is not directly included in the work. Yet, for the interested reader, this procedure can be found in appendix A. Finally, the set of equations after applying the transform is presented in (36). Same equations can be written from the point of view of rectifier operation and as a function of inductor's fluxes and capacitor's charges, which can be checked in appendix B.

$$\begin{cases} L\dot{i_d} = -Ri_d + \omega L i_q + u_d v_{dc1} - V_d \\ L\dot{i_q} = -Ri_q - \omega L i_d + u_q v_{dc1} - V_q \\ C\dot{v}_{dc1} = I_T - \dfrac{3}{2}(u_d i_d + u_q i_q) - G v_{dc1} \end{cases} \tag{36}$$

Considering the previous sets of equations, the variables i_d, i_q and v_{dc1} are associated to system state variables ψ_d, ψ_q and q_c respectively through expressions (30) and (31), while u_d and u_q are the control variables. Since the system is defined by three equations with five variables, the system's operator is able to decide the reference values of two of the states variables. In function of which set of state variables have been chosen as reference, the converter is said to be controlled as grid forming or grid feeding operation mode.

On the one hand, the grid forming converters perform in *DC voltage control mode* (also referred as *direct output voltage control*) when the VSC is required to control the reactive power and the DC voltage level. Thus, the terminology *forming* is used because this kind of converters defines the existing voltage of the HVDC grid. From the modelling point of view, the converter's DC side can be modelled along with an ideal DC current source, where the transmission line parameters are not considered. This was observed in figure 7 [49].

On the other hand, grid feeding converters operate in *PQ control mode* (or *direct current control*) when the converter is required to control both active and reactive power. Consequently, the terminology *feeding* is used, as this converters define the currents fed to the AC side. When modelling this converters, the converter's DC side can no longer be modelled as a DC current source. In this case, by contrast, the transmission line parameters are taken into account, after which a grid forming converter is generally found.

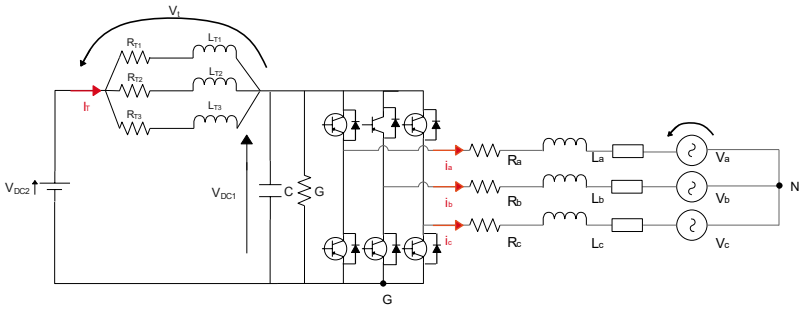

Figure 8: VSC model for grid feeding control strategy.

The most elementary HVDC system would be formed by a transmission line and two converters, each of them adopting one of control strategies. This kind of systems are presumably stable, but the aim of this work is to assure it mathematically, creating precursors for future enhancements. One of the future research lines would include the control strategies that ensure a global stability in multi-terminal systems.

3.1.2 Model description of the HVDC transmission line

A mentioned in chapter 1, traditionally π-representation is the predominant model used for transmission lines. However, in this Thesis the model presented in [6] is used in order to capture the frequency-dependent characteristics of the cable. Moreover, the representation used in [50] is implemented, since in [12] is argued that 3 parallel branches are sufficient to reproduce the frequency dependency of the series impedance of the cable in the frequency range typically considered in studies of control interactions. The model has been schematized and the current references are shown in figure 9.

After applying KVL over the model, the set of equations (37) is obtained, which describe the behaviour of the individual current at each parallel branch.

$$\begin{cases} L_{T1}\dfrac{di_{T1}}{dt} = -R_{T1}i_{T1} + v_{dc2} - v_{dc1} \\ L_{T2}\dfrac{di_{T2}}{dt} = -R_{T2}i_{T2} + v_{dc2} - v_{dc1} \\ L_{T3}\dfrac{di_{T3}}{dt} = -R_{T3}i_{T3} + v_{dc2} - v_{dc1} \end{cases} \tag{37}$$

where R_{Ti} and L_{Ti} are the theoretical resistances and inductances of each branch, and, v_{dc1} and v_{dc2} are both converters' DC voltage respectively. Take into account that the capacitances and conductances represented at both sides of the transmission lines will be added to the converters,

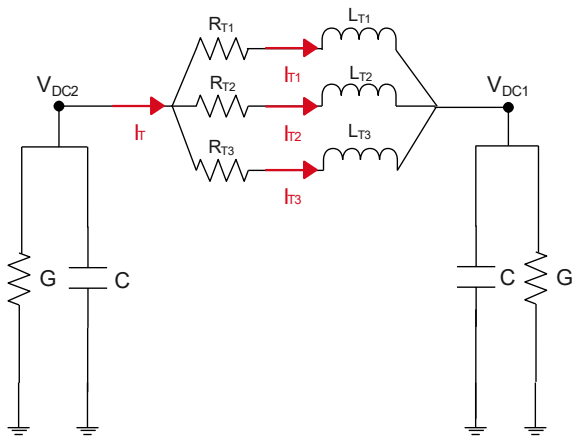

Figure 9: Schematic representation of the FD-Π model.

and thus, the dynamic of capacitances are represented in the model of the VSC. The total current flowing through the line is then obtained from (38).

$$i_T = \sum_{k=1}^{3} i_{Tk} \tag{38}$$

3.2 Port-Hamiltonian Representation

Considering the previously developed sets of equations (36) and (37), VSC and HVDC line models respectively need to be expressed under the port-Hamiltonian formalism, following the general structure for switched power electronic converters given in equation (9). In case of a VSC and HVDC transmission lines, since there are no switchable interconnection with external sources, as mentioned in section 2.2, the system should be written by means of the simplified expression (12).

For the sake of clarity, firstly the VSC representation will be developed in section 3.2.1 and then the HVDC transmission line will be also formulated in port-Hamiltonian form in section 3.2.2.

3.2.1 Port-Hamiltonian representation of 2L-VSC

In order to achieve the port-Hamiltonian representation of a VSC, it is first advisable to express the set of equations (36) in a matrix form.

$$\begin{bmatrix} L & 0 & 0 \\ 0 & L & 0 \\ 0 & 0 & C \end{bmatrix} \begin{bmatrix} \dot{i}_d \\ \dot{i}_q \\ \dot{v}_{dc1} \end{bmatrix} = \underbrace{\begin{bmatrix} -R & \omega L & u_d \\ -\omega L & -R & u_q \\ -\frac{3}{2}u_d & -\frac{3}{2}u_q & -G \end{bmatrix}}_{\mathcal{A}(u)} \begin{bmatrix} i_d \\ i_q \\ v_{dc1} \end{bmatrix} + \begin{bmatrix} -V_d \\ -V_q \\ I_T \end{bmatrix} \tag{39}$$

Analysing this matrix equation, it can be seen the use of amplitude invariant Park transformation lead to having modulation indices u_d and u_q multiplied by a factor of $\frac{3}{2}$ in the third row. This implies that skew-symmetric matrices $\mathcal{J}_1$ and $\mathcal{J}_2$ would not be skew-symmetric. This issue could be solved by applying power-invariant Park transformation instead of the amplitude-invariant one. Nonetheless, in this master thesis the following definitions are introduced to overcome such obstacle.

$$\hat{C} = \frac{2}{3}C \qquad \hat{G} = \frac{2}{3}G$$

$$\hat{I}_T = \frac{2}{3}I_T \qquad \hat{q}_c = \frac{2}{3}q_c$$

Then, equation (39) can be rewritten as the matrix expression (40), where $z = Qx$ and $x \in \mathbb{R}^n = \mathbb{R}^3$ are the state variables of the system shown in (41).

$$\underbrace{\underbrace{\begin{bmatrix} L & 0 & 0 \\ 0 & L & 0 \\ 0 & 0 & \hat{C} \end{bmatrix}}_{Q^{-1}} \underbrace{\begin{bmatrix} \dot{i}_d \\ \dot{i}_q \\ \dot{v}_{dc1} \end{bmatrix}}_{\dot{z}}}_{\dot{x}} = \underbrace{\begin{bmatrix} -R & \omega L & u_d \\ -\omega L & -R & u_q \\ -u_d & -u_q & -\hat{G} \end{bmatrix}}_{\hat{\mathcal{A}}(u)} \underbrace{\begin{bmatrix} i_d \\ i_q \\ v_{dc1} \end{bmatrix}}_{z} + \underbrace{\begin{bmatrix} -V_d \\ -V_q \\ \hat{I}_T \end{bmatrix}}_{E} \tag{40}$$

$$x = \begin{bmatrix} \psi_d \\ \psi_q \\ \hat{q}_c \end{bmatrix} \tag{41}$$

Now, the $\mathcal{A}$ matrix can be divided into four matrices with the aim of obtaining three skew-symmetric matrices $\mathcal{J}_i$ and a dissipation matrix $\mathcal{R}$ as follows:

$$\dot{x} = \left\{ \underbrace{\omega L \begin{bmatrix} 0 & 1 & 0 \\ -1 & 0 & 0 \\ 0 & 0 & 0 \end{bmatrix}}_{\mathcal{J}_0} + u_d \underbrace{\begin{bmatrix} 0 & 0 & 1 \\ 0 & 0 & 0 \\ -1 & 0 & 0 \end{bmatrix}}_{\mathcal{J}_1} + u_q \underbrace{\begin{bmatrix} 0 & 0 & 0 \\ 0 & 0 & 1 \\ 0 & -1 & 0 \end{bmatrix}}_{\mathcal{J}_2} - \underbrace{\begin{bmatrix} R & 0 & 0 \\ 0 & R & 0 \\ 0 & 0 & \hat{G} \end{bmatrix}}_{\mathcal{R}} \right\} Qx + E \tag{42}$$

Note that if the expression (12) is strictly followed, u_d and u_q should be called u_1 and u_2 respectively. Converter's stored energy can be expressed as a scalar function with the form of (11) called Hamiltonian, which is developed as follows:

$$\begin{aligned} \mathcal{H}(x) &= \frac{1}{2}x^\top Qx, \\ &= \begin{bmatrix} \psi_d & \psi_q & \hat{q}_c \end{bmatrix} \begin{bmatrix} \frac{1}{L} & 0 & 0 \\ 0 & \frac{1}{L} & 0 \\ 0 & 0 & \frac{1}{\hat{C}} \end{bmatrix} \begin{bmatrix} \psi_d \\ \psi_q \\ \hat{q}_c \end{bmatrix}, \\ &= \frac{1}{2}\left(\frac{1}{L}\psi_d^2 + \frac{1}{L}\psi_q^2 + \frac{1}{\hat{C}}\hat{q}_c^2 \right), \quad \text{(Applying equations (30)-(31))} \\ &= \frac{1}{2}\left(Li_d^2 + Li_q^2 + \hat{C}v_{dc1}^2 \right). \end{aligned}$$

As can be seen, the scalar function $\mathcal{H}(x)$ clusters the stored energy in both RL filter's inductance and DC-side's capacitance. Likewise, the effort of the energy-storing elements is expressed as the gradient of the Hamiltonian, what is developed as,

$$
\begin{aligned}
\nabla\mathcal{H} &= \begin{bmatrix} \frac{\partial}{\partial\psi_d} \\ \frac{\partial}{\partial\psi_q} \\ \frac{\partial}{\partial\hat{q}_c} \end{bmatrix} \frac{1}{2}\left(\frac{1}{L}\psi_d^2 + \frac{1}{L}\psi_q^2 + \frac{1}{\hat{C}}\hat{q}_c^2\right), \\
&= \begin{bmatrix} \frac{\psi_d}{L} \\ \frac{\psi_q}{L} \\ \frac{\hat{q}_c}{\hat{C}} \end{bmatrix}, \\
&= \begin{bmatrix} \frac{1}{L} & 0 & 0 \\ 0 & \frac{1}{L} & 0 \\ 0 & 0 & \frac{1}{\hat{C}} \end{bmatrix} \begin{bmatrix} \psi_d \\ \psi_q \\ \hat{q}_c \end{bmatrix}, \\
&= Qx.
\end{aligned}
$$

Therefore, it is shown that expression (42) can be written as (43), which has the same form than equation (12).

$$
\dot{x} = \left(\mathcal{J}_0 + u_d\mathcal{J}_1 + u_q\mathcal{J}_2 - \mathcal{R}\right)\nabla\mathcal{H}(x) + E \tag{43}
$$

Take into account that another expression such as nonlinear input-affine form shown in (8) can be derived from this port-Hamiltonian representation,

$$
\dot{x} = f(x) + g(x)u,
$$

where $u \in \mathbb{R}^m = \mathbb{R}^2$ contains u_d and u_q modulation indexes (preserving the direct-quadrature order), with vector field $f(x) : \mathbb{R}^n \to \mathbb{R}^n$ and input matrix $g(x) : \mathbb{R}^m \to \mathbb{R}^n$ given by:

$$
f(x) = \left(\mathcal{J}_0 - \mathcal{R}\right)\nabla\mathcal{H} + E \qquad\qquad g(x) = \begin{bmatrix} \mathcal{J}_1\nabla\mathcal{H} & \mathcal{J}_2\nabla\mathcal{H} \end{bmatrix}
$$

These definitions will be of interest during the 2L-VSC stability analysis later on.

3.2.2 Port-Hamiltonian representation of HVDC transmission line

The HVDC energy transmission line can be also represented as a port-Hamiltonian system. As with the power converter, the first step is to obtain a matrix expression from the set of equation (37). The corresponding formulation is presented below:

$$
\underbrace{\begin{bmatrix} L_{T1} & 0 & 0 \\ 0 & L_{T2} & 0 \\ 0 & 0 & L_{T3} \end{bmatrix}}_{Q_T^{-1}} \underbrace{\begin{bmatrix} \dot{i_{T1}} \\ \dot{i_{T2}} \\ \dot{i_{T3}} \end{bmatrix}}_{\dot{z}_T} = -\underbrace{\begin{bmatrix} R_{T1} & 0 & 0 \\ 0 & R_{T2} & 0 \\ 0 & 0 & R_{T3} \end{bmatrix}}_{\mathcal{R}_T} \underbrace{\begin{bmatrix} i_{T1} \\ i_{T2} \\ i_{T3} \end{bmatrix}}_{z_T} + \underbrace{\begin{bmatrix} V_{dc2} - v_{dc1} \\ V_{dc2} - v_{dc1} \\ V_{dc2} - v_{dc1} \end{bmatrix}}_{E_T} \tag{44}
$$

It can be seen that equation (44) is almost a port-Hamiltonian representation, where $\mathcal{R}_T$ is the dissipation matrix, E_T are the external energy sources, and the state variables of the system $x_T \in \mathbb{R}^3$ are the inductors' fluxes, which are directly related by the property (30) as $z_T = Q_T x_T$.

$$
\begin{bmatrix} \dot{\psi_{T1}} \\ \dot{\psi_{T2}} \\ \dot{\psi_{T3}} \end{bmatrix} = -\begin{bmatrix} R_{T1} & 0 & 0 \\ 0 & R_{T2} & 0 \\ 0 & 0 & R_{T3} \end{bmatrix} \begin{bmatrix} \frac{1}{L_{T1}} & 0 & 0 \\ 0 & \frac{1}{L_{T2}} & 0 \\ 0 & 0 & \frac{1}{L_{T3}} \end{bmatrix} \begin{bmatrix} \psi_{T1} \\ \psi_{T2} \\ \psi_{T3} \end{bmatrix} + \begin{bmatrix} V_{dc2} - v_{dc1} \\ V_{dc2} - v_{dc1} \\ V_{dc2} - v_{dc1} \end{bmatrix}
$$

$$\dot{x}_T = (-\mathcal{R}_T)\, Q_T x_T + E_T \tag{45}$$

The energy storage of the HVDC line is carried out mainly by the inductive behaviour of the cables, since the capacitive effect of the line is modelled along with the DC-side capacitance of the converter, and hence, this storage is considered by the VSC. The Hamiltonian ($\mathcal{H}_T(x)$) of this system is developed from equation (11) as follows:

$$\begin{aligned}
\mathcal{H}_T(x) &= \frac{1}{2} x_T^\top Q_T x_T, \\
&= \begin{bmatrix} \psi_{T1} & \psi_{T2} & \psi_{T3} \end{bmatrix} \begin{bmatrix} \frac{1}{L_{T1}} & 0 & 0 \\ 0 & \frac{1}{L_{T2}} & 0 \\ 0 & 0 & \frac{1}{L_{T3}} \end{bmatrix} \begin{bmatrix} \psi_{T1} \\ \psi_{T2} \\ \psi_{T3} \end{bmatrix}, \\
&= \frac{1}{2} \left(\frac{1}{L_{T1}} \psi_{T1}^2 + \frac{1}{L_{T2}} \psi_{T2}^2 + \frac{1}{L_{T3}} \psi_{T3}^2 \right), \quad \text{(Applying equation (30))}, \\
&= \frac{1}{2} \left(L_{T1} i_{T1}^2 + L_{T2} i_{T2}^2 + L_{T3} i_{T3}^2 \right).
\end{aligned}$$

Hence, the gradient of the Hamiltonian is then developed as,

$$\begin{aligned}
\nabla \mathcal{H}_T &= \begin{bmatrix} \frac{\partial}{\partial \psi_{T1}} \\ \frac{\partial}{\partial \psi_{T2}} \\ \frac{\partial}{\partial \psi_{T3}} \end{bmatrix} \frac{1}{2} \left(\frac{1}{L_{T1}} \psi_{T1}^2 + \frac{1}{L_{T2}} \psi_{T2}^2 + \frac{1}{L_{T3}} \psi_{T3}^2 \right), \\
&= \begin{bmatrix} \frac{\psi_{T1}}{L_{T1}} \\ \frac{\psi_{T2}}{L_{T2}} \\ \frac{\psi_{T3}}{L_{T3}} \end{bmatrix}, \\
&= \begin{bmatrix} \frac{1}{L_{T1}} & 0 & 0 \\ 0 & \frac{1}{L_{T2}} & 0 \\ 0 & 0 & \frac{1}{L_{T3}} \end{bmatrix} \begin{bmatrix} \psi_{T1} \\ \psi_{T2} \\ \psi_{T3} \end{bmatrix}, \\
&= Q_T x_T.
\end{aligned}$$

Thus, replacing the term $Q_T x_T$ by ∇H_T the port-Hamiltonian representation of the HVDC transmission line can be expressed as in equation (46).

$$\dot{x}_T = (-\mathcal{R}_T)\, \nabla H_T + E_T \tag{46}$$

3.3 2L-VSC Open-Loop Stability

Following the reachable stability points mentioned in (4), the particular case for the VSC port-Hamiltonian representation shown in section 3.2.1 is developed. The equilibrium equation states that $g(x)$ is not relevant in the equilibrium whenever the $g^\perp(x)$, the full-rank left annihilator of the input matrix, is properly defined to make the product zero.

This can be achieved when:

$$g^\perp(\bar{x}) := \nabla^\top \mathcal{H}(\bar{x}) \tag{47}$$

and, therefore,

$$g^\perp(\bar{x}) g(\bar{x}) = \begin{bmatrix} \nabla^\top \mathcal{H} \mathcal{J}_1 \nabla \mathcal{H} & \nabla^\top \mathcal{H} \mathcal{J}_2 \nabla \mathcal{H} \end{bmatrix}$$

As the control power represented by $g^{\perp}(\bar{x})g(\bar{x})u$ is zero, $\nabla^{\top}\mathcal{H}(\bar{x})\mathcal{J}_i\nabla\mathcal{H}(\bar{x}) = 0$ considering the skew-symmetry of $\mathcal{J}_i$; the system's power nature can be achieved developing (4), with the full-rank annihilator matrix defined:

$$\begin{aligned} g^{\perp}(\bar{x})f(\bar{x}) &= \nabla^{\top}\mathcal{H}(\bar{x})[(\mathcal{J}_0 - \mathcal{R})\nabla\mathcal{H}(\bar{x}) + E] \\ &= \nabla^{\top}\mathcal{H}(\bar{x})\mathcal{J}_0\nabla\mathcal{H}(\bar{x}) - \nabla^{\top}\mathcal{H}(\bar{x})\mathcal{R}\nabla\mathcal{H}(\bar{x}) + \nabla^{\top}\mathcal{H}(\bar{x})E \\ &= 0 \end{aligned} \tag{48}$$

As before, the skew-symmetry of $\mathcal{J}_0$ makes that term become zero. Consequently, only the terms related to the dissipation and external energy sources matrix remain. Considering $\nabla\mathcal{H}(\bar{x}) = Q\bar{x}$, then $\nabla^{\top}\mathcal{H}(\bar{x}) = \bar{x}^{\top}Q$ as $Q^{\top} = Q$.

$$0 = -\bar{x}^{\top}Q\mathcal{R}\nabla\mathcal{H}(\bar{x}) + \bar{x}^{\top}QE \tag{49}$$

Here two different terms can be distinguished: $-\bar{x}^{\top}Q\mathcal{R}\nabla\mathcal{H}(\bar{x})$ and $\bar{x}^{\top}QE$. Despite appearing in the same equation, both terms will be developed separately due to the different significance of each of them. On the one hand, the former one gives

$$\begin{aligned} -\bar{x}^{\top}Q\mathcal{R}\nabla\mathcal{H}(\bar{x}) &= -\begin{bmatrix}\bar{\psi}_d & \bar{\psi}_q & \bar{\tilde{q}}_c\end{bmatrix}\begin{bmatrix}\frac{1}{L} & 0 & 0\\ 0 & \frac{1}{L} & 0\\ 0 & 0 & \frac{1}{\tilde{C}}\end{bmatrix}\begin{bmatrix}R & 0 & 0\\ 0 & R & 0\\ 0 & 0 & \hat{G}\end{bmatrix}\begin{bmatrix}\frac{1}{L} & 0 & 0\\ 0 & \frac{1}{L} & 0\\ 0 & 0 & \frac{1}{\tilde{C}}\end{bmatrix}\begin{bmatrix}\bar{\psi}_d\\ \bar{\psi}_q\\ \bar{\tilde{q}}_c\end{bmatrix}, \\ &= -\begin{bmatrix}\frac{\bar{\psi}_d}{L} & \frac{\bar{\psi}_q}{L} & \frac{\bar{\tilde{q}}_c}{\tilde{C}}\end{bmatrix}\begin{bmatrix}R & 0 & 0\\ 0 & R & 0\\ 0 & 0 & \hat{G}\end{bmatrix}\begin{bmatrix}\frac{\bar{\psi}_d}{L}\\ \frac{\bar{\psi}_q}{L}\\ \frac{\bar{\tilde{q}}_c}{\tilde{C}}\end{bmatrix}, \\ &= -\left[R(\tfrac{\bar{\psi}_d}{L})^2 + R(\tfrac{\bar{\psi}_q}{L})^2 + \hat{G}(\tfrac{\bar{\tilde{q}}_c}{\tilde{C}})^2\right], \\ &= -\left[R\bar{i}_d^2 + R\bar{i}_q^2 + \hat{G}\bar{v}_{dc1}^2\right], \end{aligned}$$

and, on the other hand, the latter term of the equilibrium equation is developed as,

$$\begin{aligned} \bar{x}^{\top}QE &= \begin{bmatrix}\bar{\psi}_d & \bar{\psi}_q & \bar{\tilde{q}}_c\end{bmatrix}\begin{bmatrix}\frac{1}{L} & 0 & 0\\ 0 & \frac{1}{L} & 0\\ 0 & 0 & \frac{1}{\tilde{C}}\end{bmatrix}\begin{bmatrix}-V_d\\ -V_q\\ \hat{I}_T\end{bmatrix}, \\ &= \begin{bmatrix}\frac{\bar{\psi}_d}{L} & \frac{\bar{\psi}_q}{L} & \frac{\bar{\tilde{q}}_c}{\tilde{C}}\end{bmatrix}\begin{bmatrix}-V_d\\ -V_q\\ \hat{I}_T\end{bmatrix}, \\ &= \left[-V_d\tfrac{\bar{\psi}_d}{L} - V_q\tfrac{\bar{\psi}_q}{L} + \tfrac{\bar{\tilde{q}}_c}{\tilde{C}}\hat{I}_T\right], \\ &= \left[-V_d\bar{i}_d - V_q\bar{i}_d + \bar{v}_{dc1}\hat{I}_T\right]. \end{aligned}$$

Developing both expressions, the former can be identified as the power dissipation in the converter resistances and conductance, while the latter is just the existing difference between 2L-VSC input and output power. Finally, it can be concluded that the converter reaches an equilibrium whenever the input power is equal to the sum of output and dissipated power; this is, no extra effective power is being generated, consumed or dissipated in the system energy storing elements.

Once the equilibrium points are known, the associated input vector can be computed following what was mentioned in (5). For that, it is important to obtain the value of $g^{+}(x)$, the already mentioned Moore-Penrose left pseudoinverse. This can be obtained using the following expression:

$$g^{+}(\bar{x}) = \left(g^{\top}(\bar{x})g(\bar{x})\right)^{-1} g^{\top}(\bar{x})$$

Considering that:

$$\begin{aligned} g(\bar{x}) &= \begin{bmatrix} \mathcal{J}_1\nabla\mathcal{H} & \mathcal{J}_2\nabla\mathcal{H} \end{bmatrix}, \\ &= \left(\begin{bmatrix} 0 & 0 & 1 \\ 0 & 0 & 0 \\ -1 & 0 & 0 \end{bmatrix} \begin{bmatrix} \frac{\bar{\psi}_d}{L} \\ \frac{\bar{\psi}_q}{L} \\ \frac{\bar{q}_c}{\hat{C}} \end{bmatrix} \quad \begin{bmatrix} 0 & 0 & 0 \\ 0 & 0 & 1 \\ 0 & -1 & 0 \end{bmatrix} \begin{bmatrix} \frac{\bar{\psi}_d}{L} \\ \frac{\bar{\psi}_q}{L} \\ \frac{\bar{q}_c}{\hat{C}} \end{bmatrix} \right), \\ &= \left(\begin{bmatrix} \frac{\bar{q}_c}{\hat{C}} \\ 0 \\ -\frac{\bar{\psi}_d}{L} \end{bmatrix} \quad \begin{bmatrix} 0 \\ \frac{\bar{q}_c}{\hat{C}} \\ -\frac{\bar{\psi}_q}{L} \end{bmatrix} \right) = \begin{bmatrix} \frac{\bar{q}_c}{\hat{C}} & 0 \\ 0 & \frac{\bar{q}_c}{\hat{C}} \\ -\frac{\bar{\psi}_d}{L} & -\frac{\bar{\psi}_q}{L} \end{bmatrix}, \end{aligned}$$

and, consequently:

$$g^{\top}(\bar{x}) = \begin{bmatrix} \frac{\bar{q}_c}{\hat{C}} & 0 & -\frac{\bar{\psi}_d}{L} \\ 0 & \frac{\bar{q}_c}{\hat{C}} & -\frac{\bar{\psi}_q}{L} \end{bmatrix} = \begin{bmatrix} \bar{v}_{dc1} & 0 & -\bar{i}_d \\ 0 & \bar{v}_{dc1} & -\bar{i}_q \end{bmatrix}. \tag{50}$$

For the sake of simplicity, the term Υ is defined as follows:

$$\Upsilon := g^{\top}(\bar{x})g(\bar{x}) = \begin{bmatrix} \frac{\bar{q}_c}{\hat{C}} & 0 & -\frac{\bar{\psi}_d}{L} \\ 0 & \frac{\bar{q}_c}{\hat{C}} & -\frac{\bar{\psi}_q}{L} \end{bmatrix} \begin{bmatrix} \frac{\bar{q}_c}{\hat{C}} & 0 \\ 0 & \frac{\bar{q}_c}{\hat{C}} \\ -\frac{\bar{\psi}_d}{L} & -\frac{\bar{\psi}_q}{L} \end{bmatrix} = \begin{bmatrix} (\frac{\bar{q}_c}{\hat{C}})^2 + (\frac{\bar{\psi}_d}{L})^2 & \frac{\bar{\psi}_d\bar{\psi}_q}{L^2} \\ \frac{\bar{\psi}_d\bar{\psi}_q}{L^2} & (\frac{\bar{q}_c}{\hat{C}})^2 + (\frac{\bar{\psi}_q}{L})^2 \end{bmatrix}. \tag{51}$$

Taking into account the inverse Υ^{-1}, defined in (52), is necessary to obtain the left pseudoinverse, $|\Upsilon|$ and $adj(\Upsilon^{\top})$ are the previous stages to the final result. Obtained terms are shown in (53) and (54).

$$\Upsilon^{-1} = \frac{adj(\Upsilon)^{\top}}{|\Upsilon|} \tag{52}$$

where,

$$|\Upsilon| = \begin{vmatrix} (\frac{\bar{q}_c}{\hat{C}})^2 + (\frac{\bar{\psi}_d}{L})^2 & \frac{\bar{\psi}_d\bar{\psi}_q}{L^2} \\ \frac{\bar{\psi}_d\bar{\psi}_q}{L^2} & (\frac{\bar{q}_c}{\hat{C}})^2 + (\frac{\bar{\psi}_q}{L})^2 \end{vmatrix} = \bar{v}_{dc1}^2\left(\bar{v}_{dc1}^2 + \bar{i}_d^2 + \bar{i}_q^2\right), \tag{53}$$

and,

$$adj(\Upsilon^{\top}) = \begin{bmatrix} (\frac{\bar{q}_c}{\hat{C}})^2 + (\frac{\bar{\psi}_q}{L})^2 & -\frac{\bar{\psi}_d\bar{\psi}_q}{L^2} \\ -\frac{\bar{\psi}_d\bar{\psi}_q}{L^2} & (\frac{\bar{q}_c}{\hat{C}})^2 + (\frac{\bar{\psi}_d}{L})^2 \end{bmatrix} = \begin{bmatrix} \bar{v}_{dc1}^2 + \bar{i}_q^2 & -\bar{i}_d\bar{i}_q \\ -\bar{i}_d\bar{i}_q & \bar{v}_{dc1}^2 + \bar{i}_d^2 \end{bmatrix}. \tag{54}$$

Finally, the term of $g^{+}(\bar{x})$ is obtained.

$$\begin{aligned} g^{+}(\bar{x}) &= \left(g^{\top}(\bar{x})g(\bar{x})\right)^{-1} g^{\top}(\bar{x}) \\ &= \frac{1}{\bar{v}_{dc1}^2\left(\bar{v}_{dc1}^2 + \bar{i}_d^2 + \bar{i}_q^2\right)} \begin{bmatrix} \bar{v}_{dc1}^2 + \bar{i}_q^2 & -\bar{i}_d\bar{i}_q \\ -\bar{i}_d\bar{i}_q & \bar{v}_{dc1}^2 + \bar{i}_d^2 \end{bmatrix} \begin{bmatrix} \bar{v}_{dc1} & 0 & -\bar{i}_d \\ 0 & \bar{v}_{dc1} & -\bar{i}_q \end{bmatrix}, \\ &= \frac{1}{\bar{v}_{dc1}^2\left(\bar{v}_{dc1}^2 + \bar{i}_d^2 + \bar{i}_q^2\right)} \begin{bmatrix} \bar{v}_{dc1}\left(\bar{v}_{dc1}^2 + \bar{i}_q^2\right) & -\bar{i}_d\bar{i}_q\bar{v}_{dc1} & -\bar{i}_d\bar{v}_{dc1}^2 \\ -\bar{i}_d\bar{i}_q\bar{v}_{dc1} & \bar{v}_{dc1}\left(\bar{v}_{dc}^2 + \bar{i}_d^2\right) & -\bar{i}_q\bar{v}_{dc1}^2. \end{bmatrix} \end{aligned}$$

Once the pseudo-inverse matrix has been developed, the different input matrix terms, this is, $\bar{u}_d$ and $\bar{u}_q$; can be computed. For that, in equation (55), the matrix $f(x)$ development is obtained.

$$
\begin{aligned}
f(x) &= (\mathcal{J}_0 - \mathcal{R})\nabla\mathcal{H} + E, \\
&= \left\{ \omega L \begin{bmatrix} 0 & 1 & 0 \\ -1 & 0 & 0 \\ 0 & 0 & 0 \end{bmatrix} + \begin{bmatrix} R & 0 & 0 \\ 0 & R & 0 \\ 0 & 0 & \hat{G} \end{bmatrix} \right\} \begin{bmatrix} \frac{1}{L} & 0 & 0 \\ 0 & \frac{1}{L} & 0 \\ 0 & 0 & \frac{1}{\hat{C}} \end{bmatrix} \begin{bmatrix} \psi_d \\ \psi_q \\ \hat{q}_c \end{bmatrix} + \begin{bmatrix} -V_d \\ -V_q \\ \hat{I}_T \end{bmatrix}, \\
&= \begin{bmatrix} \omega L i_q - R i_d - V_d \\ -\omega L i_d - R i_q - V q \\ -\hat{G} v_{dc1} + \hat{I}_T \end{bmatrix}.
\end{aligned} \tag{55}
$$

Knowing the input matrix has $u \in \mathbb{R}^2$, that matrix will have the following terms u_d and u_q in the first and second positions, respectively. Considering that:

$$
\begin{aligned}
\bar{u} &= -g^{+}(\bar{x}) f(\bar{x}) \\
&= -\frac{1}{|\Upsilon|} \begin{bmatrix} \bar{v}_{dc1}\left(\bar{v}_{dc1}^2 + \bar{i}_q^2\right) & -\bar{i}_d \bar{i}_q \bar{v}_{dc1} & -\bar{i}_d \bar{v}_{dc1}^2 \\ -\bar{i}_d \bar{i}_q \bar{v}_{dc1} & \bar{v}_{dc1}\left(\bar{v}_{dc1}^2 + \bar{i}_d^2\right) & -\bar{i}_q \bar{v}_{dc1}^2 \end{bmatrix} \begin{bmatrix} \omega L \bar{i}_q - R \bar{i}_d - V_d \\ -\omega L \bar{i}_d - R \bar{i}_q - V q \\ -\hat{G} \bar{v}_{dc1} + \bar{\hat{I}}_T \end{bmatrix}
\end{aligned} \tag{56}
$$

The input vector terms are finally shown in (57)-(58). However, despite the complete derivation of these terms is trivial for the particular case of a 2L-VSC, for the sake of being didactic it is not presented in this section but attached in appendix A.

$$
\bar{u} = \begin{bmatrix} \bar{u}_d \\ \bar{u}_q \end{bmatrix}
$$

$$
\bar{u}_d = \frac{R \bar{i}_d - \omega L \bar{i}_q + V_d}{\bar{v}_{dc1}} \tag{57}
$$

$$
\bar{u}_q = \frac{R \bar{i}_q + \omega L \bar{i}_d + V_q}{\bar{v}_{dc1}} \tag{58}
$$

In order to ease the performance of the control system, the output Park-transformed voltage is coupled with the d-axis. Therefore, V_q is considered to be zero. The stability of the converter can be proven from a variety of perspectives. In this manuscript two ways are exposed, first, a more intuitive point of view, and then a mathematical interpretation.

1. If the control variables of the set of dynamic equations (36), which represent the converter, are fixed to a constant value, the system becomes an RLC linear system, which is stable.
2. In section 3.4.3 the direct method of Lyapunov is applied to the non-controlled incremental model of the VSC. After concluding that the first, second and fourth Lyapunov conditions are fulfilled, the last issue to prove the stability remains in the Lyapunov function derivative shown in (59). It can be seen if the control variables term u is replace by its open-loop solution $\bar{u}$, the second term is cancelled. Hence, the time-derivative is a negative-definite function, fulfilling the last condition.

$$
\dot{\mathcal{V}}(\tilde{x}) = \underbrace{-\nabla^{\top}\mathcal{H}(\tilde{x})\mathcal{R}\nabla\mathcal{H}(\tilde{x})}_{Dissipations} + y^{\top}(u - \bar{u}). \tag{59}
$$

Nonetheless, the direct application of the input vector to control the system, though stable, results in unacceptable oscillating behaviour caused by the low value of the system eigenvalues associated to the AC resistance and DC conductance, i.e. by the poor natural damping of the converter. This

can be also discerned in equation (59), where if $u = \bar{u}$, the speed of stabilization is just determined by the dissipation term.

Closed loop control is then implemented in order to improve the behaviour of the system. In addition, the lack of reliable accurate knowledge of the system parameters introduces errors to the control variable solution. This fact is widely studied later.

3.4 2L-VSC Stability Certificate

The stability of the VSC is analysed in this section by means of the second method of Lyapunov previously explained in section 2.3. The energy conservation law of a system is, in general, a good starting point for obtaining a Lyapunov function. However, we first start by showing in section 3.4.1 that directly using the VSC stored energy function or Hamiltonian as LCF will not be sufficient. To overcome this obstacle, an incremental model will be developed for the converter in order to be able to obtain a more useful Lyapunov function, in section 3.4.3. Finally, a controller is then designed based on the PBC strategy in section 3.4.4 before obtaining the last stability certification in section 3.4.5.

3.4.1 Lyapunov function for the physical model

The first Lyapunov Candidate Function (LCF) to be analysed is the Hamiltonian of the converter, which represents the stored energy in the system. The VSC will be stable if the LCF is proven to fulfil the four Lyapunov conditions (16)-(19). The proposed Lyapunov function is,

$$\mathcal{V}(x) = \mathcal{H}(x) = \frac{1}{2}\left(\frac{1}{L}\psi_d^2 + \frac{1}{L}\psi_q^2 + \frac{1}{\hat{C}}\hat{q}_c^2\right), \tag{60}$$

which is a positive definite scalar quadratic function. The first-order time-derivative of LCF ($\dot{\mathcal{V}}$) is obtained by means of the chain rule.

$$\begin{aligned}
\dot{\mathcal{V}} &= \frac{d\mathcal{V}(x)}{dt}, \\
&= \frac{d\mathcal{V}(x)}{dt}\frac{dx}{dx}, \\
&= \frac{d\mathcal{V}(x)}{dx}\frac{dx}{dt}, \\
&= \nabla^\top \mathcal{V}(x)\dot{x}, \\
&= \nabla^\top \mathcal{H}(x)\dot{x},
\end{aligned}$$

which can be developed as equation (49) shown in section 3.3, but with the difference that now it is a dynamic equation whilst the former described a specific equilibrium point. So, the LCF is written as in (61).

$$\dot{\mathcal{V}} = -x^\top Q\mathcal{R}\nabla\mathcal{H}(x) + x^\top QE \tag{61}$$

It can be seen that $\mathcal{V}(x)$ reaches its minimum (zero) when the state variables are also zero (i.e. $\dot{\mathcal{V}}(0) = 0$), fulfilling the fourth Lyapunov condition.

However, this LCF is equal zero only if the state variables of the converter are zero. Hence, this function would only prove that the system is stable when the converter is out of operation, which is a trivial result that is not useful in practice. In addition, equation (49) is a sign indefinite function which could take both positive and negative values, and therefore it does not comply with the third Lyapunov function condition.

Therefore, in order to obtain a Lyapunov function based on the energy conservation laws, but whose stability point is not in the origin, the non-linear incremental model in port-Hamiltonian representation of the VSC will be used instead.

3.4.2 Application of the incremental model

The idea behind using an non-linear incremental model is to obtain a Lyapunov function which converges to zero at the desired operating point. This is obtained system variables by the equilibrium point $\bar{x}$, $\bar{u}$ as shown in (62).

$$\begin{aligned} \tilde{x} &= x - \bar{x}, \\ \tilde{u} &= u - \bar{u}, \end{aligned} \tag{62}$$

where, $\tilde{x}$ and $\tilde{u}$ are the incremental state and control variables, respectively. Note that the converter control should provide a real-time open-loop solution of system equilibrium in order to be able to implement the incremental model. It can be proven that the behaviour of the incremental state variables is the same than original state variables.

$$\begin{aligned} \dot{\tilde{x}} &= \frac{d\tilde{x}}{dt}, \\ &= \frac{d}{dt}\left(x - \bar{x}\right), \\ &= \frac{dx}{dt} - \frac{d\bar{x}}{dt}, \\ &= \dot{x} - \dot{\bar{x}}, \quad \text{(The equilibrium point is constant)} \\ &= \dot{x}. \end{aligned} \tag{63}$$

The incremental model is achieved by replacing $\dot{x}$ and $\dot{\tilde{x}}$ in equation (63) by VSC nonlinear input-affine form expressions (64) and (65) respectively.

$$\dot{x} = f(x) + g(x)u = \left(\mathcal{J}_0 - \mathcal{R}\right)\nabla\mathcal{H}(x) + E + g(x)u \tag{64}$$

$$\dot{\tilde{x}} = f(\bar{x}) + g(\bar{x})\bar{u} = \left(\mathcal{J}_0 - \mathcal{R}\right)\nabla\mathcal{H}(\bar{x}) + E + g(\bar{x})\bar{u} \tag{65}$$

Therefore,

$$\begin{aligned} \dot{\tilde{x}} &= \dot{x} - \dot{\tilde{x}}, \\ &= \left(\mathcal{J}_0 - \mathcal{R}\right)\underbrace{\left(\nabla\mathcal{H}(x) - \nabla\mathcal{H}(\bar{x})\right)}_{\text{Term A}} + \underbrace{g(x)u - g(\bar{x})\bar{u}}_{\text{Term B}}. \end{aligned} \tag{66}$$

In appendix C it is proven that the terms A and B of equation (66) can be developed as expressions (67) and (68) respectively.

$$\nabla\mathcal{H}(x) - \nabla\mathcal{H}(\bar{x}) = \nabla\mathcal{H}(\tilde{x}) \tag{67}$$

$$g(x)u - g(\bar{x})\bar{u} = g(x)\tilde{u} + g(\tilde{x})\bar{u} \tag{68}$$

The dynamics of the incremental state variables can then be written as,

$$\dot{\tilde{x}} = (\mathcal{J}_0 - \mathcal{R})\,\nabla\mathcal{H}(\tilde{x}) + g(x)\tilde{u} + g(\tilde{x})\bar{u} \tag{69}$$

where,

$$g(\tilde{x}) = \begin{bmatrix}\mathcal{J}_1\nabla\mathcal{H}(\tilde{x}) & \mathcal{J}_2\nabla\mathcal{H}(\tilde{x})\end{bmatrix},$$

and thus equation (69) can be rewritten in its incremental form as in (70).

$$\dot{\tilde{x}} = (\mathcal{J}_0 + \mathcal{J}_1\bar{u}_d + \mathcal{J}_2\bar{u}_q - \mathcal{R})\,\nabla\mathcal{H}(\tilde{x}) + g(x)\tilde{u} \tag{70}$$

Alternatively, it is also possible to replace the term B of equation (66) by equation (71). In this case, the behaviour of the incremental model could be described by equation (72), which is more convenient for future developments in the converter PI-PBC control analysis.

$$g(x)u - g(\bar{x})\bar{u} = g(\tilde{x})u + g(\bar{x})\tilde{u} \tag{71}$$

$$\dot{\tilde{x}} = (\mathcal{J}_0 + \mathcal{J}_1 u_d + \mathcal{J}_2 u_q - \mathcal{R})\,\nabla\mathcal{H}(\tilde{x}) + g(\bar{x})\tilde{u} \tag{72}$$

Both expressions contain a new energy-like Hamiltonian which is now a function of the incremental state variables. However, now this *virtual* energy does not represent the actual physical energy storage in the system, but can be interpreted instead as some sort of quantification of how far is the system from the equilibrium point of interest. Following the Hamiltonian definition in (11), $\mathcal{H}(\tilde{x})$ can be expressed as in equation (73).

$$\mathcal{H}(\tilde{x}) = \frac{1}{2}\tilde{x}^\top Q\tilde{x} \tag{73}$$

3.4.3 Lyapunov function for the incremental physical model

The Hamiltonian of the new incremental model of the VSC can be now used like a Lyapunov function. As in section 3.4.1, equation (73) will be developed in order to identify if the LCF fulfils the requirements. The time-derivative of the Hamiltonian is also developed to study the last two Lyapunov conditions.

$$\begin{aligned}
\mathcal{V}(\tilde{x}) &= \mathcal{H}(\tilde{x}),\\
&= \frac{1}{2}\tilde{x}^\top Q\tilde{x},\\
&= \frac{1}{2}\begin{bmatrix}\tilde{\psi}_d & \tilde{\psi}_q & \tilde{q}_{dc1}\end{bmatrix}\begin{bmatrix}\frac{1}{L} & 0 & 0\\ 0 & \frac{1}{L} & 0\\ 0 & 0 & \frac{1}{\hat{C}}\end{bmatrix}\begin{bmatrix}\tilde{\psi}_d\\ \tilde{\psi}_q\\ \tilde{q}_{dc1}\end{bmatrix},\\
&= \frac{1}{2}\begin{bmatrix}\tilde{\psi}_d & \tilde{\psi}_q & \tilde{q}_{dc1}\end{bmatrix}\begin{bmatrix}\frac{\tilde{\psi}_d}{L}\\ \frac{\tilde{\psi}_q}{L}\\ \frac{\tilde{q}_{dc1}}{\hat{C}}\end{bmatrix},\\
&= \frac{1}{2}\left(\frac{\tilde{\psi}_d^2}{L} + \frac{\tilde{\psi}_q^2}{L} + \frac{\tilde{q}_{dc1}^2}{\hat{C}}\right).
\end{aligned} \tag{74}$$

It can be easily seen that the function is positive definite, which is zero when the incremental variables of the system are also zero. Thus, now the system fulfils the first two Lyapunov conditions, but in contrast with the original model, the equilibrium is reached when $x = \bar{x}$.

The time-derivative of this *incremental* Hamiltonian is derived by means of the chain rule, introducing equation (70) and taking into account skew-symmetric matrices properties.

$$\begin{aligned}\dot{\mathcal{V}}(\tilde{x}) &= \nabla^\top \mathcal{H}(\tilde{x})\dot{\tilde{x}}, \\ &= \nabla^\top \mathcal{H}(\tilde{x})\left(\mathcal{J}_0 + \mathcal{J}_1\bar{u}_d + \mathcal{J}_2\bar{u}_q - \mathcal{R}\right)\nabla\mathcal{H}(\tilde{x}) + \nabla^\top \mathcal{H}(\tilde{x})g(x)\tilde{u}, \\ &= -\nabla^\top \mathcal{H}(\tilde{x})\mathcal{R}\nabla\mathcal{H}(\tilde{x}) + \nabla^\top \mathcal{H}(\tilde{x})g(x)\tilde{u}. \end{aligned} \tag{75}$$

On the one hand, note that $\nabla^\top \mathcal{H}(\tilde{x}) = \tilde{x}^\top Q$. Hence, when state variables get the desired values, and then the incremental state variables are zero, $\nabla^\top \mathcal{H}(\tilde{x})$ makes zero, fulfilling the fourth Lyapunov condition.

On the other hand, the third condition is satisfied if equation (75) is negative definite. Since the dissipation term is negative semi-definite, it can be said that,

$$\dot{\mathcal{V}}(\tilde{x}) \leqslant \nabla^\top \mathcal{H}(\tilde{x})g(x)\tilde{u}. \tag{76}$$

The term $\nabla^\top \mathcal{H}(\tilde{x})g(x)$ is defined as the passive output of the incremental model ($y^\top$), whose development and interpretation for a VSC is given in appendix A. Since the resultant expression is dependant on the incremental control variables, it allows the design of a PBC which makes the term $y^\top\tilde{u}$ always negative, satisfying the third Lyapunov condition.

$$\dot{\mathcal{V}}(\tilde{x}) \leqslant y^\top\tilde{u} \tag{77}$$

Following the terminology of [28], systems that satisfy expression (77) are referred as (cyclo-)passive systems. In addition, notice that the passive output can be also expressed as follows—refer to appendix C for more details.

$$y = g^\top(\bar{x})\nabla\mathcal{H}(\tilde{x}) \tag{78}$$

3.4.4 PI-Passivity based controller

To control the 2L-VSC, we make use of the PI-PBC; i.e., a proportional-integral controller whose input is the negative value of the passive output of the VCSs, and the controller output is the modulation indices. Figure 10 depicts the block diagram of the PI-PBC.

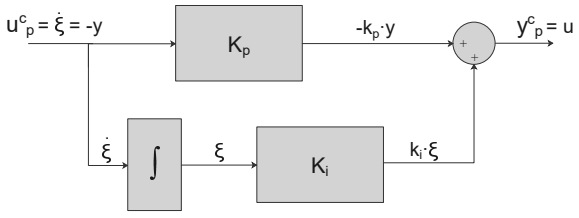

Figure 10: Block-diagram of the proposed PI-PBC.

The control input $u_p^c \in \mathbb{R}^2$ and output $y_p^c \in \mathbb{R}^2$ can be then expressed as the set of equation as follows

$$\begin{cases} u_p^c = \dot{\xi} = -y \\ y_p^c = K_p u_p^c + K_i \xi = u, \end{cases} \tag{79}$$

where $K_p = K_p^\top \in \mathbb{R}^{2\times 2}_{>0}$ and $K_i = K_i^\top \in \mathbb{R}^{2\times 2}_{>0}$ are the proportional and integral (diagonal) constants, respectively, in form of square matrices, and $\xi \in \mathbb{R}^2$ is a column vector containing the virtual state variables of the control. Henceforth, the control input and passive output of the converter will be expressed as u_p^{VSC} and y_p^{VSC} in order to avoid misunderstandings with notation. The sub-index "p" expresses they are the input and output "ports" of the port-Hamiltonian representation.

$$\xi = \begin{bmatrix} \xi_d \\ \xi_q \end{bmatrix} \qquad K_p = \begin{bmatrix} k_p^d & 0 \\ 0 & k_p^q \end{bmatrix} \qquad K_i = \begin{bmatrix} k_i^d & 0 \\ 0 & k_i^q \end{bmatrix}$$

The Lyapunov function which proves the stability of the system must contain all state variables, including recently introduced virtual state variables. However, these new variables do not have to become zero during steady state operation. Hence, an incremental model of the PI-PBC is developed where $\tilde{\xi} = \xi - \bar{\xi}$ are the incremental state variables, $\tilde{u}_p^c = u_p^c - \bar{u}_p^c$ is the incremental input port and $\tilde{y}_p^c = y_p^c - \bar{y}_p^c$ is the incremental output port of the control.

$$\begin{cases} \tilde{u}_p^c = \dot{\tilde{\xi}} = -\tilde{y}_p^{\text{VSC}} \\ K_p \tilde{u}_p^c + K_i \tilde{\xi} = \tilde{u}_p^{\text{VSC}} \end{cases} \tag{80}$$

However, this model can be also interpreted from the energetic point of view as a I-PBC controller, which store virtual energy, and an energy dissipation between the 2L-VSC and the I-PBC represented by the matrix K_p. The I-PBC incremental model is described by the set of equations (81).

$$\begin{cases} \dot{\tilde{\xi}} = \tilde{u}_p^c \\ \tilde{y}_p^c = K_i \tilde{\xi} \end{cases} \tag{81}$$

The Hamiltonian of the control (H_c) is then defined with the form of the expression (11).

$$H_c(\tilde{\xi}) = \frac{1}{2} \tilde{\xi}^\top K_i \tilde{\xi} \tag{82}$$

Take into account that the integrator Hamiltonian does not represent real energy, but a *virtual* energy quantifying how far the control is from its equilibrium point. The gradient of this Hamiltonian is computed as follows.

$$\begin{aligned} \nabla H_c(\tilde{\xi}) &= \begin{bmatrix} \frac{\partial}{\partial \xi_d} \\ \frac{\partial}{\partial \xi_d} \end{bmatrix} H_c(\tilde{\xi}), \\ &= \begin{bmatrix} \frac{\partial}{\partial \xi_d} \\ \frac{\partial}{\partial \xi_d} \end{bmatrix} \left(\frac{1}{2} k_i^d \xi_d^2 + \frac{1}{2} k_i^q \xi_q^2 \right), \\ &= \begin{bmatrix} k_i^d \xi_d \\ k_i^q \xi_q \end{bmatrix}, \\ &= \begin{bmatrix} k_i^d & 0 \\ 0 & k_i^q \end{bmatrix} \begin{bmatrix} \xi_d \\ \xi_q \end{bmatrix}, \\ &= K_i \xi. \end{aligned}$$

Therefore, the dynamic equation of the integrator can be written in the form of port-Hamiltonian representation as in equation (83).

$$\begin{cases} \dot{\tilde{\xi}} = (\mathbf{0}_{2\times 2})\,\nabla H_c(\tilde{\xi}) + \tilde{u}_p^c \\ \tilde{y}_p^c = \nabla H_c(\tilde{\xi}) \end{cases} \tag{83}$$

Comparing it with VSC incremental model in equation (72), a similar structure is observed, but without dissipation (symmetric) nor interconnection (anti-symmetric) components in the structure matrix. As commented in section 2.2, two port-Hamiltonian structures can be combine into a single port-Hamiltonian representation, despite one of them being a virtual system. The relation between both systems inputs and outputs presented in equation (80) can be written in matrix form as in (84), where the missing PI-PBC term K_p has been finally added. From power systems point of view, this interconnection can be depicted in a schematic form as in figure 11.

$$\begin{bmatrix} \tilde{u}_p^{\text{VSC}} \\ \tilde{y}_p^{\text{VSC}} \end{bmatrix} = \begin{bmatrix} -K_p & 1 \\ -1 & 0 \end{bmatrix} \begin{bmatrix} \tilde{u}_p^c \\ \tilde{y}_p^c \end{bmatrix} \tag{84}$$

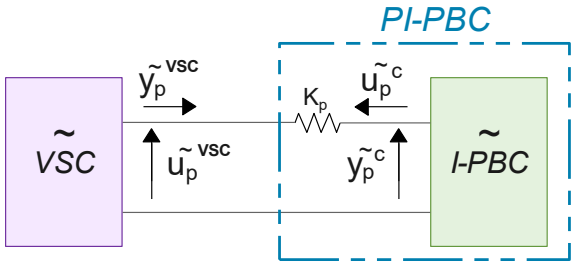

Figure 11: Interconnection between VSC and PI-PBC.

As can be seen, the interconnection matrix has a skew-symmetric part, as well as a symmetric part. This means that the *lossy* interconnection of both system has a *virtual* damping element K_p.

Equation (72) and the first expression of (80) are chosen as the most convenient set of equations to develop the interconnection.

$$\begin{cases} \dot{\tilde{x}} = (\mathcal{J}_0 + \mathcal{J}_1 u_d + \mathcal{J}_2 u_q - \mathcal{R})\,\nabla\mathcal{H}(\tilde{x}) + g(\bar{x})\tilde{u}_p^{\text{VSC}} \\ \dot{\tilde{\xi}} = -\tilde{y}_p^{\text{VSC}} \end{cases}$$

The VSC's passive output definition in (78) and the input vector computed by the control by means of the second expression of (80) are replaced in the set of equations.

$$\begin{cases} \dot{\tilde{x}} = (\mathcal{J}_0 + \mathcal{J}_1 u_d + \mathcal{J}_2 u_q - \mathcal{R})\,\nabla\mathcal{H}(\tilde{x}) + g(\bar{x})\left(-K_p g^\top(\bar{x})\nabla\mathcal{H}(\tilde{x}) + K_i\tilde{\xi}\right) \\ \dot{\tilde{\xi}} = -g^\top(\bar{x})\nabla\mathcal{H}(\tilde{x}) \end{cases}$$

Now, this set of equations can be written in matrix form obtaining a new incremental model of the interconnected port-Hamiltonian system.

$$\underbrace{\begin{bmatrix} \dot{\tilde{x}} \\ \dot{\tilde{\xi}} \end{bmatrix}}_{\dot{\tilde{v}}} = \begin{bmatrix} \dot{\tilde{x}} \\ \dot{\tilde{\xi}} \end{bmatrix} = \begin{bmatrix} \mathcal{J}_0 + \sum_{i=1}^m \mathcal{J}_i u_i - \mathcal{R} - g(\bar{x})K_p g^\top(\bar{x}) & g(\bar{x}) \\ -g^\top(\bar{x}) & 0 \end{bmatrix} \underbrace{\begin{bmatrix} \nabla\mathcal{H}(\tilde{x}) \\ \nabla\mathcal{H}_c(\tilde{\xi}) \end{bmatrix}}_{\nabla\mathcal{H}_v(v)} \tag{85}$$

The Hamiltonian of the interconnected system can be written as in equation (86), where $\tilde{v} \in \mathbb{R}^5$ is the column vector that contains all incremental state variables.

$$\mathcal{H}_v(\tilde{v}) = \frac{1}{2}\tilde{v}^\top \mathcal{Q}\tilde{v}, \qquad \mathcal{Q} = \begin{bmatrix} Q & 0 \\ 0 & K_i \end{bmatrix} \tag{86}$$

3.4.5 Lyapunov function for the physical and the virtual model

The Hamiltonian of the interconnected model of VSC and PI-PBC is used as LCF ($\mathcal{V}(\tilde{v}) = \mathcal{H}_v(\tilde{v})$). This expression is a positive definite quadratic function which contains the five state variables of the incremental model. Hence, the first Lyapunov function is fulfilled. Additionally, the incremental state variables are zero when the system is stabilize, so the second condition is also satisfied. In order to check the third and fourth Lyapunov conditions, the time derivative of the Hamiltonian must be developed.

$$\begin{aligned}
\dot{\mathcal{V}}(\tilde{v}) &= \nabla\mathcal{H}_v^\top \dot{\tilde{v}}, \\
&= \begin{bmatrix} \nabla\mathcal{H}^\top & \nabla\mathcal{H}_c^\top \end{bmatrix} \begin{bmatrix} \mathcal{J}_0 + \mathcal{J}_1 u_d + \mathcal{J}_2 u_q - \mathcal{R} - g(\bar{x})K_p g^\top(\bar{x}) & g(\bar{x}) \\ -g^\top(\bar{x}) & 0 \end{bmatrix} \begin{bmatrix} \nabla\mathcal{H} \\ \nabla\mathcal{H}_c \end{bmatrix}, \\
&= \begin{bmatrix} \nabla\mathcal{H}^\top & \nabla\mathcal{H}_c^\top \end{bmatrix} \begin{bmatrix} \mathcal{J}_0\nabla\mathcal{H} + \mathcal{J}_1\nabla\mathcal{H}u_d + \mathcal{J}_2\nabla\mathcal{H}u_q - \mathcal{R}\nabla\mathcal{H} - g(\bar{x})K_p g^\top(\bar{x})\nabla\mathcal{H} + g(\bar{x})\nabla\mathcal{H}_c \\ -g^\top(\bar{x})\nabla\mathcal{H} \end{bmatrix}, \\
&= \nabla\mathcal{H}^\top\mathcal{J}_0\nabla\mathcal{H} + \nabla\mathcal{H}^\top\mathcal{J}_1\nabla\mathcal{H}u_d + \nabla\mathcal{H}^\top\mathcal{J}_2\nabla\mathcal{H}u_q - \nabla\mathcal{H}^\top\mathcal{R}\nabla\mathcal{H} - \nabla\mathcal{H}^\top g(\bar{x})K_p g^\top(\bar{x})\nabla\mathcal{H} + \\
&\quad + \nabla\mathcal{H}^\top g(\bar{x})\nabla\mathcal{H}_c - \nabla\mathcal{H}_c^\top g^\top(\bar{x})\nabla\mathcal{H}.
\end{aligned}$$

Terms with skew-symmetric matrices will result in zero-matrices, the definition of the VSC passive output of equation (78) is replaced and the last two terms cancel each other as proven in appendix C. The Lyapunov function is then expressed as:

$$\dot{\mathcal{V}}(\tilde{v}) = \underbrace{-\nabla\mathcal{H}^\top\mathcal{R}\nabla\mathcal{H}}_{\text{Dissipations}} - y^\top K_p y \tag{87}$$

Since dissipation term is always negative, it can be stated that,

$$\dot{\mathcal{V}}(\tilde{v}) \leqslant -y^\top K_p y, \tag{88}$$

which is a negative definite quadratic function, and therefore, the third condition of Lyapunov is fulfilled. Additionally, since the converter's passive output is zero during steady state operation, the fourth condition is also satisfied. This statement is argued in appendix A.

Thus, a Lyapunov function has been obtained which demonstrates the stability of the system composed by the converter along with the PI-PBC. However, the incremental model requires the open-loop solution of the system, which cannot be accurately calculated as the system parameters are not exactly known. The Immersion & Invariance method will be applied in order to estimate the real values of those needed parameters in the next section.

4 DESIGN OF THE PARAMETERS ESTIMATORS

As reported in previous sections, the PBC strategy is based on knowledge of the desired equilibrium point of the system. However, if the different parameters are not accurately known, this point cannot be computed precisely.

The main contribution of this master's thesis is to use the I&I methodology in order to design an adaptive control based on the physical model, which estimates the value of any variable or parameter in the system. In case of a VSC, both the linkage resistance between the converter and the grid (R) and the conductance that represents the active power losses in the DC-side of the converter (G) are unknown and this uncertainty will have a negative influence in the load flow solution. Therefore, the estimation of these two parameters is the final aim of this section. In case of system inductance and capacitance, they do not affect the power-balance of the converter, and thus, the computation of the state variables associated with the desired equilibrium point does not require these parameters.

In a similar fashion to chapter 3, the structure of this section has been designed in order to be as didactic as possible. Five different estimators have been designed, trying to estimate different parameters and gradually learning from each of their shortcomings, which where subsequently taken into account to improve the next design. For the readers that are exclusively interested in the final design, we refer them to go directly to 4.5.

This section in organized as follows. First, the DC-side current (I_T) is estimated for a grid forming VSC with an HVDC line modelled as a current source. This first attempt is considered the easiest, as there is nothing multiplying I_T and since just a single dynamic equation will be used. Second, the conductance will be traced by means of a single equation estimator. However, it is important to consider that in this equation G is multiplied by the DC-side voltage. Third, an attempt to estimate the previous two parameters using just one equation will be made. Then, the linkage resistance will be tracked both with one and two dynamic equations. Finally, an estimator is designed to track both R and G based on the set of equations (36).

4.1 Single Estimation of I_T

In this first attempt, the I&I strategy is used with the aim of estimating the DC current of a VSC (I_T). The estimator is based on one of the dynamic equations of the 2L-VSC model; more precisely, the dynamic of the DC capacitance.

$$\dot{q}_c = I_T - \frac{3}{2}\left(u_d i_d + u_q i_q\right) - G v_{dc1}$$

The estimation of the DC current (I_T^E) and the error between real value and estimation (e_{I_T}) will be defined as in Equations (89) and (90) respectively.

$$I_T^E \triangleq \beta(x) + \gamma \tag{89}$$

$$e_{I_T} \triangleq I_T^E - I_T \tag{90}$$

Where $\beta(x)$ is as a function of one or more state variables depending on the equations used, and the update law (γ) will be defined in order to render the error dynamics attractive; e.g., by removing the less interesting terms. Introducing (89) into the time-derivative of (90), the error dynamic is obtained.

$$
\begin{aligned}
\dot{e}_{I_T} &= \dot{I}_T^E - \dot{I}_T, \quad (\dot{I}_T = 0) \\
&= \dot{I}_T^E, \\
&= \dot{\beta}(x) + \dot{\gamma}, \quad \text{(Applying the chain rule)} \\
&= \underbrace{\frac{\partial \beta(x)}{\partial x}}_{\beta'(x)} \dot{x} + \dot{\gamma}, \\
&= \beta'(x)\dot{x} + \dot{\gamma}.
\end{aligned}
$$

As mentioned before, the adaptive control is based on the dynamic equation of the capacitor charge, which is a state variable of the system. In order to introduce this equation in the error dynamic, β will depend on this charge ($\beta(x) = \beta(q_c)$), and therefore,

$$
\begin{aligned}
\dot{e}_{I_T} &= \beta'(q_c)\dot{q}_c + \dot{\gamma}, \\
&= \beta'(q_c)\left(I_T - \frac{3}{2}\left(u_d i_d + u_q i_q\right) - G v_{dc1}\right) + \dot{\gamma}, \quad \text{(Introducing Equations 89-90)} \\
&= \beta'(q_c)\left(\beta(q_c) + \gamma - e_{I_T} - \frac{3}{2}\left(u_d i_d + u_q i_q\right) - G v_{dc1}\right) + \dot{\gamma}.
\end{aligned}
$$

The derivative of the update law ($\dot{\gamma}$) will be defined in order to have an error dynamic with just the term that contains the error. Towards this end, we select

$$
\begin{aligned}
\dot{\gamma} &= -\beta'(q_c)\left(\beta(q_c) + \gamma - \frac{3}{2}\left(u_d i_d + u_q i_q\right) - G v_{dc1}\right), \\
&= -\beta'(q_c)\left(I_T^E - \frac{3}{2}\left(u_d i_d + u_q i_q\right) - G v_{dc1}\right).
\end{aligned} \tag{91}
$$

So the error dynamic can be express as equation (92).

$$
\dot{e}_{I_T} = -\beta'(q_c) e_{I_T} \tag{92}
$$

The design of this estimator will be over with the definition of $\beta(q_c)$. This is chosen with the aim of ensuring convergence of the estimation error to zero. For the sake of completeness two different methods are used, the first by means of the second method of Lyapunov and the second by transforming the first-order derivative equation to an expression that fulfills the desired behaviour; both leading to the same exact result.

4.1.1 Definition of $\beta(q_c)$ from Lyapunov function

A new Lyapunov function can be defined as a function of the estimation error. Equation (93) is proposed as a possible function, where the error is zero when the stability is reached ($\bar{e}_{I_T} = 0$).

$$
\mathcal{V}(e_{I_T}) = \frac{1}{2} e_{I_T}^2 \tag{93}
$$

The time derivative of the Lyapunov function is shown in equation (94).

$$
\dot{\mathcal{V}}(e_{I_T}) = e_{I_T}\dot{e}_{I_T} = -\beta'(q_c) e_{I_T}^2 \tag{94}
$$

It can be proven that this Lyapunov function fulfills the four Lyapunov conditions if $\beta'(q_c) = \lambda \in \mathbb{R}_{>0}$. Consequently, $\beta(q_c)$ is defined as in equation (95).

$$\beta'(q_c) = \frac{\partial \beta(q_c)}{\partial q_c} = \lambda$$

$$\int \partial \beta(q_c) = \int \lambda \, \partial q_c$$

$$\beta(q_c) = \lambda q_c = \lambda C v_{dc1} \tag{95}$$

- $\mathcal{V}(e_{I_T}) \geqslant 0$
- $\mathcal{V}(\bar{e}_{I_T}) = 0$
- $\dot{\mathcal{V}}(e_{I_T}) \leqslant 0$
- $\dot{\mathcal{V}}(\bar{e}_{I_T}) = 0$

Then, error behaviour can be written as follows.

$$\dot{e}_{I_T} = -\lambda e_{I_T} \longrightarrow e_{I_T}(t) = e^{-\lambda t}$$

Thus, λ can be seen as the rate of convergence of the error dynamics.

4.1.2 Definition of $\beta(q_c)$ from the desired behaviour

In this method, the desired solution of the estimation error dynamic is defined beforehand. It consists of a negative exponential function that tends to zero as shown as follow.

$$\dot{x} = -\tau x \longrightarrow x(t) = e^{-\tau t}$$

In this way, $\beta'(q_c)$ can be directly derived from equation (92).

$$\dot{e}_{I_T} = -\beta'(q_c) e_{I_T} = -\lambda e_{I_T}$$

Where $\lambda \in \mathbb{R}_{>0}$. Thus, the error will stabilize at zero after a period defined by λ, and $\beta(q_c)$ is expressed as in equation (95).

Even though the result obtained is the same for both cases, the use of Lyapunov function is of great interest for the system equilibrium certificate.

4.2 Single Estimation of G

The dynamic equation referred to the capacitor charge also includes the conductance parameter. This is commonly related to capacitors and switches non-ideal behaviour, which means this is not a real resistance in the system. Furthermore, the model capacitance would vary depending on the interconnection point between the HVDC line and the power converter. Due to this nature, the estimation of this parameter is crucial.

As done previously with the current estimator, the estimation of G and the error between the real value and the estimation (e_G) will be defined in equations (96) and (97) respectively.

$$G^E \triangleq \beta(x) + \gamma \tag{96}$$

$$e_G \triangleq G^E - G \tag{97}$$

Again, the self-defined parameter $\beta(x)$ will be dependant on the capacitor's charge state variable ($\beta(q_c)$), while γ will seek the linearization of the error dynamic.

Considering what was developed previously in section 4.1, the dynamics of the error estimation then reads

$$\begin{aligned}
\dot{e}_G &= \dot{G}^E - \dot{G}, \quad (\dot{G} = 0) \\
&= \dot{G}^E, \\
&= \dot{\beta}(q_c) + \dot{\gamma}, \quad \text{(Applying the chain rule)} \\
&= \underbrace{\frac{\partial \beta(q_c)}{\partial q_c}}_{\beta'(q_c)} \dot{q_c} + \dot{\gamma}, \\
&= \beta'(q_c)\dot{q_c} + \dot{\gamma}, \\
&= \beta'(q_c)\left(I_T - \frac{3}{2}\left(u_d i_d + u_q i_q\right) - G v_{DC1}\right) + \dot{\gamma}, \\
&= \beta'(q_c)\left(I_T - \frac{3}{2}\left(u_d i_d + u_q i_q\right) - (G^E - e_G) v_{DC1}\right) + \dot{\gamma}.
\end{aligned}$$

The dynamic expression of the update law will be defined in order to have an error dynamics with just the term that contains the error.

$$\dot{\gamma} = -\beta'(q_c)\left(I_T - \frac{3}{2}\left(u_d i_d + u_q i_q\right) - G^E v_{DC1}\right) \tag{98}$$

The error dynamics is then expressed as in equation (99), which is not only dependant on $\beta'(q_c)$, but also on v_{DC1}. This implies a non-linear behaviour with one of the system's state variables, since the DC voltage will act as a non-constant disturbance.

$$\dot{e}_{I_T} = \beta'(q_c) v_{DC1} e_G \tag{99}$$

In order to make this estimator stable two different definitions of $\beta(q_c)$ are given in the following subsections, one based on linearizing the error's dynamics and the second seeking another way to make the system stable from the point of view of Lyapunov second method.

4.2.1 Linearized G estimator from $\dot{q}_c$

As a first strategy, non-linear dynamics can be avoided defining a $\beta'(q_c)$ so that v_{DC1} term is cancelled. Therefore, $\beta'(q_c)$ must contain the state variable q_c in the denominator as shown as follows.

$$\beta'(q_c) = \frac{\partial \beta(q_c)}{\partial q_c} = -\frac{\lambda}{v_{DC1}} = -\frac{\lambda C}{q_c} \tag{100}$$

$$\beta(q_c) = -\lambda C \ln(q_c) \tag{101}$$

The stability of the system will be proven by means of a Lyapunov method. A possible function is shown in (102). First order derivative of this Lyapunov function is developed in equation (103).

$$\mathcal{V}(e_G) = \frac{1}{2} e_G^2 \tag{102}$$

$$\dot{\mathcal{V}}(e_G) = e_G \dot{e}_G = \beta'(q_c) v_{dc1} e_G^2 = \beta'(q_c) \frac{q_c}{C} e_G^2 \tag{103}$$

When this new definition is considered, the Lyapunov derivative is no longer v_{DC1} dependant.

$$\dot{\mathcal{V}}(e_G) = -\lambda \frac{C}{q_c} \frac{q_c}{C} e_G^2 = -\lambda e_G^2 \tag{104}$$

Finally, it can be proved that using this linearized method the error dynamic fulfills all the Lyapunov properties and makes the system *asymptotically stable*. However, some major drawbacks can be observed when using this topology. The main problem would appear whenever the HVDC line is initialized, as the capacitors charge is close zero value. Since $\beta(q_c)$ term includes a natural logarithm, this could lead to problems in the proper functioning of the system. Another issue is identified in equation (100). When the measurement of DC voltage was close to zero, the control would tend to infinity.

4.2.2 Non-linearized G estimator from $\dot{q}_c$

With the aim of avoiding the previously commented issues, the parameters β and, consequently β', are defined so that the non-linearity of the dynamic is not removed, but the Lyapunov function still fulfills the conditions.

$$\beta'(q_c) = \frac{\partial \beta(q_c)}{\partial q_c} = -\lambda \frac{q_c}{C} = -\lambda v_{dc1} \tag{105}$$

$$\beta(q_c) = -\frac{\lambda}{2} \frac{{q_c}^2}{C} = -\lambda C v_{dc1}^2 \tag{106}$$

Taking equation (102) as Lyapunov function again, the time-derivative is developed as follow.

$$\dot{\mathcal{V}}(e_G) = e_G \dot{e}_G = \beta'(q_c) e_G^2 \frac{q_c}{C} = -\lambda \frac{q_c}{C} e_G^2 \frac{q_c}{C} = -\lambda (e_G v_{dc1})^2 \tag{107}$$

In equation (107) can be seen that the fact of introducing DC-side voltage into $\beta'(qc)$ makes $\dot{\mathcal{V}}(e_G)$ negative semi-definite along the trajectory, what means the system will be asymptotically stable without the risk of introducing an infinite value into the control.

4.3 Combined Estimation of I_T and G

Once the estimator for a single variable is designed and implemented, the following case unifies both of them into a single estimation. The aim of this section is to estimate I_T and G parameters by means of the DC-side voltage dynamics.

Towards this end, a matrix structure is adopted. Consequently, the following matrices definitions are introduced. The new matrices $e \in \mathbb{R}^2$, $S \in \mathbb{R}^2$ and $R_S \in \mathbb{R}^2$ represent the error, the estimation and real values matrices, respectively.

$$e = \begin{bmatrix} e_{I_T} \\ e_G \end{bmatrix} \qquad S = \begin{bmatrix} I_T^E \\ G^E \end{bmatrix} \qquad R_S = \begin{bmatrix} I_T \\ G \end{bmatrix} \tag{108}$$

The relationship between these matrices is the same as in previous attempts, where the error is the existing difference between the estimated value and the real one.

$$e \triangleq S - R_S \tag{109}$$

In the same way, the estimation matrix is defined in (110) by means of the matrices $\beta(x) = \beta(q_c) \in \mathbb{R}^2$ and $\gamma \in \mathbb{R}^2$, which are shown in (111).

$$S \triangleq \beta(x) + \gamma \tag{110}$$

$$\beta(x) = \begin{bmatrix} \beta_{I_T}(q_c) \\ \beta_G(q_c) \end{bmatrix} \qquad \gamma = \begin{bmatrix} \gamma_{I_T} \\ \gamma_G \end{bmatrix} \tag{111}$$

Once all the required definitions have been introduced, the first-order time derivative of the error will be computed.

$$\begin{aligned} \dot{e} &= \dot{S} + \dot{R}_S \quad (\dot{R}_S = 0), \\ &= \dot{S}, \\ &= \dot{\beta}(x) + \dot{\gamma}, \quad \text{(Applying the chain rule)} \\ &= \underbrace{\frac{\partial \beta(x)}{\partial x}}_{\beta'(x)} \dot{x} + \dot{\gamma}, \\ &= \beta'(x)\dot{x} + \dot{\gamma}, \end{aligned}$$

where,

$$\beta'(x) = \beta'(q_c) = \frac{\partial}{\partial x} \begin{bmatrix} \beta_{I_T}(q_c) \\ \beta_G(q_c) \end{bmatrix} = \begin{bmatrix} \beta'_{I_T}(q_c) \\ \beta'_G(q_c) \end{bmatrix}.$$

It is worth mentioning that each term of error dynamics will be written in matrix form.

$$\begin{aligned} \dot{e} &= \beta'(q_c)\dot{q}_c + \dot{\gamma}, \\ &= \begin{bmatrix} \beta'_{I_T} \\ \beta'_G \end{bmatrix} \left(I_T - \frac{3}{2}\left(u_d i_d + u_q i_q\right) - G v_{DC1} \right) + \begin{bmatrix} \gamma_{I_T} \\ \gamma_G \end{bmatrix}, \\ &= \begin{bmatrix} \beta'_{I_T} \\ \beta'_G \end{bmatrix} \left(\left(I_T^E - e_{I_T}\right) - \frac{3}{2}\left(u_d i_d + u_q i_q\right) - \left(G^E - e_G\right) v_{DC1} \right) + \begin{bmatrix} \gamma_{I_T} \\ \gamma_G \end{bmatrix}. \end{aligned}$$

Then, $\dot{\gamma}$ is defined as equation (112) in order to simplify the error expression to equation (113).

$$\dot{\gamma} = \begin{bmatrix} \gamma_{I_T} \\ \gamma_G \end{bmatrix} = -\beta'(q_c) \left(I_T^E - \frac{3}{2}\left(u_d i_d + u_q i_q\right) - G^E v_{DC1} \right) \tag{112}$$

$$\dot{e} = \begin{bmatrix} e_{I_T} \\ e_G \end{bmatrix} = \begin{bmatrix} \beta'_{I_T} \\ \beta'_G \end{bmatrix} (-e_{I_T} + e_G v_{DC1}) = \begin{bmatrix} \beta'_{I_T} \ (-e_{I_T} + e_G v_{DC1}) \\ \beta'_G \ (-e_{I_T} + e_G v_{DC1}) \end{bmatrix} \tag{113}$$

However, it can be deduced from (113) that the estimator will not be stabilized in the desired equilibrium point, but there are infinite possible equilibria. In can be also concluded that once the errors are constant values, they are going to be related by equation (114).

$$\begin{aligned} 0 &= \begin{bmatrix} \beta'_{I_T} \\ \beta'_G \end{bmatrix} (-e_{I_T} + e_G v_{dc1}) \\ 0 &= (-e_{I_T} + e_G v_{dc1}) \longrightarrow e_{I_T} = v_{dc1} e_G \end{aligned} \tag{114}$$

Hence, it has not been possible to achieve the correct performance of a dual-parameter estimator with a single equation. Future work could solve the identified issues in this section by means of the Schur's component, so as to identify conditions when and how the estimator can operate satisfactorily.

4.4 Single Estimation of R

The coupling resistance between VSC and grid is also necessary for the load flow. A different estimator will be designed with the objective of obtaining the best solution.

In contrast with previous attempts, this resistance appears in the first two dynamic equations of the set (36). Thus, firstly two independent estimator will be designed by means of a single dynamic equation (direct and quadrature flux respectively) and, then, both equations will be used for a complete estimator.

4.4.1 R estimator from inductance direct flux ($\dot{\psi}_d$)

This first estimator is based on the dynamic equation of inductance's direct flux:

$$\dot{\psi}_d = -Ri_d + \omega L i_q + u_d v_{dc1} - V_d.$$

As in previous attempts, two variables are defined: the estimation of the resistance ($R^E \in \mathbb{R}$) and the error ($e_R \in \mathbb{R}$).

$$R^E \triangleq \beta(x) + \gamma \tag{115}$$

$$e_R \triangleq R^E - R \tag{116}$$

Where R is the real, constant and accurately unknown resistance. The dynamic of this error can be developed as:

$$
\begin{aligned}
\dot{e}_R &= \dot{R}^E - \dot{R} \quad (\dot{R} = 0), \\
&= \dot{R}^E, \\
&= \dot{\beta}(x) + \dot{\gamma}, \quad \text{(Applying the chain rule)} \\
&= \underbrace{\frac{\partial \beta(x)}{\partial x}}_{\beta'(x)} \dot{x} + \dot{\gamma}, \\
&= \beta'(x)\dot{x} + \dot{\gamma}.
\end{aligned}
$$

In order to introduce the flux dynamic in the estimator, $\beta(x) = \beta(\psi_d)$.

$$
\begin{aligned}
\dot{e}_R &= \beta'(\psi_d)\dot{\psi}_d + \dot{\gamma}, \\
&= \beta'(\psi_d)\left(-Ri_d + \omega L i_q + u_d v_{dc1} - V_d\right) + \dot{\gamma}, \\
&= \beta'(\psi_d)\left(-(R^E - e_R)i_d + \omega L i_q + u_d v_{dc1} - V_d\right) + \dot{\gamma}.
\end{aligned}
$$

Once again, the derivative of γ will be defined in order to have an error dynamics with just the error term and, in this case, also i_d multiplying the error.

$$
\dot{\gamma} = -\beta'(\psi_d)\left(-R^E i_d + \omega L i_q + u_d v_{dc1} - V_d\right)
$$

The error dynamic is now:

$$
\dot{e}_R = \beta'(\psi_d) i_d e_R. \tag{117}
$$

In order to specify $\beta'(\psi_d)$ and, therefore, $\beta(\psi_d)$; the second method of Lyapunov will be used to obtain a stable estimator, where the equilibrium point is reached whenever the error is made zero. The chosen Lyapunov function is shown as follows.

$$
\mathcal{V}(e_R) = \frac{1}{2} e_R^2 \tag{118}
$$

The time derivative of the Lyapunov function is developed in equation (119).

$$
\dot{\mathcal{V}}(e_R) = e_R \dot{e}_R = \beta'(\psi_d) i_d e_R^2 \tag{119}
$$

It can be proven that this Lyapunov function fulfills the four conditions if $\beta'(\psi_d) = -\lambda i_d, \lambda \in \mathbb{R}_{>0}$. Therefore, $\beta(\psi_d)$ is defined as in equation (120).

$$
\beta(\psi_d) = -\frac{1}{2L}\lambda \psi_d^2 = -\frac{1}{2}\lambda L i_d^2 \tag{120}
$$

And, then, the error with respect to time will be:

$$
\dot{e}_R = -\lambda i_d^2 e_R \longrightarrow e_R(t) = e^{-\lambda i_d^2 t}. \tag{121}
$$

4.4.2 R estimator from inductance quadrature flux ($\dot{\psi}_q$)

In this case, the estimator is based on the dynamic equation of inductance's quadrature flux:

$$\dot{\psi}_q = -Ri_q - \omega L i_d + u_q v_{dc1} - V_q.$$

Again, the estimation of the resistance ($R^E \in \mathbb{R}$) and the error ($e_R \in \mathbb{R}$) are defined.

$$R^E \triangleq \beta(x) + \gamma$$

$$e_R \triangleq R^E - R$$

After developing the error dynamic as in section 4.4.1, $\beta(x)$ has been defined as a function of quadrature flux so that the VSC's dynamic equation can be introduced into the error's behaviour.

$$\begin{aligned}
\dot{e}_R &= \beta'(x)\dot{x} + \dot{\gamma}, \\
&= \beta'(\psi_q)\dot{\psi}_q + \dot{\gamma}, \\
&= \beta'(\psi_q)\left(-Ri_q - \omega L i_d + u_q v_{dc1} - V_q\right) + \dot{\gamma}, \\
&= \dot{e}_R = \beta'(\psi_q)\left(-(R^E - e_R)i_q - \omega L i_d + u_q v_{dc1} - V_q\right) + \dot{\gamma}.
\end{aligned}$$

The derivative of γ ($\dot{\gamma}$) will be defined in order to have an error dynamic with just the error term and, in this case, also i_q multiplying the error.

$$\dot{\gamma} = -\beta'(\psi_q)\left(-R^E i_q - \omega L i_d + u_q v_{dc1} - V_q\right)$$

The error dynamic is now:

$$\dot{e}_R = \beta'(\psi_q) i_q e_R. \tag{122}$$

In order to design $\beta'(\psi_q)$ and, therefore $\beta(\psi_q)$; the second method of Lyapunov will be used again, choosing equation (123) as Lyapunov function.

$$\mathcal{V}(e_R) = \frac{1}{2}e_R^2 \tag{123}$$

The time derivative of the Lyapunov function is developed in equation (124).

$$\dot{\mathcal{V}}(e_R) = e_R \dot{e}_R = \beta'(\psi_q) i_q e_R^2 \tag{124}$$

It can be proven that this Lyapunov function fulfills the four conditions if $\beta'(\psi_q) = -\lambda i_q, \lambda \in \mathbb{R}_{>0}$. Therefore, $\beta(\psi_q)$ is defined as in equation (125).

$$\beta(\psi_q) = -\frac{1}{2L}\lambda\psi_q^2 = -\frac{1}{2}\lambda L i_q^2 \tag{125}$$

And then the error behaviour will be:

$$\dot{e}_R = -\lambda i_q^2 e_R \longrightarrow e_R(t) = e^{-\lambda i_q^2 t}. \tag{126}$$

As in the estimator for the conductance (G) with the DC side voltage, the error dynamics is disturbed by the behaviour of the AC direct or quadrature current depending the VSC dynamic equation used in the design. At the same time, the non-accurate knowledge of the inductance value would introduce an error in $\beta(\psi_q)$, and consequentially would disturb the estimation and, thus, the convergence to zero of the error.

Looking at equation (126), it can be seen that the estimator could not take the error to zero if the inductor quadrature current was zero. Note that if i_q has an arbitrary value and the reference of i_q goes to zero, the estimator should estimate the resistance before reaching the equilibrium point, which is not practical. Hence, the estimator based on quadrature flux dynamic works just if the q-current is not zero. Same issue occurs using the direct flux dynamic equations (see Equation (121)), but in this case with the d-current.

After this analysis, the first idea was to use both estimators individually, switching the used estimated resistances in case of having one of the currents at zero. However, in contrast with the DC conductance estimator, the dynamic equation of the update law contains the value of the inductance. As the known value of L is approximated, this error pollutes γ, generating a deviation in the final value of the estimated R.

In case of the first R-estimator, L is multiplied by i_q. So if the VSC was controlled only to inject or absorb active power from the grid, the quadrature current would go to zero, removing the error in γ. On the other hand, the second estimator is multiplied by i_d. Hence, the estimator would work if only reactive power is being transfered.

Therefore, the theoretical estimator based on using both equations individually would work only if one of the components of the current goes to zero or, in other words, if the VSC generates only active or reactive power.

In order to overcome this limitation, an estimator based on both direct and quadratic flux dynamics at the same time will be designed.

4.4.3 R estimator from the inductance direct and quadrature fluxes together

This estimator will be based on the dynamics of the two state variables where the resistance appears; i.e, in the dynamics of both direct and quadrature flux linkages (equation (127)).

$$\dot{x} = \begin{bmatrix} \dot{\psi}_d \\ \dot{\psi}_q \end{bmatrix} = \begin{bmatrix} -Ri_d + \omega L i_q + u_d v_{dc1} - V_d \\ -Ri_q - \omega L i_d + u_q v_{dc1} - V_q \end{bmatrix} \tag{127}$$

As in previous estimators, the estimated resistance $R^E \in \mathbb{R}$ and the error of this estimator $e_R \in \mathbb{R}$ are defined; where R is the real, constant and non-accurately known resistance.

$$R^E \triangleq \beta(x) + \gamma \tag{128}$$

$$e_R \triangleq R^E - R \tag{129}$$

The dynamics of the error can be also derived as in the previous cases.

$$\dot{e}_R = \beta'(x)\dot{x} + \dot{\gamma}$$

However, since $\dot{x} \in \mathbb{R}^{2\times 1}$, and as $\beta(x)$ must depend on both fluxes ($\beta(x) = \beta(\psi_d, \psi_q)$), $\beta'(x) = \beta'(\psi_d, \psi_q) \in \mathbb{R}^{1\times 2}$, as can be seen in equation 130.

$$\beta'(\psi_d, \psi_q) = \begin{bmatrix} \frac{\partial \beta(\psi_d, \psi_q)}{\partial \psi_d} & \frac{\partial \beta(\psi_d, \psi_q)}{\partial \psi_q} \end{bmatrix} \tag{130}$$

So the estimator's error dynamics should be,

$$\begin{aligned}
\dot{e}_R &= \beta'(\psi_d,\psi_q)\dot{x}+\dot{\gamma},\\
&= \beta'(\psi_d,\psi_q)\begin{bmatrix}-Ri_d+\omega Li_q+u_dv_{dc1}-V_d\\-Ri_q-\omega Li_d+u_qv_{dc1}-V_q\end{bmatrix}+\dot{\gamma},\\
&= \beta'(\psi_d,\psi_q)\begin{bmatrix}-(R^E-e_R)i_d+\omega Li_q+u_dv_{dc1}-V_d\\-(R^E-e_R)i_q-\omega Li_d+u_qv_{dc1}-V_q\end{bmatrix}+\dot{\gamma},\\
&= \beta'(\psi_d,\psi_q)\begin{bmatrix}e_Ri_d-R^Ei_d+\omega Li_q+u_dv_{dc1}-V_d\\e_Ri_q-R^Ei_q-\omega Li_d+u_qv_{dc1}-V_q\end{bmatrix}+\dot{\gamma}.
\end{aligned}$$

To simplify the notation, two new matrices have been defined.

$$I=\begin{bmatrix}i_d\\i_q\end{bmatrix}\qquad\qquad T=\begin{bmatrix}\omega Li_q+u_dv_{dc1}-V_d\\-\omega Li_d+u_qv_{dc1}-V_q\end{bmatrix}$$

Now the error dynamics can be written as,

$$\dot{e}_R=\beta'(\psi_d,\psi_q)(e_RI-R^EI+T)+\dot{\gamma}.$$

The derivative of γ is defined aiming to remove all terms that are not directly related with the error.

$$\dot{\gamma}\triangleq-\beta'(\psi_d,\psi_q)(-R^EI+T) \tag{131}$$

And then the error can be finally expressed as,

$$\begin{aligned}
\dot{e}_R &= \beta'(\psi_d,\psi_q)e_RI,\\
&= \frac{\partial\beta(\psi_d,\psi_q)}{\partial\psi_d}i_de_R+\frac{\partial\beta(\psi_d,\psi_q)}{\partial\psi_q}i_qe_R.
\end{aligned}$$

In order to find an appropriate definition for $\beta(\psi_d,\psi_q)$, the second method of Lyapunov has been applied to ensure that the estimator converges to an equilibrium point.

$$\mathcal{V}(e_R)=\frac{1}{2}e_R^2 \tag{132}$$

The time derivative of the Lyapunov function is shown as follows.

$$\dot{\mathcal{V}}(e_R)=e_R\dot{e}_R=\frac{\partial\beta(\psi_d,\psi_q)}{\partial\psi_d}i_de_R^2+\frac{\partial\beta(\psi_d,\psi_q)}{\partial\psi_q}i_qe_R^2 \tag{133}$$

The proposal for $\beta(\psi_d,\psi_q)$ is then given in equation (134).

$$\beta(\psi_d,\psi_q)\triangleq-\frac{1}{2}\lambda L(i_d^2+i_q^2) \tag{134}$$

Therefore, $\beta(\psi_d,\psi_q)$ is used to derived to $\beta'(\psi_d,\psi_q)$ as in equation (135).

$$\beta'(\psi_d,\psi_q)=\begin{bmatrix}\frac{\partial\beta(\psi_d,\psi_q)}{\partial\psi_d} & \frac{\partial\beta(\psi_d,\psi_q)}{\partial\psi_q}\end{bmatrix}=\begin{bmatrix}-\lambda i_d & -\lambda i_q\end{bmatrix} \tag{135}$$

Note that this derivative is true just if the behaviour of the inductance is linear, i.e. $\psi = Li \; \forall \; \psi$. The time derivative of Lyapunov function is then,

$$\dot{\mathcal{V}}(e_R) = -\lambda(i_d^2 e_R^2 + i_q^2 e_R^2). \tag{136}$$

So the four Lyapunov conditions are satisfied obtaining a stable estimator. If $\beta'(\psi_d, \psi_q)$ is replaced in the error dynamic, it can be seen that if neither of the currents are zero, the equilibrium implies that the error is zero. At the same time, as the dynamic equation contains two terms, each part with a different current; one of them can be zero without stopping the estimation. However, asymptotic convergence of the error to zero can be theoretically still be stymied when both currents are zero at the same exact time, but in such a case the converter would be practically switched off.

$$\dot{e}_R = -\lambda(i_d^2 e_R + i_q^2 e_R)$$

Going back to the definition of $\dot{\gamma}$ in (131), it clearly contains the value of the inductance in both elements. As concluded in the resistance estimators with one equation, this non-accurately known inductance introduces an error in γ that pollutes the final value of the estimator. However, for this estimator it can be proven that both terms cancel each other when they are multiplied by $\beta'(\psi_d, \psi_q)$, removing the value of L from the final equation.

$$\begin{aligned}
\dot{\gamma} &= \begin{bmatrix} -\lambda i_d & -\lambda i_q \end{bmatrix} (-R^E I + T), \\
&= \begin{bmatrix} -\lambda i_d & -\lambda i_q \end{bmatrix} \left(-R^E \begin{bmatrix} i_d \\ i_q \end{bmatrix} + \begin{bmatrix} \omega L i_q + u_d v_{dc1} - V_d \\ -\omega L i_d + u_q v_{dc1} - V_q \end{bmatrix} \right), \\
&= -\lambda \left(-R^E (i_d^2 + i_q^2) + (u_d v_{dc1} i_d + u_d v_{dc1} i_q) - (V_d i_d + V_q i_q) \right).
\end{aligned}$$

4.5 Combined Estimation of R and G

Once the individual estimator for R and G have been obtained, a unified estimator will now be designed. Note that these two parameters are the uncertain values that are used in a centralized load flow.

For this estimator the whole set of dynamic equations of a VSC converter will be used.

$$\dot{x} = \begin{bmatrix} \dot{\psi}_d \\ \dot{\psi}_q \\ \dot{q}_c \end{bmatrix} = \begin{bmatrix} -R i_d + \omega L i_q + u_d v_{dc1} - V_d \\ -R i_q - \omega L i_d + u_q v_{dc1} - V_q \\ -G v_{dc1} + I_T - \frac{3}{2}(u_d i_d + u_q i_q) \end{bmatrix}$$

In this case, the estimations will be clustered in a column vector called $S \in \mathbb{R}^2$, where the estimation of the resistance and conductance are allocated in the first and second elements of the vector, respectively. The same vector is created with the actual values of the parameters (R_S).

$$S = \begin{bmatrix} R^E \\ G^E \end{bmatrix} \qquad R_S = \begin{bmatrix} R \\ G \end{bmatrix}$$

Then, both resistance and conductance estimators' errors are also clustered in a column vector $e \in \mathbb{R}^2$.

$$e = \begin{bmatrix} e_R \\ e_G \end{bmatrix}$$

$\beta(x)$ and γ must also be column vectors of two elements, the first one controlling the dynamics of the resistance estimator and the second element for the conductance.

$$\beta(x) = \begin{bmatrix} \beta_R(x) \\ \beta_G(x) \end{bmatrix} \qquad \gamma = \begin{bmatrix} \gamma_R \\ \gamma_G \end{bmatrix}$$

The estimation vector (S) is defined as equation (137).

$$S \triangleq \beta(x) + \gamma \tag{137}$$

Once the needed matrices have been defined, the dynamic of the error can be developed following the sequence of previous estimators.

$$\begin{aligned} \dot{e} &= \dot{S} + \dot{R}_S \quad (\dot{R}_S = 0), \\ &= \dot{S}, \\ &= \dot{\beta}(x) + \dot{\gamma}, \quad \text{(Applying the chain rule)} \\ &= \underbrace{\frac{\partial \beta(x)}{\partial x}}_{\beta'(x)} \dot{x} + \dot{\gamma}, \\ &= \beta'(x)\dot{x} + \dot{\gamma}. \end{aligned}$$

$\beta'(x)$ is then defined as the Jacobian matrix of $\beta(x)$. Since the state variables of the first-order derivative equations $x \in \mathbb{R}^3$ and $\beta(x) \in \mathbb{R}^2$, $\beta'(x) \in \mathbb{R}^{2\times 3}$ as seen in equation (138).

$$\beta'(x) = \begin{bmatrix} \frac{\partial \beta_R(x)}{\partial \psi_d} & \frac{\partial \beta_R(x)}{\partial \psi_q} & \frac{\partial \beta_R(x)}{\partial q_c} \\ \frac{\partial \beta_G(x)}{\partial \psi_d} & \frac{\partial \beta_G(x)}{\partial \psi_q} & \frac{\partial \beta_G(x)}{\partial q_c} \end{bmatrix} \tag{138}$$

If $\beta_R(x) = \beta_R(\psi_d, \psi_q)$ and $\beta_G(x) = \beta_G(q_c)$, the error of each parameters are decoupled. Hence, the error of a parameter does not influence the dynamic of the other estimation. In this case, $\beta'(x)$ could be expressed as in equation (139).

$$\beta'(x) = \begin{bmatrix} \frac{\partial \beta_R(\psi_d, \psi_q)}{\partial \psi_d} & \frac{\partial \beta_R(\psi_d, \psi_q)}{\partial \psi_q} & 0 \\ 0 & 0 & \frac{\partial \beta_G(q_c)}{\partial q_c} \end{bmatrix} \tag{139}$$

It can be seen that the rank of $\beta'(x)$ is equal to the number of estimated parameters, as long as $\beta'(x) \neq 0$, what makes the estimator viable. The development of the error's dynamic is continued as follows.

$$\begin{aligned} \dot{e} &= \beta'(x)\dot{x} + \dot{\gamma}, \\ &= \beta'(x) \begin{bmatrix} -Ri_d + \omega L i_q + u_d v_{dc1} - V_d \\ -Ri_q - \omega L i_d + u_q v_{dc1} - V_q \\ -G v_{dc1} + I_T - \frac{3}{2}(u_d i_d + u_q i_q) \end{bmatrix} + \dot{\gamma}, \\ &= \beta'(x) \begin{bmatrix} -(R^E - e_R) i_d + \omega L i_q + u_d v_{dc1} - V_d \\ -(R^E - e_R) i_q - \omega L i_d + u_q v_{dc1} - V_q \\ -(G^E - e_G) v_{dc1} + I_T - \frac{3}{2}(u_d i_d + u_q i_q) \end{bmatrix} + \dot{\gamma}. \end{aligned}$$

Then, in terms of simplification, two new matrices can be defined:

$$I = \begin{bmatrix} i_d & 0 \\ i_q & 0 \\ 0 & v_{dc1} \end{bmatrix}, \qquad T = \begin{bmatrix} \omega L i_q + u_d v_{dc1} - V_d \\ -\omega L i_d + u_q v_{dc1} - V_q \\ I_T - \frac{3}{2}(u_d i_d + u_q i_q) \end{bmatrix}.$$

So, $\dot{e}$ could be rewritten as follows.

$$\dot{e} = \beta'(x)[Ie - IS + T] + \dot{\gamma}$$

The update law derivative is then defined as in equation (140) in order to remove all the terms that do not contain the error vector.

$$\dot{\gamma} = -\beta'(x)[-IS + T] \tag{140}$$

The error is now simplified to:

$$\begin{aligned} \dot{e} &= \beta'(x) I e, \\ &= \begin{bmatrix} \frac{\partial \beta_R(x)}{\partial \psi_d} & \frac{\partial \beta_R(x)}{\partial \psi_q} & 0 \\ 0 & 0 & \frac{\partial \beta_G(x)}{\partial q_c} \end{bmatrix} \begin{bmatrix} i_d & 0 \\ i_q & 0 \\ 0 & v_{dc1} \end{bmatrix} \begin{bmatrix} e_R \\ e_G \end{bmatrix}, \\ &= \begin{bmatrix} \dot{e}_R \\ \dot{e}_G \end{bmatrix} = \begin{bmatrix} \frac{\partial \beta_R(\psi_d, \psi_q)}{\partial \psi_d} i_d e_R + \frac{\partial \beta_R(\psi_d, \psi_q)}{\partial \psi_q} i_q e_R \\ \frac{\partial \beta_G(q_c)}{\partial q_c} v_{dc1} e_G \end{bmatrix}. \end{aligned}$$

The second method of the Lyapunov theory will be then used to define a $\beta(x)$ that makes the estimator reach to stability. The Lyapunov function is defined as in equation (141).

$$V(e_R, e_G) = \frac{1}{2}\left(e_R^2 + e_G^2\right) \tag{141}$$

So, the time derivative of the Lyapunov function is shown in equation (142).

$$\dot{V}(e_R, e_G) = \frac{\partial V(e_R, e_G)}{\partial e_R} \dot{e}_R + \frac{\partial V(e_R, e_G)}{\partial e_G} \dot{e}_G \tag{142}$$

This time derivative is developed as,

$$\begin{aligned} \dot{V}(e_R, e_G) &= e_R \dot{e}_R + e_G \dot{e}_G, \\ &= \left(\frac{\partial \beta_R(\psi_d, \psi_q)}{\partial \psi_d} i_d + \frac{\partial \beta_R(\psi_d, \psi_q)}{\partial \psi_q} i_q \right) e_R^2 + \frac{\partial \beta_G(q_c)}{\partial q_c} v_{dc1} e_G^2. \end{aligned}$$

In order to obtain a negative-definite scalar function from the time-derivative of Lyapunov function, the following $\beta(x)$ has been defined where $\lambda_R \in \mathbb{R}_{>0}$ and $\lambda_G \in \mathbb{R}_{>0}$, whose objective is to modify the speed of the estimator.

$$\beta(x) = \begin{bmatrix}\beta_R(x)\\ \beta_G(x)\end{bmatrix} = \begin{bmatrix}-\frac{1}{2}\lambda_R L\left(i_d^2 + i_q^2\right)\\ -\frac{1}{2}\lambda_G C v_{dc1}^2\end{bmatrix} \longrightarrow \begin{cases}\frac{\partial \beta_R(\psi_d,\psi_q)}{\partial \psi_d} = -\lambda_R i_d\\ \frac{\partial \beta_R(\psi_d,\psi_q)}{\partial \psi_q} = -\lambda_R i_q\\ \frac{\partial \beta_G(q_c)}{\partial q_c} = -\lambda_G v_{dc1}\end{cases}$$

Then, as seen in equation (143), the expression of $\dot{V}(e_R, e_G)$ is always negative except for when it reaches to the equilibrium, point at which $\dot{V}(e_R, e_G) = 0$.

$$\dot{V}(e_R, e_G) = -\lambda_R\left(i_d^2 + i_q^2\right)e_R^2 - \lambda_G v_{dc1}^2 e_G^2 \leqslant 0 \tag{143}$$

The errors will then behave as equation (144) describes (solution of the first-order derivative equation in (145)).

$$\dot{e} = \begin{bmatrix}\dot{e}_R\\ \dot{e}_G\end{bmatrix} = \begin{bmatrix}-\lambda_R i_d^2 e_R - \lambda_R i_q^2 e_R\\ -\lambda_G v_{dc1}^2 e_G\end{bmatrix} \tag{144}$$

$$e(t) = \begin{bmatrix}e_R(t)\\ e_G(t)\end{bmatrix} = \begin{bmatrix}e^{-\lambda_R i_d^2 t} + e^{-\lambda_R i_q^2 t}\\ e^{-\lambda_G v_{dc1}^2 t}\end{bmatrix} \tag{145}$$

In [50] it is proven that in case of asking the PI-PBC for a slightly erroneous equilibrium point, the converter's state variables will converge at a point near the asked equilibrium. Note that the fast dynamic of the VSC converter, thanks to the PI-PBC, will make the current and DC-voltage stabilize relatively quickly. In addition, wrong values of AC link resistance and DC-conductance do not generate a great error in the load flow solution. Therefore, if this estimator is used, the converter will converge to equilibrium point near the desired point during the first milliseconds. Afterwards, the estimator will find the real values of the parameters, recalculating the load flow and obtaining the desired equilibrium point.

On the other hand. the currents and the voltage in the exponentials of (145) act as disturbances for the error dynamic, but they do not influence the final solution of the error, *as long as they remain bounded*, which is ensured by the PI-PBC.

4.6 Estimator's Energetic Interpretation

The update law dynamic defined in equation (140) can be developed with the aim of understanding its operation from an energy balance point of view.

$$\begin{aligned}\dot{\gamma} &= -\beta'(x)[-IS + T],\\ &= -\begin{bmatrix}-\lambda_R i_d & -\lambda_R i_d & 0\\ 0 & 0 & -\lambda_G v_{dc1}\end{bmatrix}\left\{-\begin{bmatrix}i_d & 0\\ i_q & 0\\ 0 & v_{dc1}\end{bmatrix}\begin{bmatrix}R^E\\ G^E\end{bmatrix} + \begin{bmatrix}\omega L i_q + u_d v_{dc1} - V_d\\ -\omega L i_d + u_q v_{dc1} - V_q\\ I_T - \frac{3}{2}(u_d i_d + u_q i_q)\end{bmatrix}\right\}.\end{aligned}$$

Note that λ_R and λ_G can be extracted from $\beta'(x)$, forming a new matrix $\lambda = \lambda^\top \in \mathbb{R}^{2\times 2}_{>0}$.

$$
\begin{aligned}
\dot{\gamma} &= \begin{bmatrix}\lambda_R & 0\\ 0 & \lambda_G\end{bmatrix}\begin{bmatrix}i_d & i_q & 0\\ 0 & 0 & v_{dc1}\end{bmatrix}\left\{-\begin{bmatrix}i_d & 0\\ i_q & 0\\ 0 & v_{dc1}\end{bmatrix}\begin{bmatrix}R^E\\ G^E\end{bmatrix}+\begin{bmatrix}\omega L i_q + u_d v_{dc1} - V_d\\ -\omega L i_d + u_q v_{dc1} - V_q\\ I_T - \frac{3}{2}(u_d i_d + u_q i_q)\end{bmatrix}\right\},\\
&= \lambda\begin{bmatrix}i_d & i_q & 0\\ 0 & 0 & v_{dc1}\end{bmatrix}\begin{bmatrix}-R^E i_d + \omega L i_q + u_d v_{dc1} - V_d\\ -R^E i_q - \omega L i_d + u_q v_{dc1} - V_q\\ -G^E v_{dc1} + I_T - \frac{3}{2}(u_d i_d + u_q i_q)\end{bmatrix},\\
&= \lambda\begin{bmatrix}-R^E i_d^2 + \omega L i_d i_q + u_d v_{dc1} i_d - V_d i_d - R^E i_q^2 - \omega L i_d i_q + u_q v_{dc1} i_q - V_q i_q\\ -G^E v_{dc1}^2 + v_{dc1} I_T - \frac{3}{2} v_{dc1}(u_d i_d + u_q i_q)\end{bmatrix},\\
&= \lambda\begin{bmatrix}-R^E\left(i_d^2 + i_q^2\right) + (u_d v_{dc1} i_d + u_q v_{dc1} i_q) - (V_d i_d + V_q i_q)\\ -G^E v_{dc1}^2 + v_{dc1} I_T - \frac{3}{2} v_{dc1}(u_d i_d + u_q i_q)\end{bmatrix}.
\end{aligned}
$$

As can be seen, the value of the inductance disappears from the dynamic, what means the error of this parameter does not affect neither the behaviour nor the final value of γ. Additionally, the remaining terms of the expression have units of power, and therefore, it can be rewritten as in (146).

$$
\dot{\gamma} = \lambda\begin{bmatrix}-P_{L.AC}^E + P_{AC}^{VSC} - P_{AC}^{Grid}\\ -P_{L.DC}^E + P_{DC}^{HVDC} - P_{DC}^{VSC}\end{bmatrix} \tag{146}
$$

Where $P_{L.AC}^E$ is the estimated power losses in the AC side, P_{AC}^{VSC} is the AC power going out from the converter, P_{AC}^{Grid} is the AC power that reaches to the PCC, $P_{L.DC}^E$ is the estimated power losses in the DC side, P_{DC}^{HVDC} is the power that comes from the HVDC line and P_{DC}^{VSC} is the final power that enters to the VSC from the DC side. Take into account all powers in the AC equation are multiplied by $\frac{2}{3}$ as park transformation was carried out in amplitude invariant mode. Moreover, all power are active powers, since the chosen $\beta(x)$ removes the terms that are related to reactive component.

In conclusion, during the transitory state of the estimator, the power imbalance between real input-output powers and the estimated dissipations leads to a variation of the update law with the aim of tracking the accurate value of both parameters. On the other hand, the velocity of the system can be modified through the tuning of the constant matrix λ, whose elements can take different values for each parameter's estimation.

Finally, the chosen $\beta(x)$ also has an interpretation from the point of view of energy. As can be seen in equation (147), $\beta_R(\psi_d, \psi_q)$ and $\beta_G(q_c)$ are the stored energy in the inductances and the capacitance respectively.

$$
\beta(x) = \begin{bmatrix}\beta_R(\psi_d, \psi_q)\\ \beta_G(q_c)\end{bmatrix} = -\lambda\begin{bmatrix}\frac{1}{2}L\left(i_d^2 + i_q^2\right)\\ \frac{1}{2}C v_{dc1}^2\end{bmatrix} = -\lambda\begin{bmatrix}H_L(\psi_d, \psi_q)\\ H_C(q_c)\end{bmatrix} \tag{147}
$$

Note that the both elements of $\beta(x)$ contains either the inductance or the capacitance value. These parameters, as it happens with R and G, cannot be accurately measured. However, the error that these values introduces into $\beta(x)$ is corrected by the power balance of the update law. Therefore, even though the transient behaviour can be affected, the steady-state result should be correct. This fact is evaluated and proven in section 5.4.5.

4.7 Energy Balance Based Adaptive Controller

Previously in this project, it was described how traditional VSC controllers are typically composed by an inner current loop controller, which computes the modulation indices from the reference currents, and an outer loop to calculate q-axis current from the wanted reactive power and direct current from either the active power or DC side voltage.

However, this strategy is based on the direct comparison of references and measurements, without any physical interpretation which can be taken as a starting point for the system's stability analysis.

The studied resistance and conductance estimator can be joined with the VSC load flow calculator to obtain a new outer-loop strategy for the computation of the desired system's equilibrium, which has been called *Energy Balance Based Adaptive (EBBA)* outer-loop.

An interesting advantage of EBBA is that it replace the traditional outer-loops without destroying the stability certificate and by means of an elegant energetic interpretation. This fact is fundamental for the future expansion of the HVDC power grids, as new terminals and components can be added to the power system without compromising its operation. Figure 12 depicts a brief scheme of the EBBA controller, whose output is the desired equilibrium point and inputs are the real time measurements of VSC currents and voltages, the desired references and the used control variables.

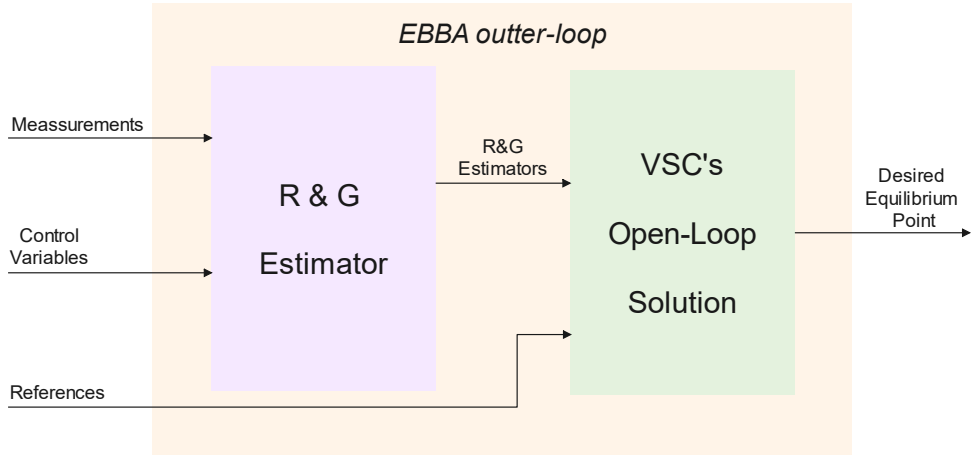

Figure 12: Schematic representation of EBBA outer-loop.

Additionally, the modulation indices of the VSC are calculated by means of the PBC strategy, based on the passive output of the converter which also has units of power. Therefore, it can be said that the whole control can be analysed from an energetic point of view.

5 SIMULATIONS

The control strategies commented and developed in sections 3 and 4 will be simulated by means of Matlab/Simulink. The major aim of this chapter is to demonstrate that the predicted behaviours of the systems, obtained from the analytical development of the models, are indeed correct.

First, two Simulink models are presented, one for the grid forming control and another one for the grid feeding strategy. Second, we test the performance of the open-loop control via simulations to highlight its limitations in HVDC applications. Third, the PI-PBC is introduced to obtain a better performance of the converter. In this case, the simulation will be carried out with and without an accurate knowledge of the system parameters. Finally, the estimators designed in section 4 are tested and their performance analysed.

5.1 Description of Matlab/Simulink Models

In relation to what has been already mentioned in previous chapters, the performance of the alternative nonlinear control will be tested numerically via time-domain simulations. Accordingly, the different model control diagrams will be presented and briefly explained. Towards this end, we proceed by first presenting the model illustrated in figure 13. This model represents an HVDC system consisting of two 2-Level VSCs and a DC transmission line. Of course, each of the VSCs needs to work with one of the possible control strategies, this is, grid forming and grid feeding control methods.

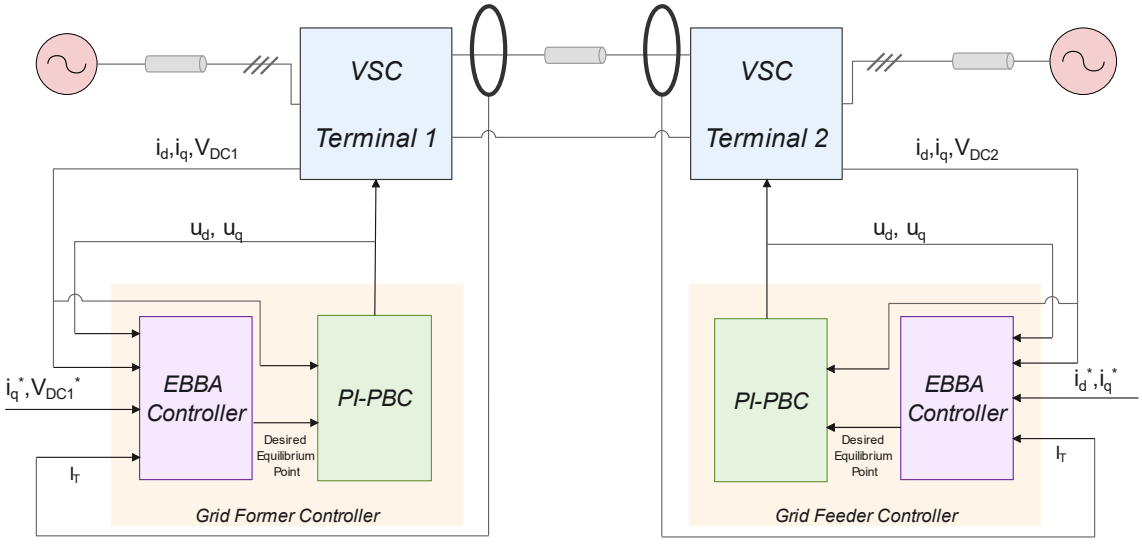

Figure 13: HVDC Simulink Model diagram.

Figure 13 shows a complete centralized model composed of three main submodels, two for each of the converters and the third one associated to the transmission line. In addition, both VSC submodels have a controller associated to them. In this specific case where the system is uniquely composed by two converters, one of the terminal controllers is required to control the active (and reactive) power; i.e., operating in grid feeding control mode; whilst the other needs to regulate the DC voltage (and reactive power) with a grid forming strategy.

Focusing on a specific submodel, e.g. the grid forming terminal, of figure 13; two main components can be distinguished. First, the VSC Terminal 1 models the functioning of the power converter by means of the set of dynamic equations (36) in port Hamiltonian representation. This block requires the state and control variables together with the transmission current (I_T) as inputs; returning the updated state variables, which will be then introduced to the controller.

This controller combines the EBBA outer-loop controller (shown in figure 12) with the PI-PBC, as depicted. This block requires multiples inputs, such as the state and control variables, the

established references and the transmission current. Finally, the optimum control variables u_d and u_q, which introduced to the terminal block bring the system to equilibrium.

Delving deeper into this control block, this not only includes important elements of the system, but also the major contribution of this work which is the use of I&I philosophy in order to estimate the erroneous system parameters. This is properly addressed in section 4.7, where figure 12 depicts the composition of EBBA where the estimators can be distinguished.

Both VSC models work with a similar structure, only rearranging the load-flow equations to change the estimated reference variable. On the other hand, the third model represents the HVDC system transmission line, which has linear dynamics only dependant on the DC voltages on the VSC terminals. This returns, in the end, the transmission line current as the sum of the parallel branches currents.

Additionally, it is important to characterize the model with the different parameters employed. Accordingly, tables 1 and 2 are included in order to specify the converter nominal values and parameters, respectively. In this respect, it is necessary to point out that the parameters established for the converters refer to both of them (grid forming and greed feeding one). This is a consideration which is not significant, since these parameters will be treated as incorrect in the following simulation scenarios and where the level of uncertainty can be different for each of the converters.

Electrical Nominal Values		
Voltage (kV)	Apparent Power (MVA)	Frequency (Hz)
200	200	50

Table 1: Electrical Nominal Values of the System

Converter Passive Elements (per phase)			
Resistance (Ω)	Inductance (H)	Capacitance (F)	Conductance (G)
0.075	0.0239	3.5×10^{-5}	1×10^{-5}

Table 2: Converter Passive Elements (per phase)

Finally, it is important to mention that the parametrization of the system has been done following the existing MATLAB/Simulink model called *VSC-Based HVDC Transmission System (Detailed Model)*.

5.2 Open-Loop Control

The open-loop control is the most fundamental and basic control strategy that can be implemented to operate a VSC, having a large-signal stability certificate. As mentioned in section 2.1, the set of equations that describe the system are used to compute constant modulation indices corresponding to a desired load flow solution. Indeed, this method does not take into account the instantaneous state of the system for any feedback action, leaving the performance of the system to its natural time constants, which could lead to an unacceptable behaviour.

The set of equations (36) is used in the case of a VSC, which consists on three first-order time derivative functions with five variables. This enables the operator to choose the reference of two state variables (AC currents or DC voltage in case of this set) and solve the system, obtaining the modulation indices and the value that the third state variable must take at the corresponding equilibrium. Note that the result of this third variable has to respect the operation limits.

In the performed simulation, only the open-loop load-flow solver has been used, applying the resultant u_d and u_q directly to the model of the converter. A single terminal without DC transmission line has been used in order to simplify the model, focusing on the analysis of the VSC itself.

Therefore, the DC side of the system is represented by a constant current that flows towards a

grid-forming converter. This strategy has been chosen due to the interest of showing and analysing the what we consider to be the worst case scenario, since the addition of the transmission line model to allow grid feeding operation introduces extra dissipation, improving the performance of the system.

Figure 14 depicts the behaviour of the direct and quadrature currents along with the DC side voltage. The simulation is launched asking for the nominal DC voltage and for zero reactive current. The incoming DC current is of 1000 A, the maximum power that the converts is able to manage. During a simulation of six seconds, two steps have been introduced. First, the incoming DC current is reduced 25% at $t = 2s$. At $t = 4s$, the reactive current reference is set at -1000 A, making the converter operate at nominal apparent power. Due to the chosen references in figure 7 this negative current means the converter is injecting reactive power to the PCC.

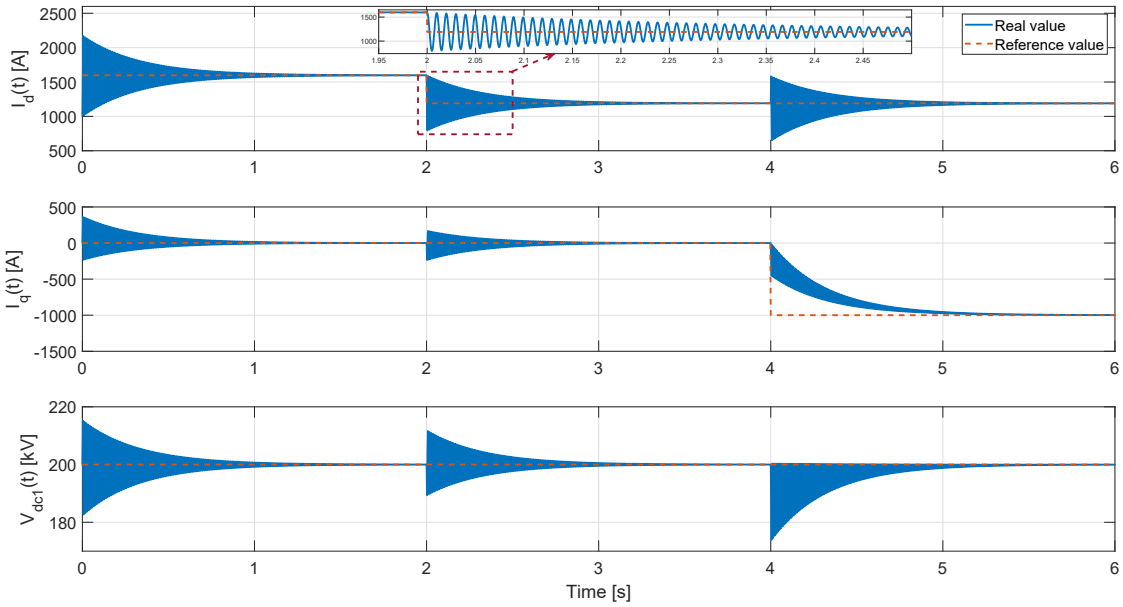

Figure 14: VSC AC currents and DC voltage in an open-loop control.

Evaluating the results, a large oscillatory performance can be seen in both currents and voltage. This inadmissible behaviour is repeated in every reference step in the converter or, in other words, each time that the converter has to vary its operation point.

The maximum direct current ripple is of 1151 A, which is 70.5% of the maximum allowed current of 1633 A. Furthermore, the quadrature current has a ripple of 624 A and the DC voltage of 32 KV, i.e. the 16% of the nominal voltage.

Needless to say, these huge oscillations cannot be managed by a real converter, as semiconductors and insulation are not prepared for those levels of stress. Furthermore, there is no control over the transient periods, due to the lack of state feedback action. However, during steady state operation the converter is *always* stable, reaching the equilibrium point.

The active and reactive powers injected by the power converter are depicted in figure 15.

In case of active and reactive powers, the same oscillatory performance is observed. When talking about the active power, a peak power greater than 250 MW can be observed, overcoming the maximum allowed power in more than 25%.

As a result of this simulation, it can be clearly seen that for the simulated 2L-VSC, a more complex control strategy which takes into account the instantaneous state of the converter, is required for improving the performance.

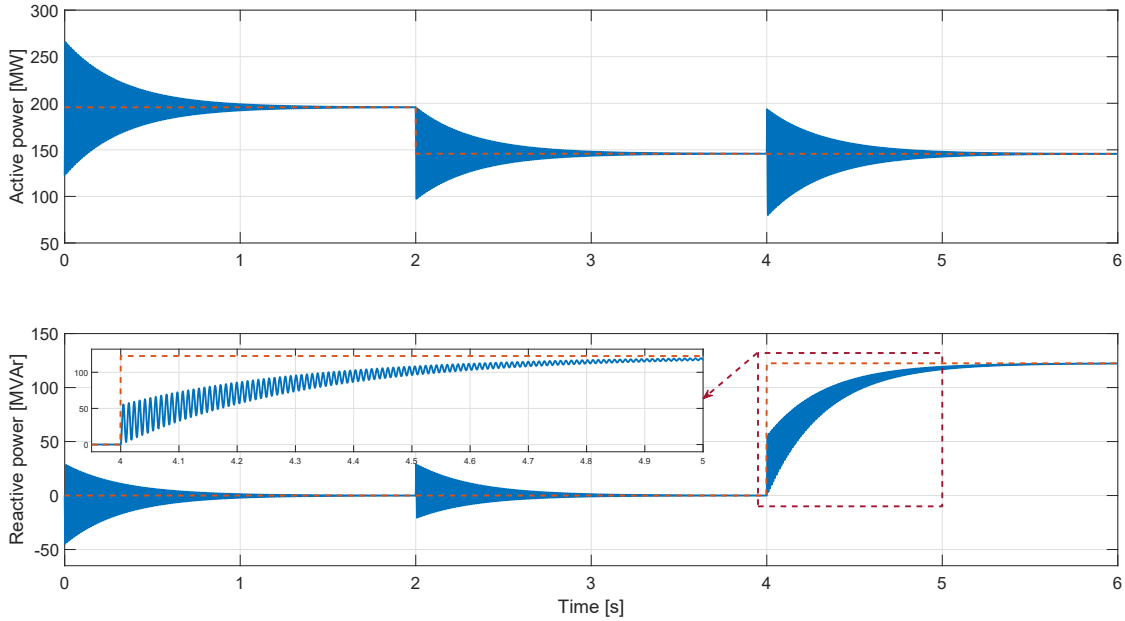

Figure 15: Injected active and reactive powers into the grid in an open-loop control.

5.3 PI-Passivity Based Control

With the aim of enhancing the performance of the 2L-VSC, in this section a PI-PBC is introduced. Comparing with traditional closed-loop controllers, this strategy has a large-signal stability certification by means of analytical methods, avoiding the use of numerical methods to demonstrate the correct operations in a finite number of situations.

Since in this simulation the modulation indices are obtained from the PI-PBC, the computed indices by the load-flow are used only for the calculation of the Lyapunov function developed in section 3.4.5 and its time-derivative. As in the open-loop simulations, a single grid-forming terminal which is fed through the DC side by a ideal current source is tested.

Two simulations are performed. First, the PI-PBC strategy is used and analysed under nominal parameters. Afterwards, an error will be introduced in both the resistance and the conductance of the converter, which implies an error in the calculation of the desired equilibrium point.

5.3.1 PI-PBC with nominal parameters

In this first simulation the set of equations that describes the converter behaviour is solved in steady-state with nominal parameters. Therefore, a reliable equilibrium point will be obtained from the two given references.

The tuning proportional and integral gains for the PI-PBC are presented in table 3. Take into account that although the converter's performance could be improved by a more optimal tuning, the final objective of this simulation is to test the overall performance of the system.

PI-PBC parameters	
K_p	K_i
$5 \cdot 10^{-8}$	$1 \cdot 10^{-8}$

Table 3: PI-PBC proportional and integral parameters

The AC currents in dq-framework and the DC voltage have been represented in figure 16 using the same reference steps and simulation time than in previous simulations.

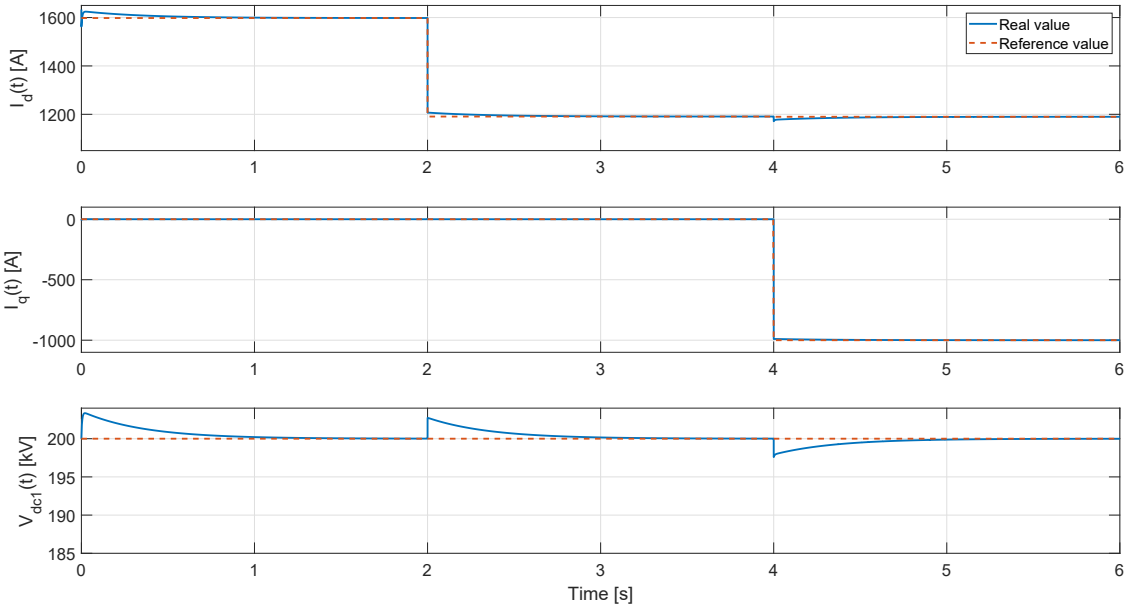

Figure 16: VSC AC currents and DC voltage with PBC strategy

As can be seen, the oscillatory behaviour of the converter analysed with the open-loop control is corrected by the PI-PBC controller. In this case, the reference steps generate a transient disturbance in both currents and voltage, which reach to the desired equilibrium point after a period of around a second. The maximum direct current error when 1600 A have been asked is of 23A, i.e. a ripple of 1.43%. In case of DC voltage, the maximum deviations respect to the reference of 200 kV has been of 3.342 KV, an error of 1.67%.

The stability of the system can also be analysed plotting, in figure 17, the designed Lyapunov function and its time-derivative defined in equations (86) and (87), respectively. In case of the Lyapunov function, it is proven that it is a positive-definite function, which reaches its minimum (zero) when the system is stable. It is important to remember that this function can be seen as the level of deviation between the current state of the VSC and the desired point.

On the other hand, the time derivative is a negative-definite function. It can be seen that whenever a reference step is introduced, the time-derivative becomes negative, which means a reduction on the Lyapunov function value over time and, thus, an approach to the desired equilibrium.

Since the correct performance of the system control led by a PI-PBC has been proven via simulation, some parametric uncertainty is now going to be introduced in both the AC side inductor resistance and in the DC side conductance.

5.3.2 PI-PBC with erroneous parameters

The PI-PBC operation will be tested under parametric uncertainty. Such uncertainty could be caused by inaccuracies in the measurement of these parameters or because they take different values depending on the operation of the converter.

For this simulation, the value used in the system solution for the AC side inductor resistance has been increased by 5%. In case of the DC side conductance, it has been multiplied by a factor of 0.94. The obtained currents and voltage are represented in figure 18 following the same references than in the previous sections.

As can be seen, even though the transient-state period and the behaviour of the curves is the same, the system is stabilized in an erroneous equilibrium point. When the system is asked for a d-current of 1600A, the VSC is stabilized at 1516.06 A. Looking at figure 19, where active and reactive powers are depicted, this error carries an active power deviation of around 10 MW, 5.13%

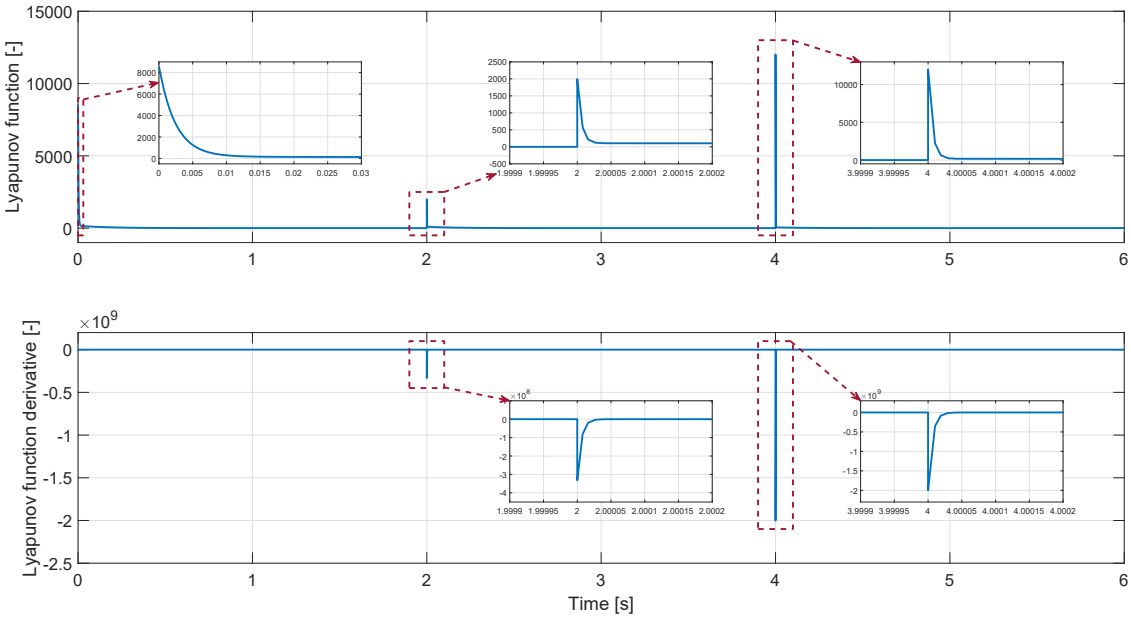

Figure 17: Systems Lyapunov function and its time-derivative

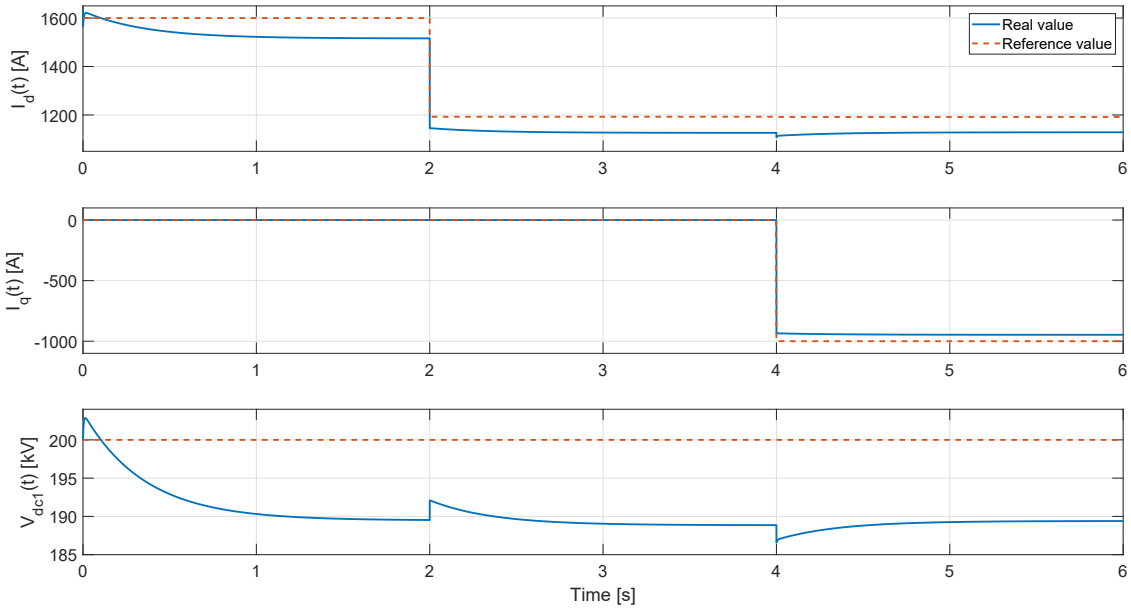

Figure 18: VSC AC currents and DC voltage with PBC strategy and erroneus parameters

of the injected power.

A similar deviation occurs in the quadrature current after $t = 4s$, which presents an error of 5.3%. On the other side, the error of the DC voltage is around 10 KV, which means an offset of 5%.

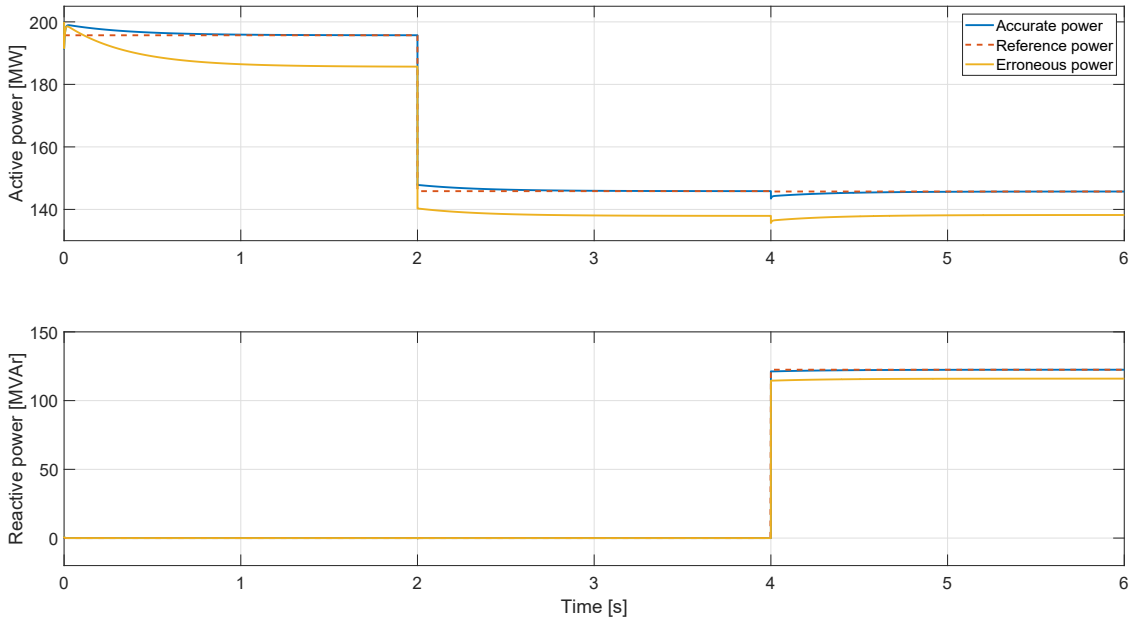

Figure 19: Active and reactive powers with PBC strategy and erroneus parameters

In conclusion, an error in the parameters used for the calculation of the equilibrium point can cause an unbalance between demanded and injected power. This could lead to further issues with the detailed component forming the AC network, which we have let unmodelled, restricting the direct integration of this control to high power HVDC transmission lines. In order to restore the nominal operating conditions under this parametric uncertainty, the Inmersion & Invariance methodology is used to find the real value of the parameters.

5.4 Adaptive Passivity Based Control

The estimators designed in chapter 4 will be tested via time-domain simulations in the following subsections. The main aim of these simulations is to validate the results obtained during the analytical development, and test their performance.

The estimators performance can be varied by means of the tuning parameter λ, as explained in chapter 4. In order to improve the interpretation of this variable, it has been divided into two terms as expressed in equation (148).

$$\lambda = \frac{\lambda'}{\rho}, \tag{148}$$

where ρ is introduced in the denominator to compensate–at least in magnitude–the effect of λ being sometimes multiplied by a disturbance such as the VSC current or voltage. This parameter should then take a constant value close to the nominal operation. In this way, λ' approximates to the inverse of the time constant of a first-order system, and hence, the system should stabilize in 4-5 times $\frac{1}{\lambda'}$.

This chapter follows the same structure than section 4, trying again to be as didactic as possible, showing the performance of every adaptive estimation proposal described in the previous section. However, for the readers interested exclusively in the final result (the EBBA), we refer them to section 5.4.5.

5.4.1 Estimation of I_T

In this first approach, again for a grid-forming VSC, the transmission current I_T value is supposed to be incorrectly known, with an error of 10%. This will cause the computation of an incorrect–and likely inadmissible–equilibrium point as reported previously in section 5.3.2. However, in this case the estimators are designed to correct the divergence between the real and the estimated parameters, so that within a short period of time both take the same value. As in the previous cases, a change of 25% of I_T is introduced at $t = 2s$, while 1000 A of quadrature current are asked for at $t = 4s$. The estimator has been tuned with the parameters summarized in table 4. The parameter ρ takes a value of unity because the dynamic equation (92) of this estimator does not have any disturbance multiplying this time constant.

Estimator's parameters	
λ'	ρ
100	1

Table 4: I_T estimator parameters

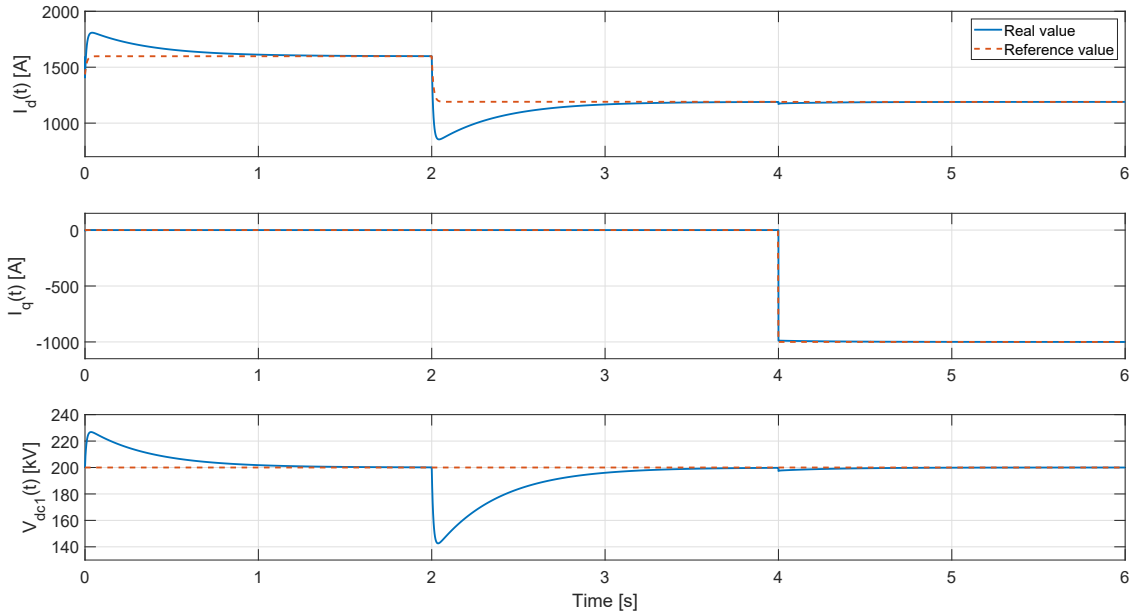

Figure 20: VSC AC currents and DC voltage with I&I philosophy for I_T estimation.

The system behaviour can be observed, reflected in the state variables, in figure 20. Indeed, the performance is enhanced when compared to the erroneous parameter PI-PBC case without adaptive control. More precisely, the three state variables stabilize at the desired reference, which means the required power injection is achieved. This is thanks to the good performance of the estimator, which is depicted in figure 21. Such figure shows how despite the fact that the initial transmission current is not accurate, the designed adaptive controller rapidly reaches the real value.

However, despite improving the performance shown previously, significant peak values during the non-stationary period are obtained when checking the different state variables. For the case of the direct current, a peak surpassing 1800 A is obtained, which means an error of 12.5%, during the initializing period. However, when the transmission current is reduced at $t = 2s$, the current descends down to 855 A. This represents an error of 28%, as the new reference current is settled in 1190 A.

In the same way, the DC voltage presents an over voltage of 13.5% during the initializing transient period. On the other hand, the reduction of the transmission current causes this voltage to decrease a 28.75% of its nominal value, reaching a minimum value of 142.5 kV. This is clearly related to the

transmission current reduction after two seconds of operation. When this occurs, the direct current reference value remains invariant during the first lapse of time; meaning during some miliseconds the converter injects to the AC grid more power than it receives. Assuring the proper functioning of the system, the DC side capacitor is forced to deliver the difference in currents, reason why it is partially discharged. Once the direct current reference is updated, this capacitor is charged again up to its nominal value.

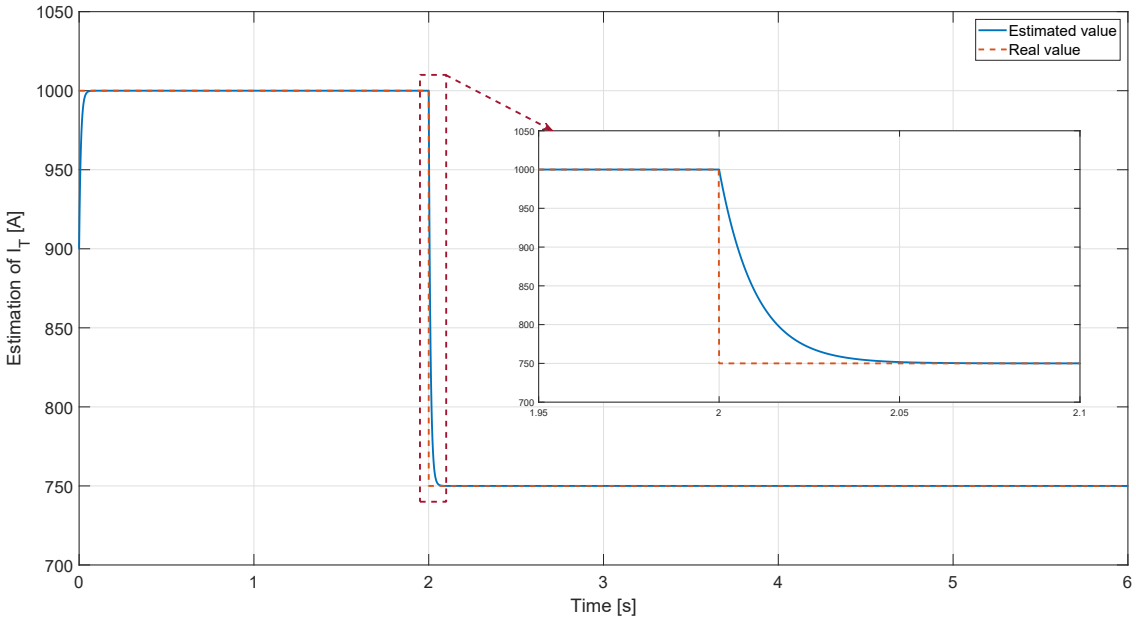

Figure 21: I_T estimation.

Focusing on figures 21, it can be stated that the estimator's dynamic is considerably fast, as the real and estimated values adopt the same value after 0.05 seconds. This time corresponds to five times the inverse of the chosen λ' value. However, the big deviations of the state variables can correspond to the significant influence that the transmission current has on the load flow calculation. Consequently, an small divergence can cause big oscillations as the ones presented previously.

Furthermore, the system currents are supposed to be measurable with a relatively high level of precision. For that reason, the next estimator is focused on a system parameter which is harder to know, as it can be the conductance. This difficulty of the measurement is attached to the fact that this element captures in the model the non-ideal (lossy) behaviour of various components.

5.4.2 Estimation of G

We now shift our attention to the estimation of a physical parameter of the HVDC system, more specifically the converter conductance; as acquiring a precise knowledge of this kind of variable is arguably more difficult than I_T. This is due to the conductance not being exactly a physical component, but it represents, as mentioned, the non-ideal behaviour of the different components of the converter and can vary depending on the point of interconnection between the transmission line and the VSC, as explained in section 4.2.

As discussed in the above mentioned section of the previous chapter, only the results for the non-linearized G estimation will be presented. This is due to the intrinsic malfunctioning of the linearized estimator when the system is initializing.

As in the previous attempts, the grid-forming case will be analysed; reducing first the transmission current from its nominal value to 75% two seconds after the beginning. Two seconds later, the demand of quadrature current is increased from 0 to 1000 A. Additionally, a factor of 0.9 is introduced to the known conductance value; this is, at the beginning a 10% error is assigned to

the conductance. The chosen parameters for this estimators are found in table 5, where the value of ρ is selected as the square of the DC side nominal voltage. The obtained simulation results are shown in figures 22 and 23.

Estimator parameters	
λ'	ρ
100	$(200 \cdot 10^3)^2$

Table 5: G estimator parameters

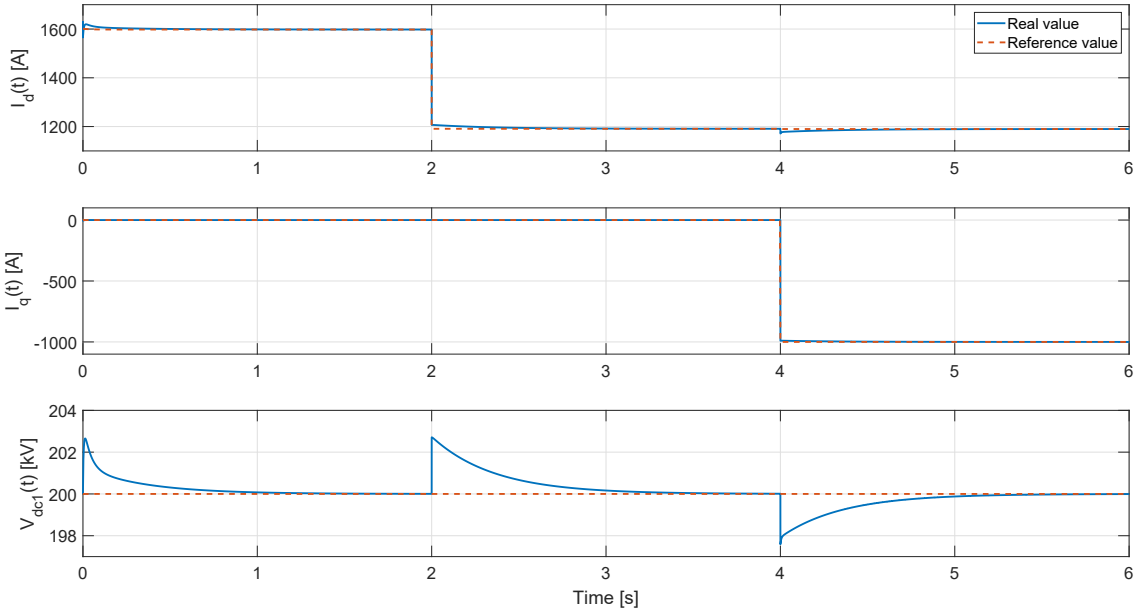

Figure 22: VSC AC currents and DC voltage with I&I philosophy for G estimation.

By analysing figure 22, it can be seen that this estimator performs better when compared to the previous one. This is due to the relevance that the conductance has on the load flow calculation. In this case the performance is always closer to the reference values given. As an example, the direct current reaches a peak value of 1620 A, meaning an error of 1.25%. On the other hand, the quadrature current follows perfectly the reference value, with no significant over or under peak values. Finally, the DC voltage value presents maximum deviations of 2 kV, which means an error of 1%. In addition, notice that in this case there is no oscillatory behaviour.

The fast correction of the divergences between reference and real values can be attributed to the fast dynamic of the estimator, which is shown in figure 23. As explained previously, this can be modified thanks to the λ' parameter; on which the estimator speed depends. The estimation time in this simulation is around 0.2 seconds, fitting perfectly with the prediction of five time the time constant. This means the introduced ρ parameter counteracts to a certain extent the DC voltage properly.

The estimator is indeed stable, as predicted thanks to the analytical development in case of choosing a positive λ. Considering the good performance of the estimator, the next step attempts to cluster the estimation of two different parameters, in this case I_T and G, simultaneously.

5.4.3 Estimation of I_T and G

Following the good performance of the conductance presented in section 5.4.2, this approach pretends to implement a combined estimator. This is aimed to follow transmission line current and converter conductance real values at the same time. After running different simulations, the res-

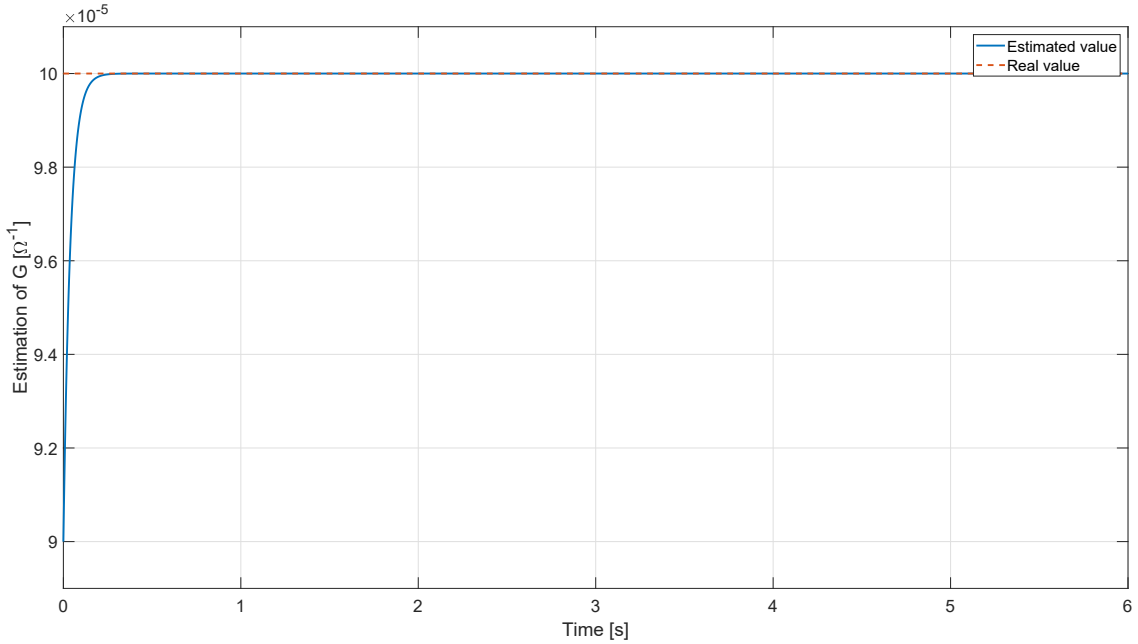

Figure 23: Conductance estimation for a 10% of initial error.

ults obtained can be seen in figures 24 and 25; showing the direct-quadrature currents and the DC voltage in the former and the estimators in the latter.

The first and second elements of the term $\beta(x)$ are the ones used in section 5.4.1 and 5.4.2, whose parameters are shown in table 6.

Estimator parameters		
	λ'	ρ
I_T	25	1
G	25	$(200 \cdot 10^3)^2$

Table 6: Estimator parameters of DC current and conductance

As concluded in section 4.3, although the estimator reaches an equilibrium point, the system does not necessarily stabilize in the desired point, which implies that the estimator fails to find the real value of the parameters. Interestingly, in this simulation the currents and voltage reach the references after $t = 2s$, even though asymptotic convergence of the error variables is not guaranteed analytically.

This fact could be linked to the same energetic interpretation of the estimator. When the system is stable, the DC side power express by the term $I_T^E - G^E v_{dc1}$ in the update law is equal by the known input power. Therefore, although the estimations are wrong, the term itself is correct. As the converter load flow solver contains both estimations in the term $I_T^E - G^E \bar{v}_{dc1}$, when the DC voltage gets close to the desired value, both expressions are set equal, what leads to a correct operation of the control.

Nevertheless, it cannot be proven that the estimator works correctly at every operation point, as seen during the first two seconds of simulation. Therefore, this design is not recommended.

5.4.4 Estimation of R

Since the combined approach from a unique equation does not present a proper performance and considering that the measurement of I_T is more feasible than accurately predicting a system

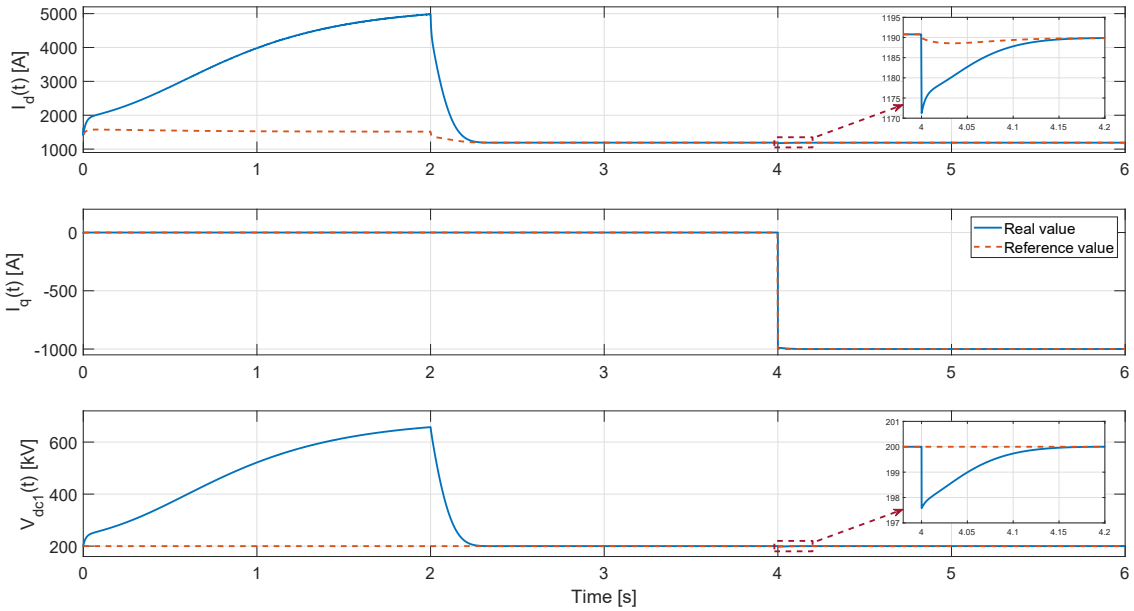

Figure 24: VSC AC currents and DC voltage with I&I philosophy for I_T and G estimation.

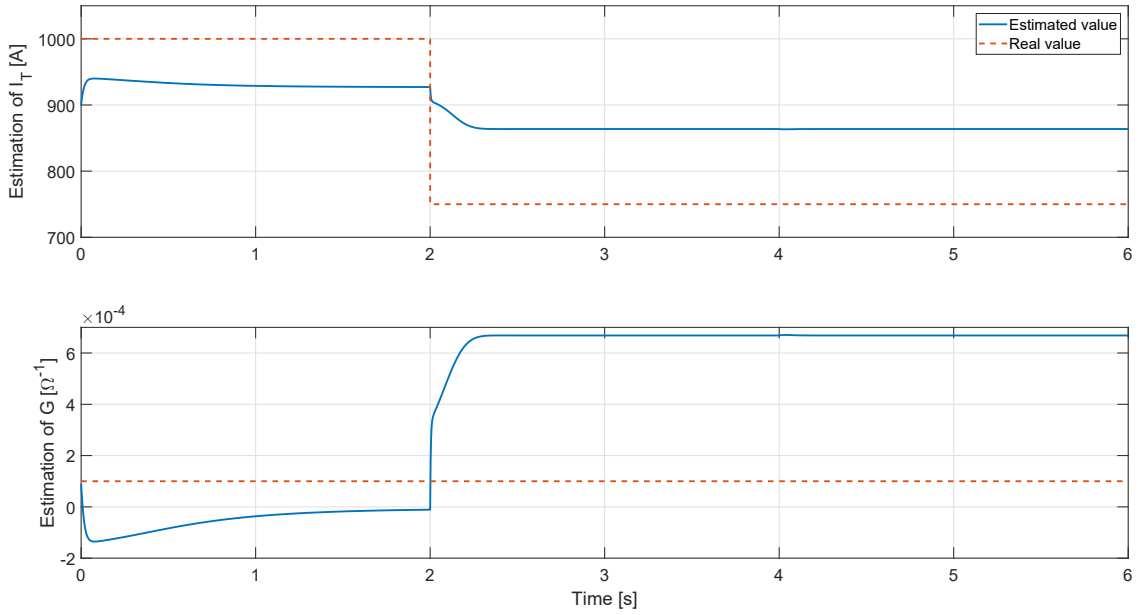

Figure 25: Transmission current and conductance estimation for a 10% of initial error.

parameter, the following approach aims to design an estimator focused on the inductor resistor of the VSC.

For this purpose, two different methods are applied as demonstrated in section 4.4. In the first method, the estimator is designed based on a single dynamical equation from the VSC, which depending on the requirements can vary between $\dot{\psi}_d$ and $\dot{\psi}_q$. Due to the unsatisfactory results, a second approach is pursued, in which the estimation is based on both inductance fluxes dynamics, simultaneously.

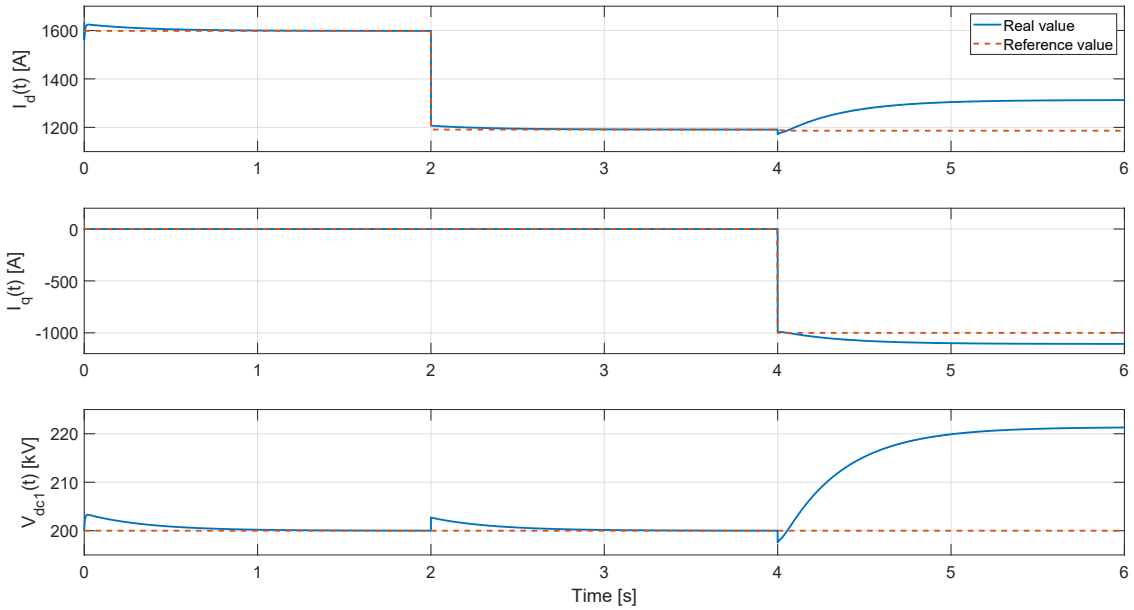

Figure 26: VSC AC currents and DC voltage with I&I philosophy for R estimation from one equation.

When working with the approach on which the flux equations are used individually, figures 26 and 27 show system's performance. The first figure focuses again on the state variables, depicting a proper parameter estimation during the initializing period and after the step introduced for the transmission current. However, once the reactive current references is changed, the estimator is not able to follow the real value and stabilizes on 0.2 Ω. Considering the real resistor value is 0.075 Ω, this is an error of 166.6%.

The non-desired behaviour can be explained when considering estimator functioning and design, which explained in 4.4. In relation to what has already been discussed in depth in that section, the controller chooses by design the flux equation to be used. If the converter is asked to provide exclusively direct current, the equation of quadrature flux ($\dot{\psi}_q$) is applied. On the other hand, whenever the converter is only required to deliver quadrature current, the direct flux ($\dot{\psi}_d$) equation is used for the estimator design. It is in these particular cases that the term including the erroneous inductor value is omitted, as it is multiplied by what is supposed to be zero. However, as an be seen in figure 26, the estimator fails to find the correct value when both currents are required to be non-zero, as the estimator starts to malfunction since the quadrature current reference is applied in second 4. At this point, regardless of the equation used, the term containing L is not removed. This affects directly the estimator, polluting the update law, with the corresponding deviation in the resistor estimated value.

For that reason, the design is improved considering both flux equations at the same time; as explained theoretically in 4.4.3. Implementing a properly defined $\beta(\psi_d, \psi_q)$, the terms including the erroneous inductor value are removed between themselves. Consequently, the value of L is no longer appearing in γ, which is reflected in the proper functioning of the system. As a conclusion, satisfactory results are obtained as shown in the following figures 28 and 29.

Considering what is depicted in 28, the state variables follow the established references appropri-

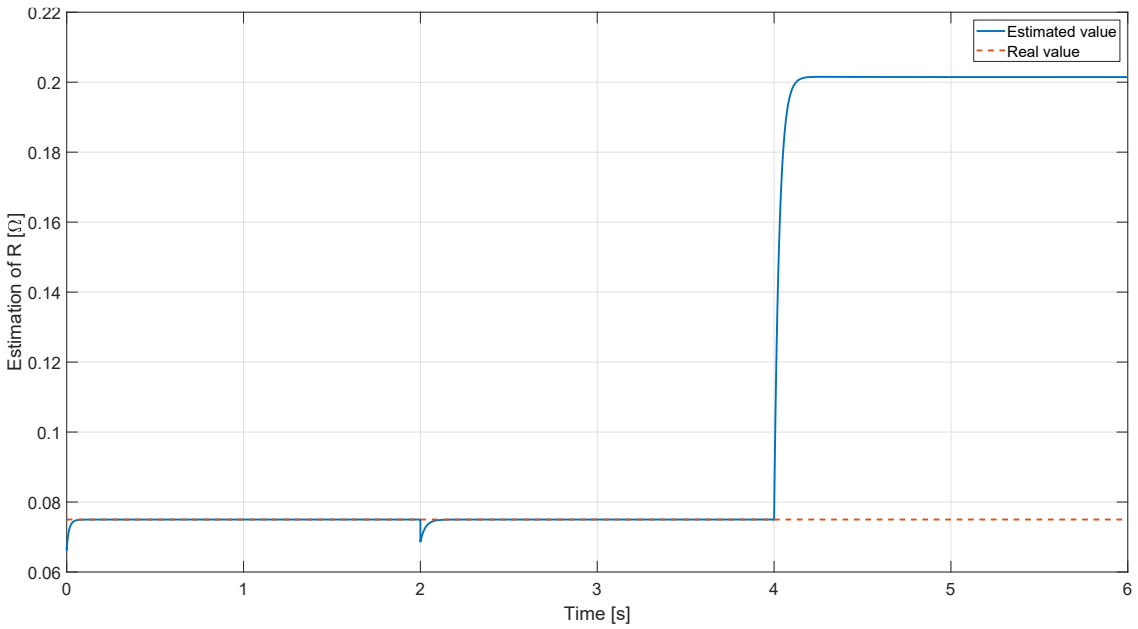

Figure 27: Inductor resistance estimation for a 10% of initial error.

ately. The direct current hardly reaches the maximum and minimum values of 1624A and 1171A when initializing and changing the quadrature current reference respectively. These deviations mean errors of 1.6 %, which are rapidly reduced. The quadrature current, meanwhile, follows the reference closely.

Estimator parameters	
λ'	ρ
25	1000^2

Table 7: R estimator parameters.

When talking about the DC voltage level, it is confirmed that the performance of the system is enhanced by the implementation of both flux equations at the same time. With a maximum oscillation of 3 kV during transient periods, the voltage reference is correctly followed when the two current dynamics are used in the design.

The correct operation can be also corroborated looking at the estimator dynamic in figure 29. Unlike in the previous case, as mentioned before, this estimator is capable of finding the correct value of the parameters even if both the active and reactive currents are non-zero. For that reason, the estimator presents a peak in the fourth second, reaching a resistor estimated value of 0.082 Ω; which is rapidly reduced up to the real value.

Focusing on the speed of response in the time period from 1.9 to 2.3 seconds, i.e. when the direct current step is introduced, the behaviour is in line with the parameters presented in table 7, since the estimator stabilizes in four or five times λ^{-1}.

5.4.5 EBBA outer-loop: Estimation of R and G

Once the single estimators both for the DC conductance and the AC resistance have been analysed, the single design for both parameters is tested via time-domain simulations in this section. A grid forming strategy with the same reference steps is still used as in the previous sections, analysing a single converter without any disturbance from the DC transmission line.

The estimator has been tuned with the parameters shown in table 8. The used ρ values are the

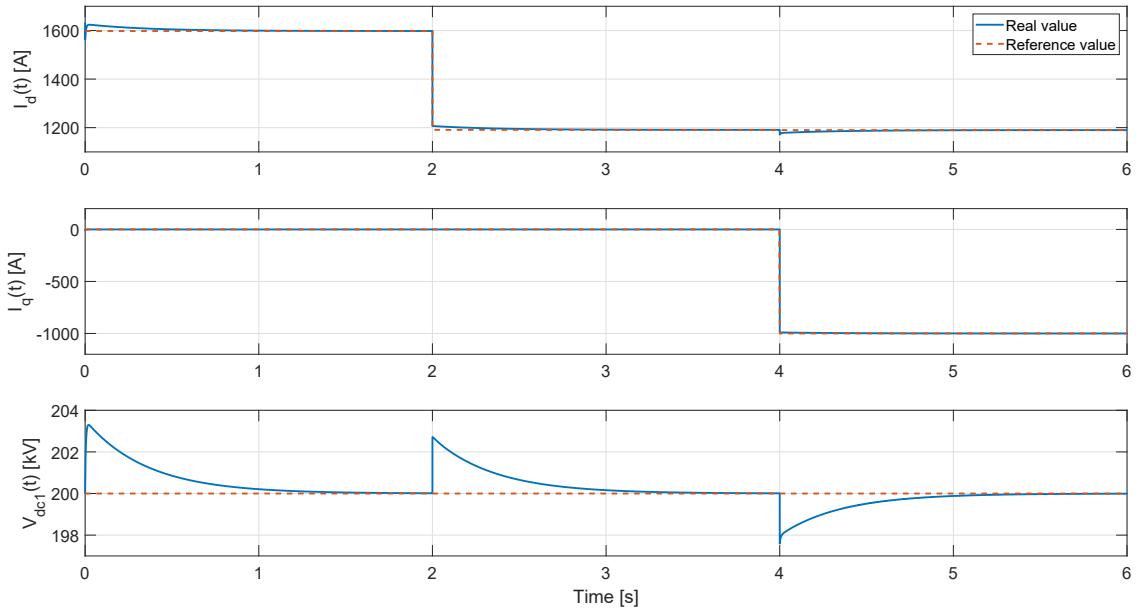

Figure 28: VSC AC currents and DC voltage with I&I philosophy for R estimation from two equations.

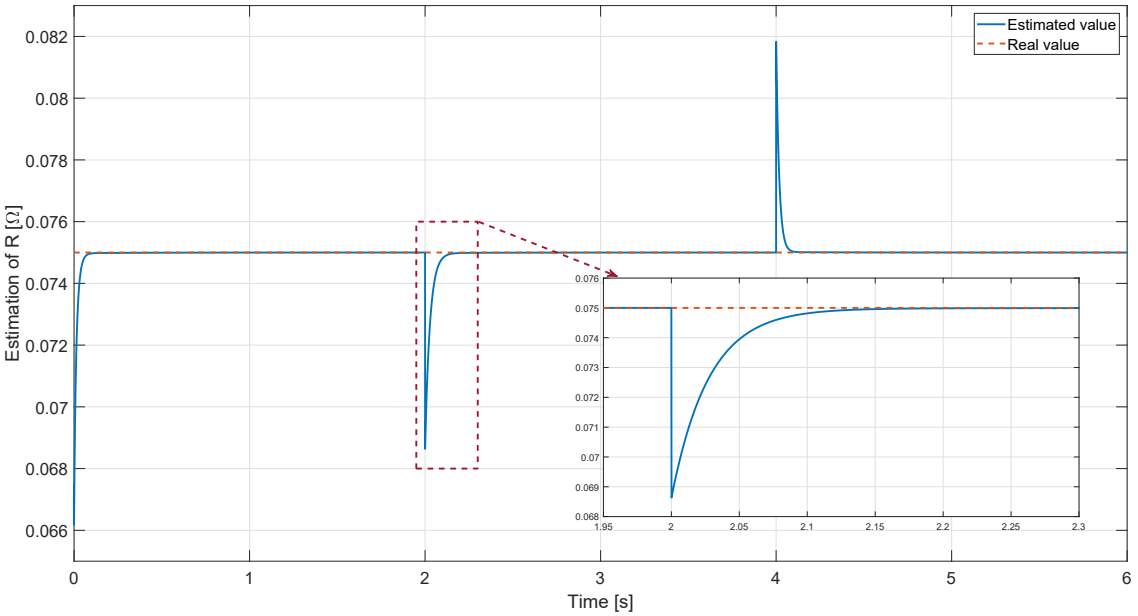

Figure 29: Inductor resistance estimation for a 10% of initial error.

same than in section 5.4.2 and 5.4.4. The obtained AC direct-quadrature currents and DC voltage are depicted in figure 30.

Estimator's parameters		
	λ'	ρ
R	100	1000^2
G	100	$(200 \cdot 10^3)^2$

Table 8: AC resistance and DC conductance estimator parameters

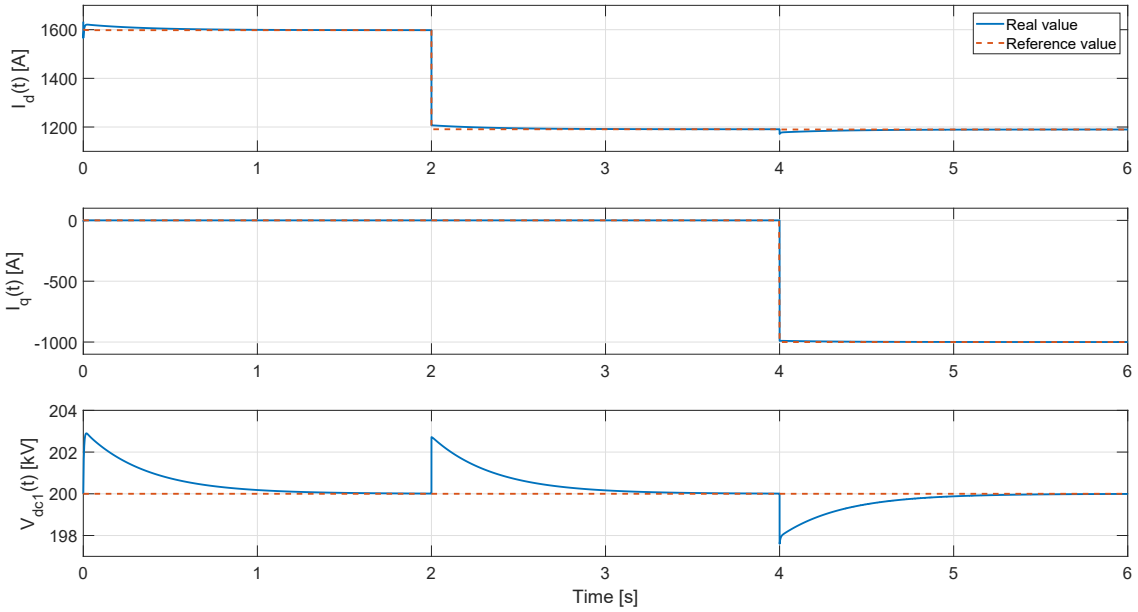

Figure 30: VSC AC currents and DC voltage with I&I philosophy for R and G estimation.

By analysing figure 30, it can be seen that the behaviour of both currents and voltage is almost identical to the ideal case of non-erroneous parameters. Therefore, from this first simulation it can be said that the estimator is able to correct the possible errors in the knowledge of R and G.

Looking at the estimation performance in figure 31, a fast tracking of the parameters is observed. During the approach of the first mili-seconds, it is seen that the estimation of R is faster than for G. This is caused by the disturbance that the direct current has over the estimator. Since the current is of around 1600 A and the chosen ρ is of 1000^2, the actual λ value is increased, reducing the system's time constant.

Nonetheless, this simulation has been run without introducing an error in the inductance and capacitance values to calculate $\beta(x)$, a requirement which is fundamental for the calculation of the estimations. As commented in section 4.6, this fact should have an effect on the transient behaviour, but the steady-state solution should be kept right.

Figure 32 depicts the estimations of R and G for a variety of inductance and capacitance errors. Apart from the already analysed estimation, simulations with errors of -20%, -10%, +10% and +20% in both inductance and capacitance have been performed.

It can be seen that although larger peaks appear during transient operation, the steady-state solution reaches the actual parameter value. A zoom of these curve is represented in figure 33 between seconds 1.98 and 2.10 to analysed the transient behaviour.

The DC current step in the second two is responsible of the estimation step both for the resistance and the conductance. This occurs because until the dynamics of the update law correct the error of the inductance and capacitance, the calculated $\beta(x)$ is incorrect. Nevertheless, the stabilization time is still low, around 30 mili-second.

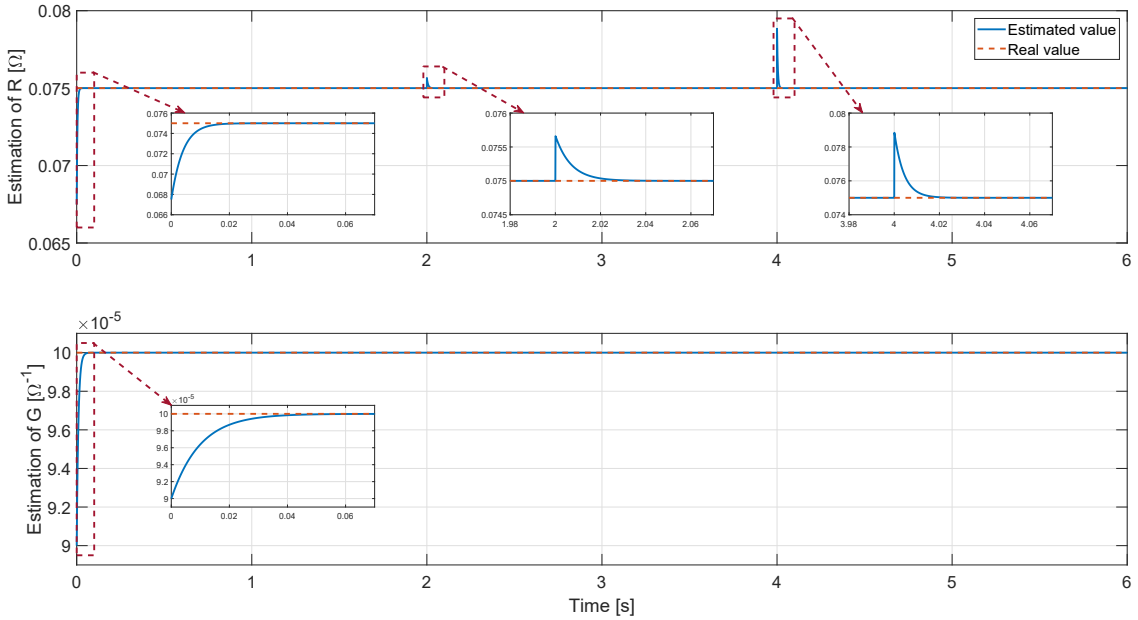

Figure 31: R and G estimations.

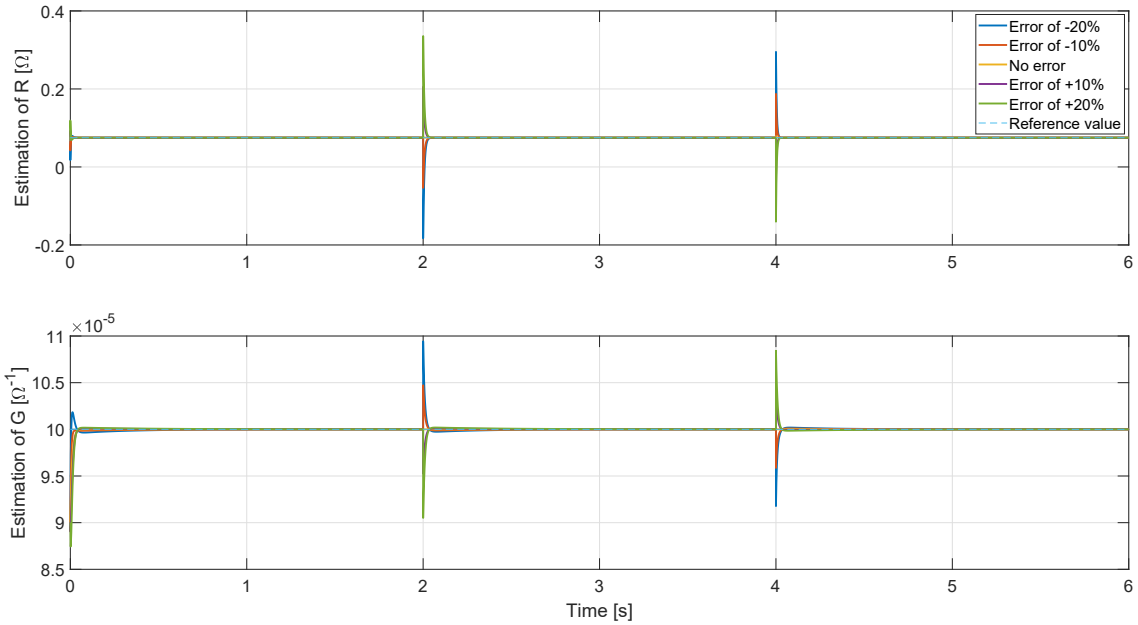

Figure 32: R and G estimations for different inductance and capacitance error.

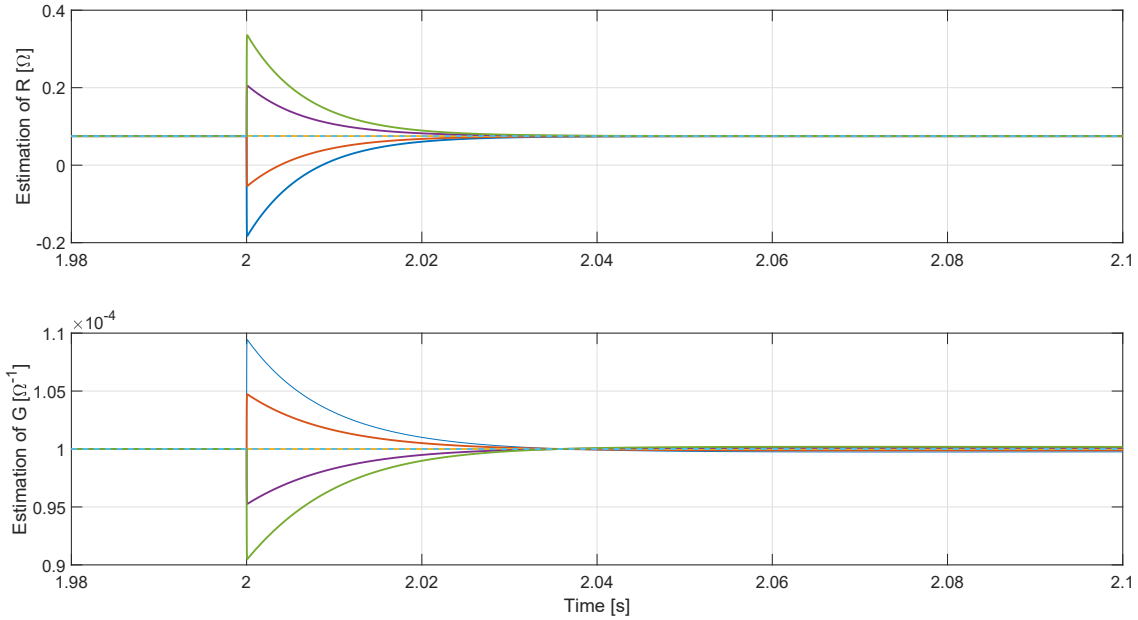

Figure 33: Zoom of R and G estimations for different inductance and capacitance error.

Figures 34 and 35 show the AC currents and DC voltage for the different errors. The second figure represents the curve between seconds 4 and 4.5.

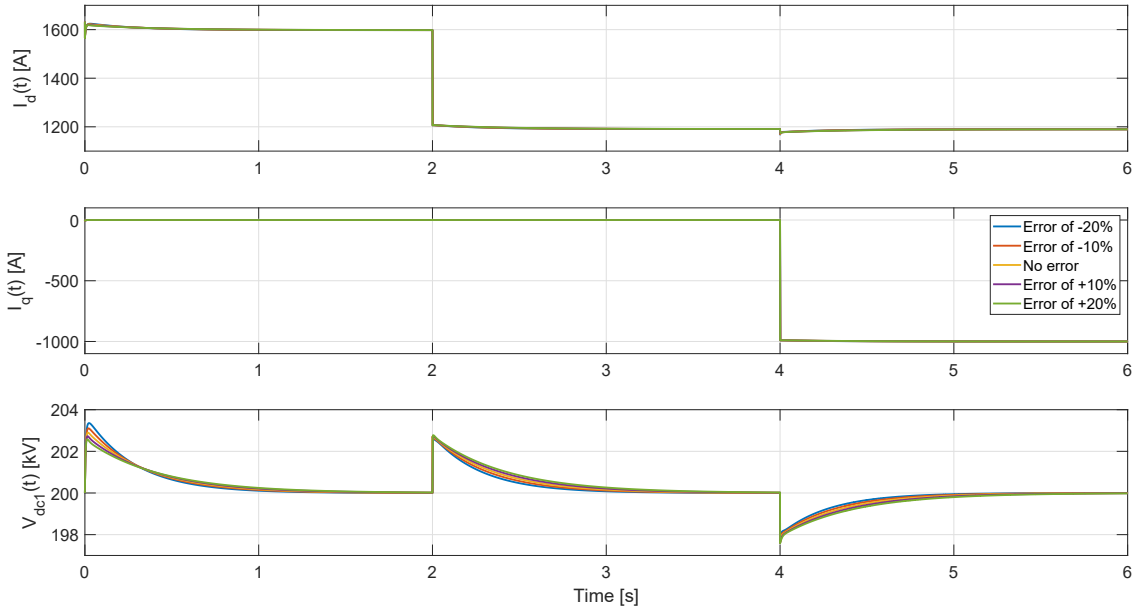

Figure 34: VSC AC currents and DC voltage with I&I philosophy for R and G estimation and for different inductance and capacitance error.

Comparing with figure 30, neither the currents nor the voltage have a different behaviour due to the estimation errors of the parameters during the first mili-seconds. Looking at figure 35, it can be seen that although there is a small change in the behaviour, it is not significant. In case of the DC voltage, the minimum peak caused by the reactive current step keeps the same value. The same observation can be made for the different simulated steps.

Now that this design has been validated numerically, it is interesting to evaluate its performance after the introduction of a DC transmission grid. For this simulation the second terminal will be presented by an ideal voltage source, aiming to avoid introducing the second terminal controller details, for the sake of simplicity. The use of an HVDC transmission system allows the implement-

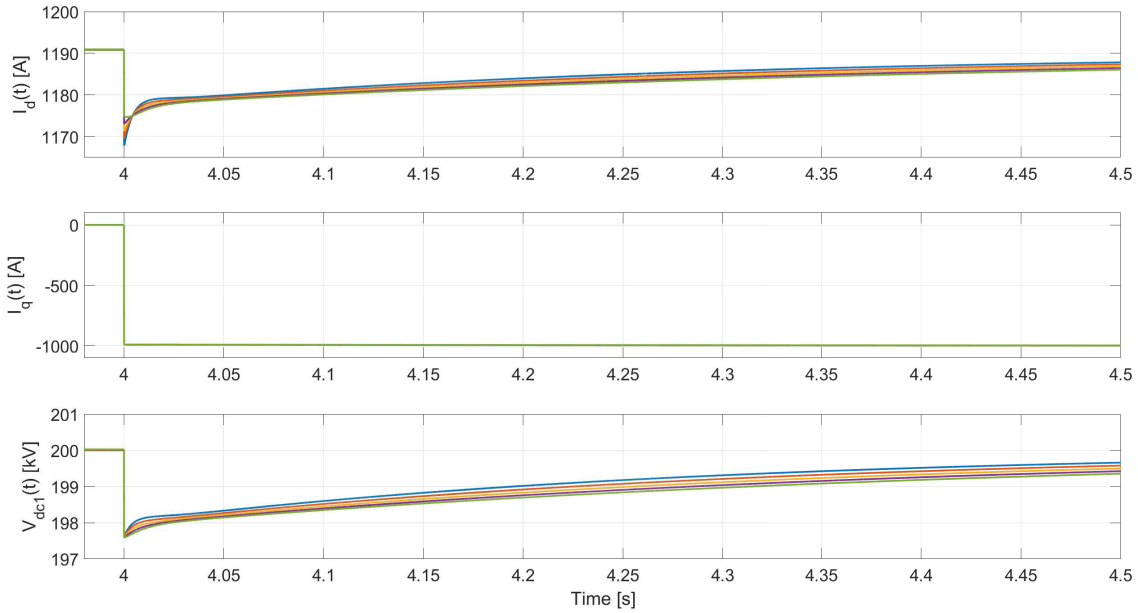

Figure 35: Zoom of VSC AC currents and DC voltage with I&I philosophy for R and G estimation and for different inductance and capacitance error.

ation of a grid feeding strategy. The inductance value error has been multiplied by a factor of 1.1 whilst the capacitance has been decreased a 10%. These error have been applied in order to simulate parametric uncertainties of a real situation as much as possible.

Figure 36 represents the AC currents and DC voltage of the converter. Comparing with the grid forming strategy, the transient periods are shorter in the current simulation. This occurs because the implemented transmission line is adding extra dissipation to the system, accelerating the rate of convergence. However, the voltage disturbances due to the reference steps are larger than in the previous simulations. However, this issue could be further improved by appropriately tuning the PI-PBC parameters.

Nonetheless, from the point of view of this thesis objectives, the system behaves successfully, since the converter reaches the desired equilibrium point.

The estimations, depicted in figure 37, also track the parameters values properly. As with grid forming control, during the references steps there is a disturbance during the first mili-seconds. However, this is eliminated thanks to the update law.

Analysing the estimations dynamics between second 1.98 and 2.10, it can be seen that the curve is not exponential. This is caused due to the fast dynamics of the current and voltage, which disturb the estimations during transient operation. Nevertheless, the real parameter value is correctly traced after few milliseconds.

5.4.6 Two terminal HVDC system

A last simulation has been carried out enabling all the submodules presented in section 5.1. Two terminals are interconnected by means of the HVDC transmission line used in section 5.4.5. The first terminal uses a grid forming strategy, regulating both the DC voltage in the grid and the AC side reactive power. On the other hand, the second converter is in grid feeding mode of operation, imposing the injected or absorbed active and reactive power towards the AC grid. The system is operated in a *centralized* manner, so it is required that the terminals are able to communicate.

Both control strategies are based on the EBBA outer-loop, and hence, each terminal is responsible for estimating their AC grid side resistances and their DC side conductance. Both sides have been tuned with the parameter shown in table 9.

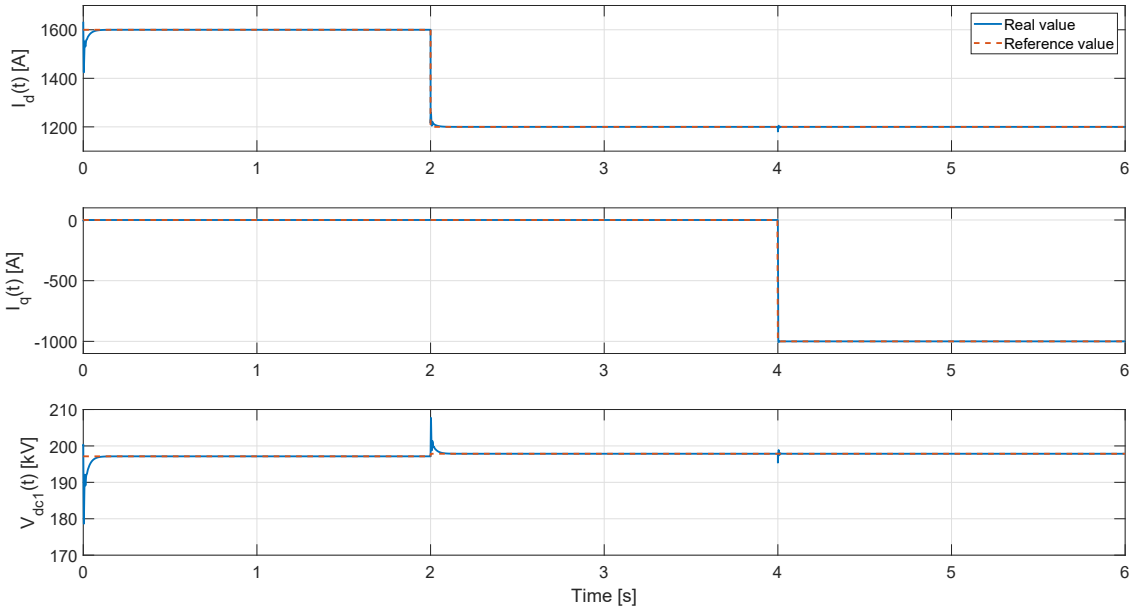

Figure 36: VSC AC currents and DC voltage with I&I philosophy for R and G estimation and for different inductance and capacitance error (Grid feeder control with DC transmission grid).

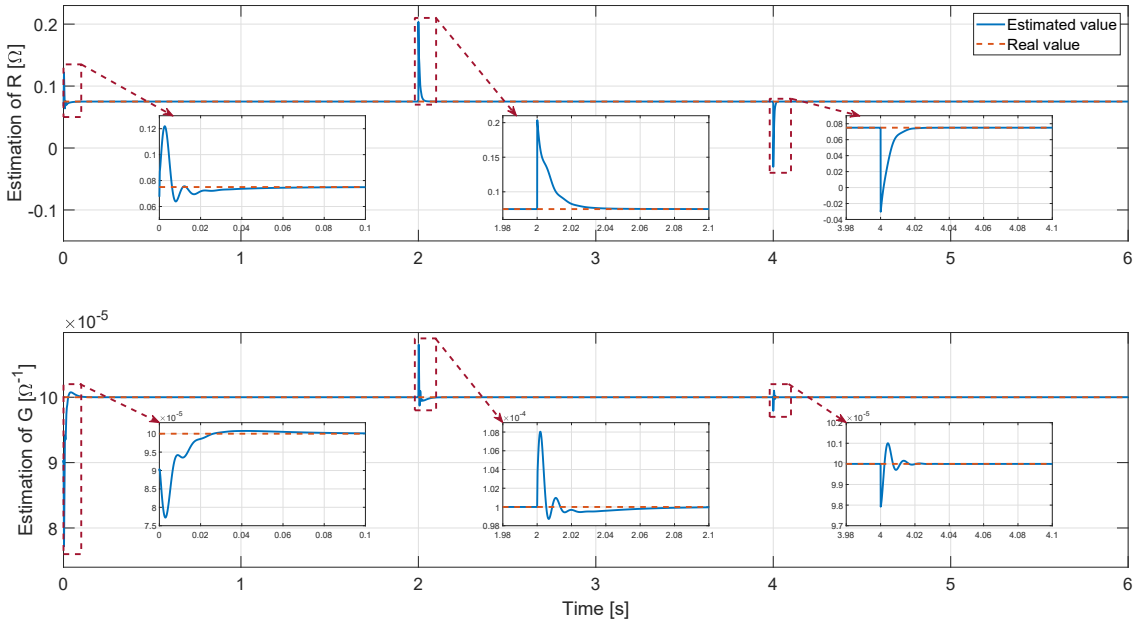

Figure 37: Zoom of R and G estimations for different inductance and capacitance error (Grid feeder control with DC transmission grid).

Terminals parameters					
PI-PBC		EBBA outer-loop			
K_p	K_i	λ_R	ρ_R	λ_G	ρ_G
$5 \cdot 10^{-8}$	$1 \cdot 10^{-8}$	100	1000^2	100	$(200 \cdot 10^3)^2$

Table 9: Terminals PI-PBC and EBBA controler parameters

For this last test, multiple reference steps have been applied during the 12 seconds simulation. During this time period the converters should be able to inject and absorb a certain amount of reactive power. The active power flow is also suddenly reversed in order to test the performance of the system under a large disturbance. In case of the grid forming converter, it should be able to maintain the DC voltage at 200 kV, whilst the grid feeding one must absorb or inject the desired current onto the transmission grid. The chosen reference steps are summarize in table 10.

	Termina 1		Terminal 2	
	V_{dc1} (kV)	I_q (A)	I_d (A)	I_q (A)
Initial cond.	200	0	-1633	0
Sec. 2	200	0	-1000	0
Sec. 4	200	-1000	-1000	-1000
Sec. 6	200	-1000	1000	-1000
Sec. 8	200	-1000	1000	250
Sec. 10	200	500	1000	250

Table 10: Terminal references though the simulation

Figure 38 depicts the AC currents and DC voltages of both terminals. Analysing the active current, each terminal absorb or inject current with almost the same magnitude but in the opposite direction. This is because the active power must flow from one side to another. Looking at the steps, the PI-PBC has been able to follow the references without any error during the steady state. However, these variations are responsible for the larger DC voltage disturbances in both sides. In case of the sixth second, there is a voltage peak of around 30% in the first terminal and a drop of the same magnitude in the second terminal. However, this issue can be solve as in previous simulations by means of a better tuning of the controller.

On the other hand, the terminals are able to absorb or inject the required reactive power. The voltage disturbances due to the q-current dynamics are not significant compared with previous steps. Looking to the DC current in figure 39 (positive current when power flows towards terminal 1), it can be seen that the variations of current occurs during the active power steps. In case of reactive current steps, the DC current is just disturbed.

At figure 40 the voltages shown in figure 38 and the DC current are compared after the active power reversal, i.e. under the largest disturbance. It can be observed that the time period between the step and the voltages peaks is the same than between the step and the moment at which the DC current reaches to the steady-state values. This occurs as the AC current dynamics are faster than the DC current ones. Consequently, during a small lapse of time, there is a power unbalance between AC and DC sides, so the converter extracts or injects charge to the capacitor in order to provide the power difference.

On the other side, analysing the estimations shown in figure 41, the same results than in the previous section are obtained. After any reference step, the disturbance introduced by the current or voltage variation are correctly eliminated by the update law.

In conclusion, even though the dynamics of the system could be improved, convergence to the equilibrium of the system is guaranteed. After trying a variety of operation points the system has never been unstable, proving the effectiveness of the developed global stability certificate. However, it must be taken into account that a communication link between both terminals is fundamental for the correct operation of the adaptive control law.

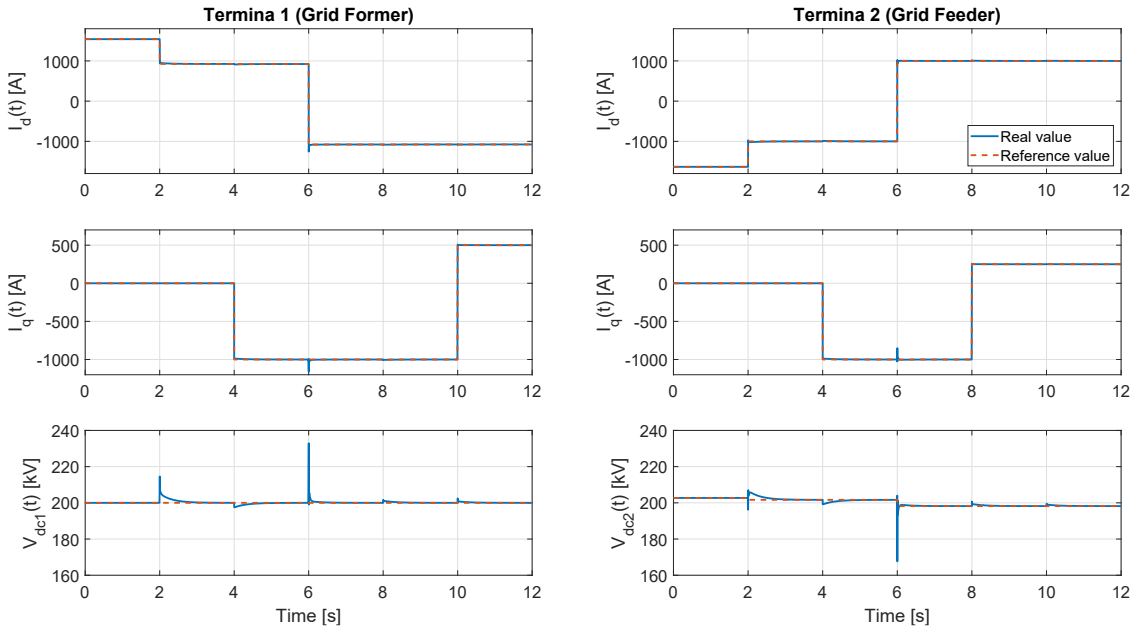

Figure 38: Both terminals AC currents and DC voltages.

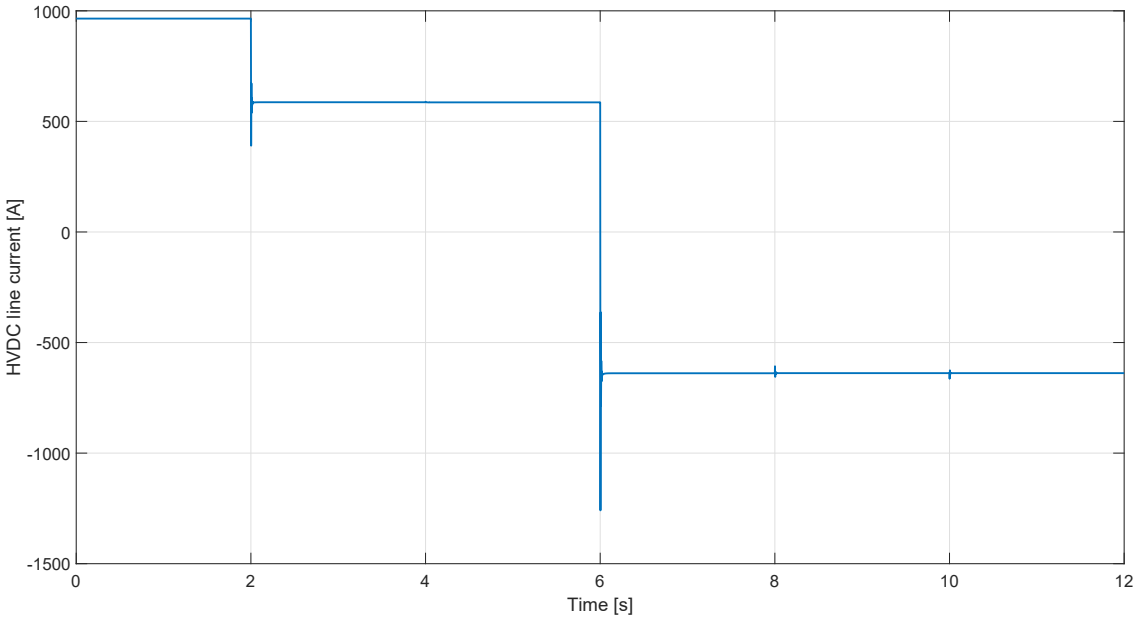

Figure 39: DC transmission line current (Reference from terminal 2 to 1).

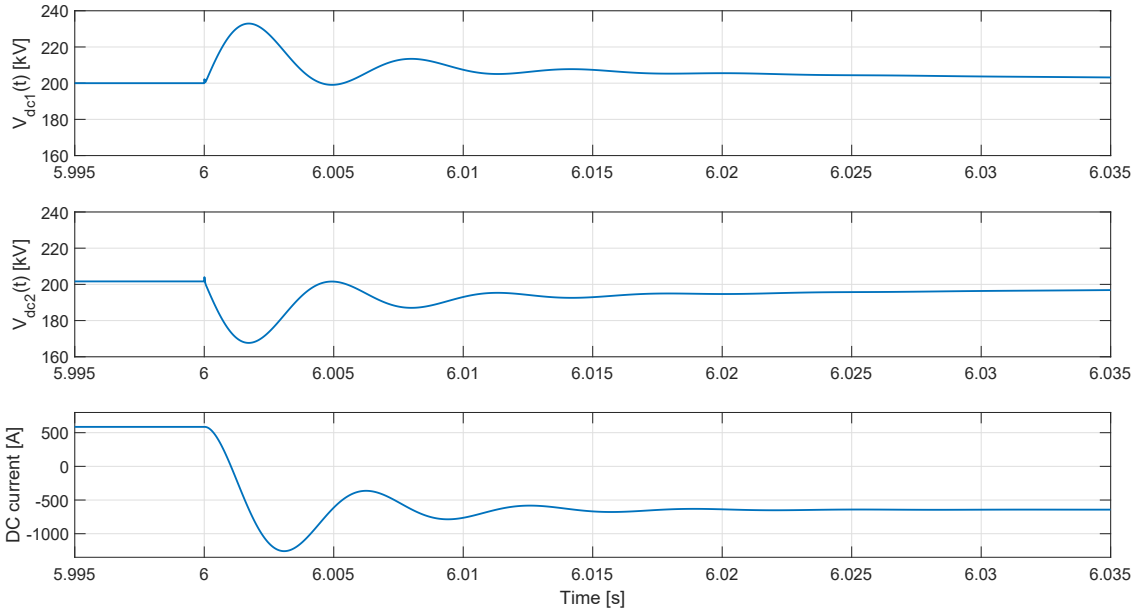

Figure 40: Zoom of both terminals DC voltages and DC transmission line current.

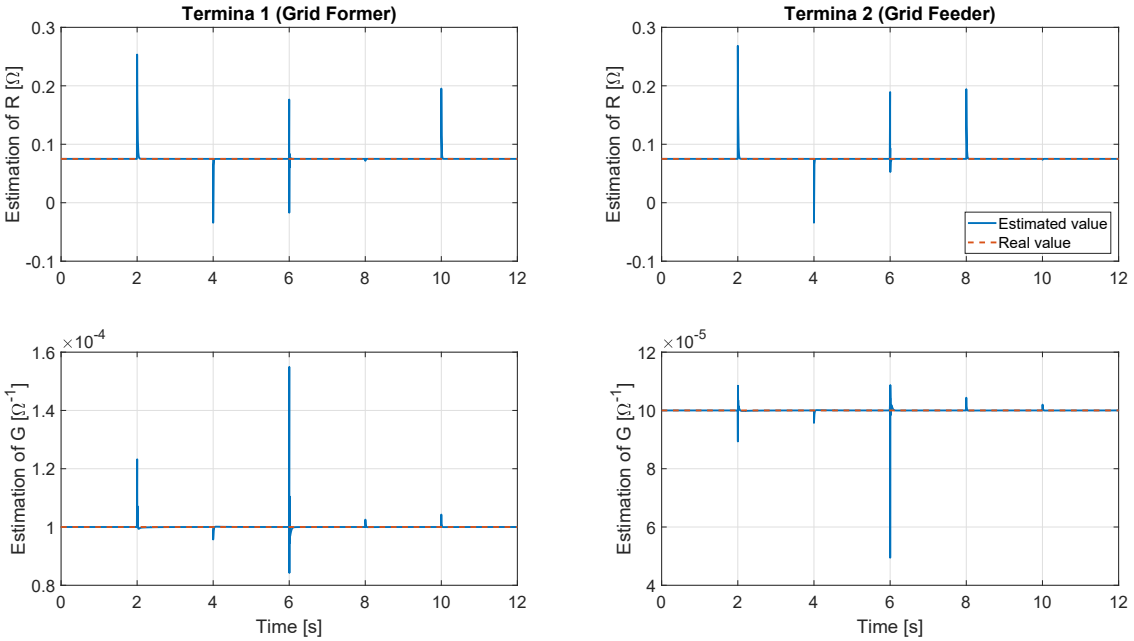

Figure 41: Both terminals R and G estimations.

5.5 Discussion of Results

Throughout this thesis several results have been obtained and evaluated, both from analytical development and from numerical simulations. In this chapter the most relevant ones will be discussed with the aim of bringing a brief summary of the accomplished objectives.

The first goal of this project is to control Voltage Source Converters via PI-Passivity Based Control while also reviewing its global asymptotic stability guarantees. This certificate is obtained by means of Lyapunov theory, which brings an analytical proof taking into account the highly nonlinear nature of these converters.

This certificate has been validated in section 5.4.6 for a two terminal HVDC power system, where a variety of desired equilibrium points were evaluated successfully. Some little over- and under-voltages were observed during the largest steps of active power. Nonetheless, these transient dynamics are not of interest for this thesis, as they can be corrected by means of an optimal tuning of the PI-PBC parameters. Moreover, additional control methods are recommended in chapter 6.2.

Furthermore, the main objective of the thesis is achieved with the development of an estimator of AC side filters resistances and DC side conductance based on the Immersion&Invariance methodology. Thanks to the implementation of this estimator, the error introduced into the system load flow computation is removed, obtaining the exact desired equilibrium point. Consequently, power-balance mismatches are avoided during the operation.

During simulations, it has been seen how estimators tracks both parameters in a few millisecond. Some disturbances appears during the variations of the equilibrium point, but they are rapidly corrected thanks to the robustness of the update law γ, which can be also interpreted from energy-balance point of view.

On the other hand, both the converter and the control can be interpreted from an energetic point of view. This gives a greater insight in how the designed estimator uses balancing mechanisms that are routed in the power preservation principles of the converter. Furthermore, the parameters estimator is combined with the converter load flow solution which ended in our main result, the called EBBA outer-loop, which replaces the traditional outer-loop based on the comparison between instantaneous DC voltage of active power and their references.

6 CONCLUSIONS AND FUTURE WORKS

This section presents the general conclusions of the manuscript as well as proposing research lines for future works that may help to improve different features which have not been addressed.

6.1 Conclusions

The present work unifies different control philosophies, perspectives and techniques in order to design a robust control method, with a large-signal stability certificate. The main contribution is an *Energy Balance Based Adaptive Controller (EBBA)* which has been implemented for a couple of 2-Level Voltage Source Converters which, together with the transmission line, constitute the simplest functional HVDC system.

Initially, a brief technology review is presented, introducing the current state of the art of HVDC converters and transmission line models. Later on, VSCs are addressed in detail, exposing the main equations that govern their operation. This recapitulation is concluded with a summary of traditional control methods, including open and closed loop control methods.

Bearing in mind the final target of the work, a more specialized literature review is performed, delving deeper into concepts such us port-Hamiltonian representation, Passivity Based Controllers, Lyapunov function and Inmersion&Invariance. Having performed an overall review, all the previously mentioned concepts are put into practice simultaneously giving as a result the EBBA.

When dealing with complex and ever-growing electrical systems, the final objective is to transfer power from the point where the resource is located to the final consumer. In order to preserve the system stability certificate as the system expands and/or changes, we chose to base our work on the PI-PBC control method, with well-known *Plug&Play* features. Towards this end, we began by making use of the Port-Hamiltonian representation as a starting point for the HVDC system modelling and gaining insight in the PI-PBC control design. This strategy is indeed strongly rooted in Lyapunov function stability theory and ensures that the system will tend to the desired point regardless of system initial state. Finally, in order to avoid the computation of possible erroneous equilibrium points, the I&I methodology is used for the design of estimators that obtain the accurate value of system parameters.

Thanks to the joint use of all these various resources, different controller testings and developments are performed trying to solve the encountered weaknesses or deficiencies. Starting with the estimation of a single unknown parameter for a unique VSC, the process migrates towards the combined use two estimators. At the end, estimators for linkage resistance and system's conductance are implemented in the mentioned two VSC HVDC system. This case includes the already mentioned EBBA outer-loop controller.

6.2 Future Works

A future research line pertains to the testing, and adapting if needed, of EBBA controller on multi-terminal systems composed by multi-level VSCs. Further on, migration to decentralized systems would be of interest, as it would reduce dependence on communications through the appropriate use of estimators. All of these ideas do not go far beyond what has been mentioned in section 1.3.

However, potential challenges and enhancements have also appeared for the specific EBBA case. In the first instance, the tests presented show an improvable stabilisation time. For that reason, it is concluded that a more accurate proportional-integer tuning is required; as current PIs are arbitrarily adjusted to provide an acceptable performance. Until now, system's dynamic depends highly on the power dissipation attached to the conductance. When increasing this parameter, the system is faster but also has an impact on the power delta between sending and receiving terminals. Therefore, the inclusion of a virtual resistance that is capable of having influence on the speed is presented as a promising solution.

Additionally, existing current but, specially, voltage peaks should be limited in order to preserve the system and protection integrity. For this, different alternatives appear. On the one hand, it would be positive to work on reducing the differences between the rates of convergences associated to the different electrical variables. Considering the current is significantly faster than voltage dynamic; if the former is reduced, large voltage drops could be avoided. On the other hand, the sizing of system parameters could be further examined, specially the converter capacitance; hindering these falls.

Finally, it would be interesting to devote effort in understanding the potential performance of the system when applying ramp profiles instead of steps. This is due to the incremental model design, which is designed to be used with non-varying equilibrium points. However, ramp profiles imply a fluctuation of this point, having a direct consequence on the Lyapunov function. It would therefore be crucial to know whether this type of reference destroys the stability certificate or not.

Bibliography

[1] J Á Acosta et al. 'A constructive solution for stabilization via immersion and invariance: The cart and pendulum system'. In: *Automatica* 44.9 (2008), pp. 2352–2357. ISSN: 00051098. DOI: 10.1016/j.automatica.2008.01.006.

[2] Abdulrahman Alassi et al. 'HVDC Transmission: Technology Review, Market Trends and Future Outlook'. In: *Renewable and Sustainable Energy Reviews* 112.June (2019), pp. 530–554. ISSN: 18790690. DOI: 10.1016/j.rser.2019.04.062. URL: https://doi.org/10.1016/j.rser.2019.04.062.

[3] Alin Albu-Schäffer, Christian Ott and Gerd Hirzinger. 'A unified passivity-based control framework for position, torque and impedance control of flexible joint robots'. In: *International Journal of Robotics Research* 26.1 (2007), pp. 23–39. ISSN: 02783649. DOI: 10.1177/0278364907073776.

[4] A Astolfi, R Ortega and A Venkatraman. 'A globally exponentially convergent immersion and invariance speed observer for mechanical systems with non-holonomic constraints'. In: *Automatica* 46.1 (2010), pp. 182–189. ISSN: 00051098. DOI: 10.1016/j.automatica.2009.10.027. URL: http://dx.doi.org/10.1016/j.automatica.2009.10.027.

[5] Alessandro Astolfi, Dimitrios Karagiannis and Romeo Ortega. 'Nonlinear and adaptive control with applications'. In: *Communications and Control Engineering*. 9781848000650. 2008, pp. 1–290. ISBN: 978-1-84800-065-0. DOI: 10.1007/978-1-84800-066-7. URL: https://www.springer.com/gp/book/9781848000650.

[6] Jef Beerten, Salvatore D'Arco and Jon Are Suul. 'Frequency-dependent cable modelling for small-signal stability analysis of VSC-HVDC systems'. In: *IET Generation, Transmission and Distribution* 10.6 (2016), pp. 1370–1381. ISSN: 17518687. DOI: 10.1049/iet-gtd.2015.0868.

[7] Gilbert Bergna-Diaz et al. 'PI Passivity-Based Control and Performance Analysis of MMC Multiterminal HVDC Systems'. In: *IEEE Journal of Emerging and Selected Topics in Power Electronics* 7.4 (2019), pp. 2453–2466. ISSN: 21686785. DOI: 10.1109/JESTPE.2018.2889152.

[8] Felix Berkenkamp et al. 'Safe learning of regions of attraction for uncertain, nonlinear systems with Gaussian processes'. In: *2016 IEEE 55th Conference on Decision and Control, CDC 2016* Cdc (2016), pp. 4661–4666. DOI: 10.1109/CDC.2016.7798979. arXiv: 1603.04915.

[9] Pablo Borja, Romeo Ortega and Emmanuel Nuño. 'New results on PID passivity-based controllers for port-Hamiltonian systems'. In: *IFAC-PapersOnLine* 51.3 (2018), pp. 175–180. ISSN: 24058963. DOI: 10.1016/j.ifacol.2018.06.049. URL: https://doi.org/10.1016/j.ifacol.2018.06.049.

[10] Pablo Borja, Romeo Ortega and Jacquelien M.A. Scherpen. 'New Results on Stabilization of Port-Hamiltonian Systems via PID Passivity-Based Control'. In: *IEEE Transactions on Automatic Control* 66.2 (2021), pp. 625–636. ISSN: 15582523. DOI: 10.1109/TAC.2020.2986731.

[11] Massimo Ceraolo and Davide Poli, eds. *Fundamentals of Electric Power Engineering*. Hoboken, New Jersey: John Wiley & Sons, Inc., Apr. 2014. ISBN: 9781118922583. DOI: 10.1002/9781118922583. URL: http://doi.wiley.com/10.1002/9781118922583.

[12] Salvatore D'Arco, Jon Are Suul and Jef Beerten. 'Analysis of accuracy versus model order for frequency-dependent Pi-model of HVDC cables'. In: *2016 IEEE 17th Workshop on Control and Modeling for Power Electronics, COMPEL 2016* (2016), pp. 27–30. DOI: 10.1109/COMPEL.2016.7556700.

[13] Salvatore D'Arco, Jon Are Suul and Marta Molinas. 'Implementation and analysis of a control scheme for damping of oscillations in VSC-based HVDC grids'. In: *16th International Power Electronics and Motion Control Conference and Exposition, PEMC 2014* (2014), pp. 586–593. DOI: 10.1109/EPEPEMC.2014.6980558.

[14] European Parliament. 'Directive (EU) 2018/2001 of the European Parliament and of the Council on the promotion of the use of energy from renewable sources'. In: *Official Journal of the European Union* 2018.L 328 (2018), pp. 82–209.

[15] Cuauhtemoc Guerrero et al. 'Control of velocity of DC motors by classical and passivity methods measuring only position: Theory and experimental comparison'. In: *IEEE Latin America Transactions* 18.5 (2020), pp. 962–970. ISSN: 15480992. DOI: 10.1109/TLA.2020.9082926.

[16] Wei He et al. 'Incremental passivity based control for DC-DC boost converters under time-varying disturbances via a generalized proportional integral observer'. In: *Journal of Power Electronics* 18.1 (2018), pp. 147–169. ISSN: 20934718. DOI: 10.6113/JPE.2018.18.1.147.

[17] Michael Hernandez-Gomez et al. 'Adaptive PI stabilization of switched power converters'. In: *IEEE Transactions on Control Systems Technology* 18.3 (2010), pp. 688–698. ISSN: 10636536. DOI: 10.1109/TCST.2009.2023669.

[18] IEA. 'Share of renewables in power generation in the Sustainable Development Scenario'. In: (2020). URL: https://www.iea.org/data-and-statistics/charts/share-of-renewables-in-power-generation-in-the-sustainable-development-scenario-2000-2030.

[19] Bayu Jayawardhana et al. 'Passivity of nonlinear incremental systems: Application to PI stabilization of nonlinear RLC circuits'. In: *Proceedings of the IEEE Conference on Decision and Control* (2006), pp. 3808–3812. ISSN: 01912216. DOI: 10.1109/cdc.2006.377132.

[20] H K Khalil. 'Nonlinear Systems, Third Edition'. In: *Cdswebcernch* (2002), p. 750. ISSN: 03784371. DOI: 10.1016/j.physa.2006.08.011. URL: http://cdsweb.cern.ch/record/1173048.

[21] Hassan K Khalil. *Lyapunov stability*. 2009.

[22] Gen Li, Chuanyue Li and Dirk Hertem. 'HVDC technology overview'. In: *HVDC Grids for Transmission of Electrical Energy: Offshore Grids and a Future Supergrid* (2016), pp. 45–78. DOI: 10.1002/9781119115243.ch3.

[23] Xiangbin Liu et al. 'Immersion and Invariance adaptive control of nonlinearly parameterized nonlinear systems'. In: *IEEE Transactions on Automatic Control* 55.9 (2010), pp. 2209–2214. ISSN: 00189286. DOI: 10.1109/TAC.2010.2052389.

[24] Rogelio Lozano, Bernard Brogliato and I. D. Landau. 'Passivity and global stabilization of cascaded nonlinear systems'. In: *IEEE Transactions on Automatic Control* 37.9 (1992), pp. 1386–1388. ISSN: 15582523. DOI: 10.1109/9.159577.

[25] Sudip K. Mazumder and Eduardo Pilo De La Fuente. 'Transient stability analysis of power system using polynomial Lyapunov function based approach'. In: *IEEE Power and Energy Society General Meeting* 2014-Octob.October (2014), pp. 5808–5815. ISSN: 19449933. DOI: 10.1109/PESGM.2014.6939524.

[26] Romeo Ortega and Eloísa García-Canseco. 'Interconnection and damping assignment passivity-based control: A survey'. In: *European Journal of Control* 10.5 (2004), pp. 432–450. ISSN: 09473580. DOI: 10.3166/ejc.10.432-450.

[27] Romeo Ortega, Liu Hsu and Alessandro Astolfi. 'Immersion and invariance adaptive control of linear multivariable systems'. In: *Systems and Control Letters* 49.1 (2003), pp. 37–47. ISSN: 01676911. DOI: 10.1016/S0167-6911(02)00341-9.

[28] Romeo Ortega et al. 'Control by interconnection and standard passivity-based control of port-hamiltonian systems'. In: *IEEE Transactions on Automatic Control* 53.11 (2008), pp. 2527–2542. ISSN: 00189286. DOI: 10.1109/TAC.2008.2006930.

[29] Romeo Ortega et al. 'Interconnection and damping assignment passivity-based control of port-controlled Hamiltonian systems'. In: *Automatica* 38.4 (2002), pp. 585–596. ISSN: 00051098. DOI: 10.1016/S0005-1098(01)00278-3.

[30] Romeo Ortega et al. 'Orbital stabilization of nonlinear systems via the immersion and invariance technique'. In: *International Journal of Robust and Nonlinear Control* 30.5 (2020), pp. 1850–1871. ISSN: 10991239. DOI: 10.1002/rnc.4861. arXiv: 1810.00601.

[31] Romeo Ortega et al. 'Permanent magnet synchronous motors are globally asymptotically stabilizable with PI current control'. In: *Automatica* 98 (2018), pp. 296–301. ISSN: 00051098. DOI: 10.1016/j.automatica.2018.09.031. arXiv: 1806.01419. URL: https://doi.org/10.1016/j.automatica.2018.09.031.

[32] Marcelo Pérez, Romeo Ortega and José Espinoza. 'Passivity-based PI control of switched power converters'. In: *European Control Conference, ECC 2003* 12.6 (2003), pp. 542–547. DOI: 10.23919/ecc.2003.7085012.

[33] Policy Recommendations. 'Roadmap 2050'. In: *Policy* (). DOI: 10.2833/10759.

[34] Maija Ruska and Juha Kiviluoma. *Renewable electricity in Europe: Current state, drivers, and scenarios for 2020*. 2584. 2011, pp. 1–72. ISBN: 9789513877125.

[35] Olaf Saksvik. 'HVDC technology and Smart Grid'. In: *IET Conference Publications* 2012.616 CP (2012), pp. 1–6. DOI: 10.1049/cp.2012.2169.

[36] La Salle. 'C3. Lyapunov Stability and Stability Regions of Nonlinear'. In: (2007), pp. 29–50.

[37] Shankar Sastry. *Nonlinear Systems*. Vol. 10. Interdisciplinary Applied Mathematics. New York, NY: Springer New York, 1999. ISBN: 978-1-4419-3132-0. DOI: 10.1007/978-1-4757-3108-8. URL: https://link.springer.com/content/pdf/10.1007%7B%5C%%7D2F978-1-4757-3108-8.pdf%20http://link.springer.com/10.1007/978-1-4757-3108-8.

[38] Arjan Van Der Schaft. 'Port-Hamiltonian systems : an introductory survey'. In: 3 (2006), pp. 1339–1365. URL: https://research.utwente.nl/en/publications/port-hamiltonian-systems-an-introductory-survey.

[39] A. Shiriaev et al. 'On global properties of passivity-based control of an inverted pendulum'. In: *International Journal of Robust and Nonlinear Control* 10.4 (2000), pp. 283–300. ISSN: 10498923. DOI: 10.1002/(SICI)1099-1239(20000415)10:4⟨283::AID-RNC473⟩3.0.CO;2-I.

[40] F. Silva, T. Hélie and W. Victor. 'Port-Hamiltonian Representation of Dynamical Systems. Application to Self-Sustained Oscillations in the Vocal Apparatus'. In: 2019. URL: https://hal.archives-ouvertes.fr/hal-03020400/.

[41] U.S. Energy Information Admnistration. 'Internaltional Energy Outlook 2019'. In: *U.S. Energy Information Administration* September.09 (2019), pp. 25–150. ISSN: 0009-4978.

[42] Arjan Van Der Schaft and Dimitri Jeltsema. 'Port-Hamiltonian systems theory: An introductory overview'. In: *Foundations and Trends in Systems and Control* 1.2-3 (2014), pp. 173–378. ISSN: 23256826. DOI: 10.1561/2600000002.

[43] Neville Watson and Jos Arrillaga. *Power Systems Electromagnetic Transients Simulation*. The Institution of Engineering and Technology, Michael Faraday House, Six Hills Way, Stevenage SG1 2AY, UK: IET, Jan. 2003. ISBN: 9780852961063. DOI: 10.1049/PBPO039E. URL: https://digital-library.theiet.org/content/books/po/pbpo039e.

[44] Bo Yang et al. 'Energy reshaping based passive fractional-order PID control design and implementation of a grid-connected PV inverter for MPPT using grouped grey wolf optimizer'. In: *Solar Energy* 170.April (2018), pp. 31–46. ISSN: 0038092X. DOI: 10.1016/j.solener.2018.05.034.

[45] B. Erik Ydstie. 'Passivity based control via the second law'. In: *Computers and Chemical Engineering* 26.7-8 (2002), pp. 1037–1048. ISSN: 00981354. DOI: 10.1016/S0098-1354(02)00041-8.

[46] Tsuneo Yoshikawa. 'Lyapunov Stability Theory'. In: *Foundations of Robotics: Analysis and Control (MIT Press)* (2003), pp. 272–276.

[47] Burak Yüksel et al. 'Aerial physical interaction via IDA-PBC'. In: *International Journal of Robotics Research* 38.4 (2019), pp. 403–421. ISSN: 17413176. DOI: 10.1177/0278364919835605.

[48] Meng Zhang et al. 'PID Passivity-Based Control of Port-Hamiltonian Systems'. In: *IEEE Transactions on Automatic Control* 63.4 (2018), pp. 1032–1044. ISSN: 00189286. DOI: 10.1109/TAC.2017.2732283.

[49] Daniele Zonetti, Romeo Ortega and Abdelkrim Benchaib. 'Modeling and control of HVDC transmission systems from theory to practice and back'. In: *Control Engineering Practice* 45 (2015), pp. 133–146. ISSN: 09670661. DOI: 10.1016/j.conengprac.2015.09.012. arXiv: arXiv:1406.4392v3.

[50] Daniele Zonetti et al. 'PID passivity-based control of power converters: Large-signal stability, robustness and performance'. In: January (2021). arXiv: 2101.05047. URL: http://arxiv.org/abs/2101.05047.

Appendix

A Mathematical Developments

A VSC Matrix Representation

This appendix section is focused on demonstrating the matrix representation of a VSC set of equations. As known, the converter can be analysed from the point of view of an inverter or a rectifier. In this case, equations are developed as a rectifier, but different alternatives are given at the end of section B.

As a starting point, Kirchhoff's Voltage Law is applied to the converter, getting the following set of three equations in *abc* framework:

$$\begin{aligned} -v_a + \frac{d}{dt}(\psi_a) + Ri_a(t) + V_{QN} + u_a v_{DC} = 0 \\ -v_b + \frac{d}{dt}(\psi_b) + Ri_b(t) + V_{QN} + u_b v_{DC} = 0 \\ -v_c + \frac{d}{dt}(\psi_c) + Ri_c(t) + V_{QN} + u_c v_{DC} = 0 \end{aligned}$$

Where $v_k(t)$ is the AC input voltage, $\psi_k(t)$ are each linkage inductor's flux, R is the resistance in the input of the converter, $i_k(t)$ is the current through inductors, V_{QN} is the voltage between the neutral and the negative side of the DC-capacitor, u_k is the modulation index of each phase and $v_{DC}(t)$ is the capacitor's or DC side voltage. In the same way, it is important to take into account following definitions and properties:

$$L = \frac{\psi_k}{i_k}$$

$$C = \frac{q_C}{v_{DC}}$$

$$i_C = C\frac{dv_{DC}}{dt}$$

So when applied to set of three equations, the next expression is achieved:

$$\begin{aligned} \frac{d}{dt}(\psi_a) = \dot{\psi}_a = v_a - \frac{R}{L}\psi_a - V_{QN} - \frac{1}{C}u_a q_C \\ \frac{d}{dt}(\psi_b) = \dot{\psi}_b = v_b - \frac{R}{L}\psi_b - V_{QN} - \frac{1}{C}u_b q_C \\ \frac{d}{dt}(\psi_c) = \dot{\psi}_c = v_c - \frac{R}{L}\psi_c - V_{QN} - \frac{1}{C}u_c q_C \end{aligned}$$

Afterwards, as the structure of each equation is the same and considering the electrical components are equal for each of the phases, the matrix form can be applied as shown in the following equation:

$$\begin{bmatrix} \dot{\psi}_a \\ \dot{\psi}_b \\ \dot{\psi}_c \end{bmatrix} = \begin{bmatrix} v_a \\ v_b \\ v_c \end{bmatrix} - \frac{R}{L}\begin{bmatrix} \psi_a \\ \psi_b \\ \psi_c \end{bmatrix} - \begin{bmatrix} V_{QN} \\ V_{QN} \\ V_{QN} \end{bmatrix} - \frac{1}{C}q_C \begin{bmatrix} u_a \\ u_b \\ u_c \end{bmatrix}$$

And in a more simplified way:

$$[\dot{\psi}_{abc}] = [v_{abc}] - \frac{R}{L}[\psi_{abc}] - [V_{QN}] - \frac{1}{C}q_C[u_{abc}]$$

On the other side, DC side's dynamic is obtain from a Kirchhoff's Current Law over the capacitor. The equation is developed as follows:

$$i_a u_a + i_b u_b + i_c u_c = i_C + I_{DC}$$

$$i_C = -I_{DC} + (i_a u_a + i_b u_b + i_c u_c)$$

$$C\frac{dv_{DC}}{dt} = -I_{DC} + (i_a u_a + i_b u_b + i_c u_c)$$

$$\frac{d(q_C)}{dt} = \dot{q}_C = -I_{DC} + (i_a u_a + i_b u_b + i_c u_c)$$

If this equation is written in a matrix way as done previously with the KVL developed equations, the next final expression is achieved:

$$\dot{q}_C = -I_{DC} + \begin{bmatrix} u_a & u_b & u_c \end{bmatrix} \begin{bmatrix} i_a \\ i_b \\ i_c \end{bmatrix}$$

$$\dot{q}_C = -I_{DC} + [u_{abc}]^T [i_{abc}]$$

$$\dot{q}_C = -I_{DC} + \frac{1}{L}[u_{abc}]^T [\psi_{abc}]$$

B Park Transformation

In order to simplify the power control, differentiating explicitly active and reactive power, the final set of three equations developed in A will be transformed to rotational dq-framework. The aim is to obtain a set of three equations, where two of them describe the dynamics of AC side inductors, using choke's current ot flux; while the third describes the dynamic of capacitors charge or voltage. This is achieved by means of Park transformation, also called direct-quadrature-zero transformation; which can be described by the following two expressions.

$$[X_{dq0}] = [P] \cdot [X_{abc}]$$

$$[X_{abc}] = [P]^{-1} \cdot [X_{dq0}]$$

Where the matrix $[P]$ is defined as:

$$[P] = \frac{3}{2} \begin{bmatrix} cos(\omega t) & cos(\omega t - \frac{2\pi}{3}) & cos(\omega t + \frac{2\pi}{3}) \\ -sin(\omega t) & -sin(\omega t - \frac{2\pi}{3}) & -sin(\omega t + \frac{2\pi}{3}) \\ \frac{1}{2} & \frac{1}{2} & \frac{1}{2} \end{bmatrix}$$

And then matrix $[P]^{-1}$ as:

$$[P]^{-1} = \begin{bmatrix} cos(\omega t) & -sin(\omega t) & 1 \\ cos(\omega t - \frac{2\pi}{3}) & -sin(\omega t - \frac{2\pi}{3}) & 1 \\ cos(\omega t + \frac{2\pi}{3}) & -sin(\omega t + \frac{2\pi}{3}) & 1 \end{bmatrix}$$

Considering [P] is the Park matrix, $[P]^{-1}$ is the inverse of Park transformation and $[X] \in \mathbb{R}^3$; the following lines describe the transform from *abc* to *dq0* of the set of equations obtained at the end of the previous section.

Applying Park matrix to AC side's dynamic equations, the following is obtained:

$$\frac{d}{dt}([P]^{-1})[\psi_{dq0}] + [P]^{-1}\frac{d}{dt}([\psi_{dq0}]) = [P]^{-1}[v_{dq0}] - \frac{R}{L}[P]^{-1}[\psi_{dq0}] - [V_{QN}] - \frac{1}{C}q_C[P]^{-1}[u_{dq0}]$$

However, multiplying $[P]^{-1}$ from left to all the terms, considering the matrix property $[P]^{-1}[P] = I$, an equation with the terms in *dq0* framework is obtained:

$$\begin{aligned}[P][P]^{-1}\frac{d}{dt}([\psi_{dq0}]) = \\ - [P]\frac{d}{dt}([P]^{-1})[\psi_{dq0}] + [P][P]^{-1}[v_{dq0}] - \frac{R}{L}[P][P]^{-1}[\psi_{dq0}] - [P][V_{QN}] - \frac{1}{C}q_C[P][P]^{-1}[u_{dq0}]\end{aligned}$$

$$\frac{d}{dt}([\psi_{dq0}]) = [\dot{\psi}_{dq0}] = -[P]\frac{d}{dt}([P]^{-1})[\psi_{dq0}] + [v_{dq0}] - \frac{R}{L}[\psi_{dq0}] - [P][V_{QN}] - \frac{1}{C}q_C[u_{dq0}]$$

Despite most of the terms are easily simplified, two remaining terms, "$-[P]\frac{d}{dt}([P]^{-1})$" and "$[P][V_{QN}]$", need further development. Following equations show the development together with the final result of these expressions. First the derivative of -$[P]^{-1}$ is obtained, as

$$\begin{aligned} -\frac{d([P]^{-1})}{dt} &= -\begin{bmatrix} \frac{d}{dt}(cos(\omega t)) & \frac{d}{dt}(-sin(\omega t)) & \frac{d}{dt}(1) \\ \frac{d}{dt}(cos(\omega t - \frac{2\pi}{3})) & \frac{d}{dt}(-sin(\omega t - \frac{2\pi}{3})) & \frac{d}{dt}(1) \\ \frac{d}{dt}(cos(\omega t + \frac{2\pi}{3})) & \frac{d}{dt}(-sin(\omega t + \frac{2\pi}{3})) & \frac{d}{dt}(1) \end{bmatrix}, \\ &= -\begin{bmatrix} -\omega sin(\omega t) & -\omega cos(\omega t) & 0 \\ -\omega sin(\omega t - \frac{2\pi}{3}) & -\omega cos(\omega t - \frac{2\pi}{3}) & 0 \\ -\omega sin(\omega t + \frac{2\pi}{3}) & -\omega cos(\omega t + \frac{2\pi}{3}) & 0 \end{bmatrix}, \\ &= \begin{bmatrix} \omega sin(\omega t) & \omega cos(\omega t) & 0 \\ \omega sin(\omega t - \frac{2\pi}{3}) & \omega cos(\omega t - \frac{2\pi}{3}) & 0 \\ \omega sin(\omega t + \frac{2\pi}{3}) & \omega cos(\omega t + \frac{2\pi}{3}) & 0 \end{bmatrix}. \end{aligned}$$

Considering this term, "$-[P]\frac{d}{dt}([P]^{-1})$" is developed as:

$$-[P]\frac{d([P]^{-1})}{dt} = \frac{2}{3}\begin{bmatrix} cos(\omega t) & cos(\omega t - \frac{2\pi}{3}) & cos(\omega t + \frac{2\pi}{3}) \\ -sin(\omega t & -sin(\omega t - \frac{2\pi}{3}) & -sin(\omega t + \frac{2\pi}{3}) \\ \frac{1}{2} & \frac{1}{2} & \frac{1}{2} \end{bmatrix}\begin{bmatrix} \omega sin(\omega t) & \omega cos(\omega t) & 0 \\ \omega sin(\omega t - \frac{2\pi}{3}) & \omega cos(\omega t - \frac{2\pi}{3}) & 0 \\ \omega sin(\omega t + \frac{2\pi}{3}) & \omega cos(\omega t + \frac{2\pi}{3}) & 0 \end{bmatrix}$$

Applying the following trigonometrical properties

$$sin(x)cos(x) = \frac{1}{2}sin(2x), \tag{149}$$

$$\begin{aligned} sin(x) + sin(x + \frac{2\pi}{3}) + sin(x - \frac{2\pi}{3}) = 0, \\ cos(x) + cos(x + \frac{2\pi}{3}) + cos(x - \frac{2\pi}{3}) = 0, \end{aligned} \tag{150}$$

$$\begin{aligned} sin^2(x) + sin^2(x + \frac{2\pi}{3}) + sin^2(x - \frac{2\pi}{3}) = \frac{3}{2}, \\ cos^2(x) + cos^2(x + \frac{2\pi}{3}) + cos^2(x - \frac{2\pi}{3}) = \frac{3}{2}, \end{aligned} \tag{151}$$

"$-[P]\frac{d}{dt}([P]^{-1})$" term can be reduced to the expression shown as follows:

$$-[P]\frac{d}{dt}([P]^{-1}) = \omega \begin{bmatrix} 0 & 1 & 0 \\ -1 & 0 & 0 \\ 0 & 0 & 0 \end{bmatrix}.$$

On the other hand, "$[P][V_{QN}]$" is reduced by the following procedure:

$$\begin{aligned} [P][V_{QN}] &= \frac{2}{3} \begin{bmatrix} cos(\omega t) & cos(\omega t - \frac{2\pi}{3}) & cos(\omega t + \frac{2\pi}{3}) \\ -sin(\omega t & -sin(\omega t - \frac{2\pi}{3}) & -sin(\omega t + \frac{2\pi}{3}) \\ \frac{1}{2} & \frac{1}{2} & \frac{1}{2} \end{bmatrix} \begin{bmatrix} V_{QN} \\ V_{QN} \\ V_{QN} \end{bmatrix}, \\ &= \frac{2}{3} \begin{bmatrix} (cos(\omega t) + cos(\omega t - \frac{2\pi}{3}) + cos(\omega t + \frac{2\pi}{3}))V_{QN} \\ -(sin(\omega t) + sin(\omega t - \frac{2\pi}{3}) + sin(\omega t + \frac{2\pi}{3}))V_{QN} \\ (\frac{1}{2} + \frac{1}{2} + \frac{1}{2})V_{QN} \end{bmatrix}, \\ &= V_{QN} \begin{bmatrix} 0 \\ 0 \\ 1 \end{bmatrix}. \end{aligned}$$

Once this is known, the developed dq0 matrix form is finally reached for the AC flux dynamics.

$$\begin{bmatrix} \dot{\psi}_d \\ \dot{\psi}_q \\ \dot{\psi}_0 \end{bmatrix} = \omega \begin{bmatrix} 0 & 1 & 0 \\ -1 & 0 & 0 \\ 0 & 0 & 0 \end{bmatrix} \begin{bmatrix} \psi_d \\ \psi_q \\ \psi_0 \end{bmatrix} + \begin{bmatrix} v_d \\ v_q \\ v_0 \end{bmatrix} - \frac{R}{L} \begin{bmatrix} \psi_d \\ \psi_q \\ \psi_0 \end{bmatrix} - \frac{1}{C} q_C \begin{bmatrix} u_d \\ u_q \\ u_0 \end{bmatrix} - V_{QN} \begin{bmatrix} 0 \\ 0 \\ 1 \end{bmatrix}$$

By undoing the matrix form simplification, dq0 set of expressions are shown hereunder:

$$\begin{aligned} \dot{\psi}_d &= -\frac{R}{L}\psi_d + \omega\psi_q - \frac{1}{C}q_C u_d + v_d \\ \dot{\psi}_q &= -\frac{R}{L}\psi_q - \omega\psi_d - \frac{1}{C}q_C u_q + v_q \\ \dot{\psi}_0 &= -\frac{R}{L}\psi_0 - \frac{1}{C}q_C u_0 + v_0 - V_{QN} \end{aligned}$$

Obtained first couple of equations, the ones related to d and q axis, will be used for the converter model. The third equation is representative uniquely during unbalanced operation. Being completely decoupled from "d" and "q" axes, it can be omitted. It is important to highlight that "d" axis will be coupled to grid voltage vector, so that v_q component will be null.

In order to achieve the third equation, DC side's dynamic equation is also transformed to *dq0*-framework.

$$\dot{q}_C = -I_{DC} + \frac{1}{L}\{[P]^{-1}[u_{dq0}]\}^T[P]^{-1}[\psi_{dq0}]$$

Taking into account the property $\{[A][B]\}^T = [B]^T[A]^T$, the capacitors charge equation can be written as:

$$\dot{q}_C = -I_{DC} + \frac{1}{L}[u_{dq0}]\{[P]^{-1}\}^T[P]^{-1}[\psi_{dq0}]$$

Again, the non-simplified term $\{[P]^{-1}\}^T[P]^{-1}$ remains. This is developed as follows:

$$\{[P]^{-1}\}^T[P]^{-1} = \begin{bmatrix} cos(\omega t) & cos(\omega t - \frac{2\pi}{3}) & cos(\omega t + \frac{2\pi}{3}) \\ -sin(\omega t) & -sin(\omega t - \frac{2\pi}{3}) & -sin(\omega t + \frac{2\pi}{3}) \\ 1 & 1 & 1 \end{bmatrix} \begin{bmatrix} cos(\omega t) & -sin(\omega t) & 1 \\ cos(\omega t - \frac{2\pi}{3}) & -sin(\omega t - \frac{2\pi}{3}) & 1 \\ cos(\omega t + \frac{2\pi}{3}) & -sin(\omega t + \frac{2\pi}{3}) & 1 \end{bmatrix}$$

Applying the trigonometrical properties of equations (149)-(151), the final value for $\{[P]^{-1}\}^T[P]^{-1}$ is shown in (152).

$$\{[P]^{-1}\}^T[P]^{-1} = \begin{bmatrix} \frac{3}{2} & 0 & 0 \\ 0 & \frac{3}{2} & 0 \\ 0 & 0 & 3 \end{bmatrix} \tag{152}$$

Once this value is known, charge's dynamic equation is fully developed in *dq0*-framework.

$$\dot{q}_C = -I_{DC} + \frac{1}{L}\begin{bmatrix} u_d & u_q & u_0 \end{bmatrix} \begin{bmatrix} \frac{3}{2} & 0 & 0 \\ 0 & \frac{3}{2} & 0 \\ 0 & 0 & 3 \end{bmatrix} \begin{bmatrix} \psi_d \\ \psi_q \\ \psi_0 \end{bmatrix}$$

$$\dot{q}_C = -I_{DC} + \frac{3}{2}\frac{1}{L}(u_d\psi_d + u_q\psi_q) + \frac{3}{L}u_0\psi_0$$

Assuming that the modulation index and inductor's flux in the zero axis does not exit during balanced operation, the third equation required is obtained:

$$\dot{q}_C = -I_{DC} + \frac{3}{2}\frac{1}{L}(u_d\psi_d + u_q\psi_q)$$

As a conclusion, the set of dynamic equations for a VSC from the point of view of rectifier operation and as a function of inductor fluxes and capacitor charge can be presented as:

$$\begin{aligned} \dot{\psi}_d &= -\frac{R}{L}\psi_d + \omega\psi_q - \frac{1}{C}q_C u_d + v_d \\ \dot{\psi}_q &= -\frac{R}{L}\psi_q - \omega\psi_d - \frac{1}{C}q_C u_q \\ \dot{q}_C &= -I_{DC} + \frac{3}{2}\frac{1}{L}(u_d\psi_d + u_q\psi_q) \end{aligned}$$

C VSC Incremental Passive Output

The passive output of the converter is developed in order to interpret the meaning of this result. The expression presented in (78) is taken as starting point.

$$
\begin{aligned}
y &= g^\top(\bar{x})\nabla\mathcal{H}(\tilde{x}),\\
&= g^\top(\bar{x})\left(\nabla\mathcal{H}(x)-\nabla\mathcal{H}(\bar{x})\right),\\
&= \begin{bmatrix}\nabla^\top\mathcal{H}(\bar{x})\mathcal{J}_1^\top & \nabla^\top\mathcal{H}(\bar{x})\mathcal{J}_2^\top\end{bmatrix}\left(\nabla\mathcal{H}(x)-\nabla\mathcal{H}(\bar{x})\right),\\
&= \begin{bmatrix}\nabla^\top\mathcal{H}(\bar{x})\mathcal{J}_1^\top\nabla\mathcal{H}(x) & \nabla^\top\mathcal{H}(\bar{x})\mathcal{J}_2^\top\nabla\mathcal{H}(x)\end{bmatrix} - \underbrace{\begin{bmatrix}\nabla^\top\mathcal{H}(\bar{x})\mathcal{J}_1^\top\nabla\mathcal{H}(\bar{x}) & \nabla^\top\mathcal{H}(\bar{x})\mathcal{J}_2^\top\nabla\mathcal{H}(\bar{x})\end{bmatrix}}_{\text{Zero matrix}},\\
&= \begin{bmatrix}\nabla^\top\mathcal{H}(\bar{x})\mathcal{J}_1^\top\nabla\mathcal{H}(x) & \nabla^\top\mathcal{H}(\bar{x})\mathcal{J}_2^\top\nabla\mathcal{H}(x)\end{bmatrix}.
\end{aligned}
$$

The first element of the obtained matrix can be expressed as follows.

$$
\begin{aligned}
\nabla^\top\mathcal{H}(\bar{x})\mathcal{J}_1^\top\nabla\mathcal{H}(x) &= \begin{bmatrix}\bar{i}_d & \bar{i}_q & \bar{v}_{dc1}\end{bmatrix}\begin{bmatrix}0 & 0 & -1\\ 0 & 0 & 0\\ 1 & 0 & 0\end{bmatrix}\begin{bmatrix}i_d\\ i_q\\ v_{dc1}\end{bmatrix},\\
&= \begin{bmatrix}\bar{i}_d & \bar{i}_q & \bar{v}_{dc1}\end{bmatrix}\begin{bmatrix}-v_{dc1}\\ 0\\ i_d\end{bmatrix},\\
&= i_d\bar{v}_{dc1}-\bar{i}_d v_{dc1}.
\end{aligned}
$$

Same process is repeated for the second element.

$$
\begin{aligned}
\nabla^\top\mathcal{H}(\bar{x})\mathcal{J}_2^\top\nabla\mathcal{H}(x) &= \begin{bmatrix}\bar{i}_d & \bar{i}_q & \bar{v}_{dc1}\end{bmatrix}\begin{bmatrix}0 & 0 & 0\\ 0 & 0 & -1\\ 0 & 1 & 0\end{bmatrix}\begin{bmatrix}i_d\\ i_q\\ v_{dc1}\end{bmatrix},\\
&= \begin{bmatrix}\bar{i}_d & \bar{i}_q & \bar{v}_{dc1}\end{bmatrix}\begin{bmatrix}0\\ -v_{dc1}\\ i_q\end{bmatrix},\\
&= i_q\bar{v}_{dc1}-\bar{i}_q v_{dc1}.
\end{aligned}
$$

The passive output can be then written as:

$$
y = \begin{bmatrix}i_d\bar{v}_{dc1}-\bar{i}_d v_{dc1} & i_q\bar{v}_{dc1}-\bar{i}_q v_{dc1}\end{bmatrix}.
$$

Analysing the expression, it can be seen that both elements have units of power, what means the converter's output is actually a power which can be analytically developed with the aim of obtaining the stability certificate. When the state variables of the converters reach to the reference values, i.e. to the equilibrium point, the passive output becomes a zero matrix. This feature is what the PI-PBC exploits to stabilize the system.

D Final Steps for the Obtention of Expressions of the Modulation Indices

In this annex the final steps for the acquisition of the modulation indices are developed. Equation (56) is taken as starting point, computing each element of the vector $\bar{u}$ separately.

$$
\bar{u} = \begin{bmatrix}\bar{u}_d\\ \bar{u}_q\end{bmatrix} = \frac{1}{|\Upsilon|}\begin{bmatrix}\bar{v}_{dc1}\left(\bar{v}_{dc1}^2+\bar{i}_q^2\right) & -\bar{i}_d\bar{i}_q\bar{v}_{dc1} & -\bar{i}_d\bar{v}_{dc1}^2\\ -\bar{i}_d\bar{i}_q\bar{v}_{dc1} & \bar{v}_{dc1}\left(\bar{v}_{dc1}^2+\bar{i}_d^2\right) & -\bar{i}_q\bar{v}_{dc1}^2\end{bmatrix}\begin{bmatrix}\omega L\bar{i}_q - R\bar{i}_d - V_d\\ -\omega L\bar{i}_d - R\bar{i}_q - Vq\\ -\hat{G}\bar{v}_{dc1}+\hat{I}_T\end{bmatrix}
$$

D.1 Development of direct modulation index

$$\bar{u}_d = \frac{-1}{|\Upsilon|}\left[\bar{v}_{dc1}(\bar{v}_{dc1}^2+\bar{i}_q^2)\left[\omega L\bar{i}_q - R\bar{i}_d - V_d\right] - \bar{i}_d\bar{i}_q\bar{v}_{dc1}\left[-\omega L\bar{i}_d - R\bar{i}_q - V_q\right] - \bar{i}_d\bar{v}_{dc1}^2\left[-\hat{G}\bar{v}_{dc1} + \bar{\hat{I}}_T\right]\right]$$

Rearranging the equation and taking into account that the DC current can be computed as in (153).

$$\hat{I}_T = \frac{P_{AC}+P_{Losses}}{v_{dc1}} = \frac{V_d i_d + V_q i_q + R\left(i_d^2+i_q^2\right) + \hat{G}v_{dc1}^2}{v_{dc1}} \tag{153}$$

$$\begin{aligned}\bar{u}_d &= \frac{-1}{\bar{v}_{dc1}\left(\bar{v}_{dc1}^2+\bar{i}_d^2+\bar{i}_q^2\right)}\left[\left(\bar{v}_{dc1}^2+\bar{i}_d^2+\bar{i}_q^2\right)\left(-R\bar{i}_d+\omega L\bar{i}_q - V_d\right)\right]\\ &= \frac{R\bar{i}_d - \omega L\bar{i}_q + V_d}{\bar{v}_{dc1}}\end{aligned}$$

D.2 Development of quadrature modulation index

$$\bar{u}_q = \frac{-1}{|\Upsilon|}\left[-\bar{i}_d\bar{i}_q\bar{v}_{dc1}\left[\omega L\bar{i}_q - R\bar{i}_d - V_d\right] + \bar{v}_{dc1}(\bar{v}_{dc1}^2+\bar{i}_d^2)\left[-\omega L\bar{i}_d - R\bar{i}_q - V_q\right] - \bar{i}_q\bar{v}_{dc1}^2\left[-\hat{G}\bar{v}_{dc1} + \bar{\hat{I}}_T\right]\right]$$

Rearranging the obtained equation and taking into account the DC current equation (153) again.

$$\begin{aligned}\bar{u}_q &= \frac{-1}{\bar{v}_{dc1}\left(\bar{v}_{dc1}^2+\bar{i}_d^2+\bar{i}_q^2\right)}\left[\left(\bar{v}_{dc1}^2+\bar{i}_d^2+\bar{i}_q^2\right)\left(-R\bar{i}_q-\omega L\bar{i}_d - V_q\right)\right]\\ &= \frac{R\bar{i}_q + \omega L\bar{i}_d + V_q}{\bar{v}_{dc1}}\end{aligned}$$

B Sets of Equations for VSC converters

A Set of equations from the point of view of a rectifier operation and as a function of inductor fluxes and capacitor charge

$$\begin{aligned}
\dot{\psi}_d &= -\frac{R}{L}\psi_d + \omega\psi_q - \frac{1}{C}q_C u_d + v_d \\
\dot{\psi}_q &= -\frac{R}{L}\psi_q - \omega\psi_d - \frac{1}{C}q_C u_q \\
\dot{q}_C &= -I_T + \frac{3}{2}\frac{1}{L}(u_d\psi_d + u_q\psi_q)
\end{aligned} \tag{154}$$

B Set of equations from the point of view of a rectifier as a function of inductor's currents and capacitor's voltage

$$\begin{aligned}
L\dot{i_d} &= -Ri_d + \omega L i_q - u_d v_{dc} + V_d \\
L\dot{i_q} &= -Ri_q - \omega L i_d - u_q v_{dc} \\
C\dot{v}_{dc} &= -I_T + \frac{3}{2}(u_d i_d + u_q i_q)
\end{aligned} \tag{155}$$

C Set of equations from the point of view of an inverter as a function of inductor's fluxes and capacitor's charge

$$\begin{aligned}
\dot{\psi}_d &= -\frac{R}{L}\psi_d + \omega\psi_q + \frac{1}{C}q_C u_d - v_d \\
\dot{\psi}_q &= -\frac{R}{L}\psi_q - \omega\psi_d + \frac{1}{C}q_C u_q \\
\dot{q}_C &= I_T - \frac{3}{2}\frac{1}{L}(u_d\psi_d + u_q\psi_q)
\end{aligned} \tag{156}$$

D Set of equations from the point of view of an inverter as a function of inductor's currents and capacitor's voltage

$$\begin{aligned}
L\dot{i_d} &= -Ri_d + \omega L i_q + u_d v_{DC} - v_d \\
L\dot{i_q} &= -Ri_q - \omega L i_d + u_q v_{DC} \\
C\dot{v}_{DC} &= I_T - \frac{3}{2}(u_d i_d + u_q i_q)
\end{aligned} \tag{157}$$

C Proofs

A Proof 1: Property of a Skew-Matrix

If $\mathcal{J}$ is a skew-matrix and C is a column vector, then $C^\top \mathcal{J} C$ is a zero-matrix.

Let's suppose a symmetric-skew matrix $\mathcal{J} \in \mathbb{R}^{3\times 3}$ and a column vector $C \in \mathbb{R}^3$.

$$\mathcal{J} = \begin{bmatrix} 0 & -a & -b \\ a & 0 & -c \\ b & c & 0 \end{bmatrix} \qquad C = \begin{bmatrix} x \\ y \\ z \end{bmatrix}$$

Then,

$$\begin{aligned} C^\top \mathcal{J} C &= \begin{bmatrix} x & y & z \end{bmatrix} \begin{bmatrix} 0 & -a & -b \\ a & 0 & -c \\ b & c & 0 \end{bmatrix} \begin{bmatrix} x \\ y \\ z \end{bmatrix}, \\ &= \begin{bmatrix} x & y & z \end{bmatrix} \begin{bmatrix} -ay - bz \\ ax - cz \\ bx + cy \end{bmatrix}, \\ &= -axy - bxz + axy - cyz + bxz + cyz, \\ &= (axy - axy) + (bxz - bxz) + (cyz - cyz), \\ &= 0. \end{aligned}$$

B Proof 2: Incremental Hamiltonian Gradient

$\nabla\mathcal{H}(x) - \nabla\mathcal{H}(\bar{x}) = \nabla\mathcal{H}(\tilde{x})$

$$\begin{aligned} \nabla\mathcal{H}(x) - \nabla\mathcal{H}(\bar{x}) &= Qx - Q\bar{x}, \\ &= Q\left(x - \bar{x}\right), \\ &= Q\tilde{x}, \\ &= \nabla\mathcal{H}(\tilde{x}). \end{aligned}$$

C Proof 3: Relation Between Input Matrix and Vector

$g(x)u - g(\bar{x})\bar{u} = g(x)\tilde{u} + g(\tilde{x})\bar{u}$

$$\begin{aligned} g(x)u - g(\bar{x})\bar{u} &= g(x)\tilde{u} + g(x)\bar{u} - g(\bar{x})\bar{u}, \\ &= g(x)\tilde{u} + \left(g(x) - g(\bar{x})\right)\bar{u}, \\ &= g(x)\tilde{u} + \left(\begin{bmatrix} \mathcal{J}_1\nabla\mathcal{H}(x) & \mathcal{J}_2\nabla\mathcal{H}(x) \end{bmatrix} - \begin{bmatrix} \mathcal{J}_1\nabla\mathcal{H}(\bar{x}) & \mathcal{J}_2\nabla\mathcal{H}(\bar{x}) \end{bmatrix}\right)\bar{u}, \\ &= g(x)\tilde{u} + [\mathcal{J}_1 \underbrace{\left(\nabla\mathcal{H}(x) - \nabla\mathcal{H}(\bar{x})\right)}_{\nabla\mathcal{H}(\tilde{x})} \quad \mathcal{J}_2 \underbrace{\left(\nabla\mathcal{H}(x) - \nabla\mathcal{H}(\bar{x})\right)}_{\nabla\mathcal{H}(\tilde{x})}]\bar{u}, \\ &= g(x)\tilde{u} + \begin{bmatrix} \mathcal{J}_1\nabla\mathcal{H}(\tilde{x}) & \mathcal{J}_2\nabla\mathcal{H}(\tilde{x}) \end{bmatrix}\bar{u}, \\ &= g(x)\tilde{u} + g(\tilde{x})\bar{u}. \end{aligned}$$

D Proof 4: Relation Between Passive Output Terms

$y = g^\top(x)\nabla\mathcal{H}(\tilde{x}) = g^\top(\bar{x})\nabla\mathcal{H}(\tilde{x})$

$$
\begin{aligned}
y &= g^\top(x)\nabla\mathcal{H}(\tilde{x}), \\
&= \begin{bmatrix} x^\top Q\mathcal{J}_1^\top \\ x^\top Q\mathcal{J}_2^\top \end{bmatrix} Q\tilde{x}, \\
&= \begin{bmatrix} x^\top Q\mathcal{J}_1^\top Q\,(x-\bar{x}) \\ x^\top Q\mathcal{J}_2^\top Q\,(x-\bar{x}) \end{bmatrix}, \\
&= \underbrace{\begin{bmatrix} x^\top Q\mathcal{J}_1^\top Qx \\ x^\top Q\mathcal{J}_2^\top Qx \end{bmatrix}}_{\text{(Zero-matrix)}} - \begin{bmatrix} x^\top Q\mathcal{J}_1^\top Q\bar{x} \\ x^\top Q\mathcal{J}_2^\top Q\bar{x} \end{bmatrix}, \\
&= \begin{bmatrix} -x^\top Q\mathcal{J}_1^\top Q\bar{x} \\ -x^\top Q\mathcal{J}_2^\top Q\bar{x} \end{bmatrix} \quad \text{(Both elements can be transposed as they are scalars)}, \\
&= \begin{bmatrix} -\bar{x}^\top Q\mathcal{J}_1 Qx \\ -\bar{x}^\top Q\mathcal{J}_2 Qx \end{bmatrix}, \\
&= \underbrace{\begin{bmatrix} -\bar{x}^\top Q\mathcal{J}_1 \\ -\bar{x}^\top Q\mathcal{J}_2 \end{bmatrix}}_{-\mathcal{J}_i = \mathcal{J}_i^\top} Qx, \\
&= \begin{bmatrix} \bar{x}^\top Q\mathcal{J}_1^\top \\ \bar{x}^\top Q\mathcal{J}_2^\top \end{bmatrix} (Q\bar{x} + Q\tilde{x}), \\
&= \begin{bmatrix} \nabla^\top\mathcal{H}(\bar{x})\mathcal{J}_1^\top \\ \nabla^\top\mathcal{H}(\bar{x})\mathcal{J}_2^\top \end{bmatrix} (\nabla\mathcal{H}(\bar{x}) + \nabla\mathcal{H}(\tilde{x})), \\
&= \underbrace{\begin{bmatrix} \nabla^\top\mathcal{H}(\bar{x})\mathcal{J}_1^\top\nabla\mathcal{H}(\bar{x}) \\ \nabla^\top\mathcal{H}(\bar{x})\mathcal{J}_2^\top\nabla\mathcal{H}(\bar{x}) \end{bmatrix}}_{\text{(Zero-matrix)}} + \underbrace{\begin{bmatrix} \nabla^\top\mathcal{H}(\bar{x})\mathcal{J}_1^\top \\ \nabla^\top\mathcal{H}(\bar{x})\mathcal{J}_2^\top \end{bmatrix}}_{g^\top(\bar{x})} \nabla\mathcal{H}(\tilde{x}), \\
&= g^\top(\bar{x})\nabla\mathcal{H}(\tilde{x}).
\end{aligned}
$$

E Proof 5: Terms Cancellation in the Physical-Virtual System Lyapunov Function

$\nabla\mathcal{H}^\top g(\bar{x})\nabla\mathcal{H}_c - \nabla\mathcal{H}_c^\top g^\top(\bar{x})\nabla\mathcal{H} = 0$

It can be seen that the second term is the transposed of the first one. As first step, the dimension of the first terms is analysed.

$$
\underbrace{\underbrace{\nabla\mathcal{H}^\top}_{1\times 3}\underbrace{g(\bar{x})}_{3\times 2}\underbrace{\nabla\mathcal{H}_c}_{2\times 1}}_{1\times 1}
$$

Since the term is actually a scalar, the transposed of this term has the same value. Therefore, the subtraction of the terms makes zero.